National Library
of Canada

Acquisitions and
Bibliographic Services Branch

395 Wellington Street
Ottawa, Ontario
K1A 0N4

Bibliothèque nationale
du Canada

Direction des acquisitions et
des services bibliographiques

395, rue Wellington
Ottawa (Ontario)
K1A 0N4

Your file Votre référence

Our file Notre référence

NOTICE

The quality of this microform is heavily dependent upon the quality of the original thesis submitted for microfilming. Every effort has been made to ensure the highest quality of reproduction possible.

If pages are missing, contact the university which granted the degree.

Some pages may have indistinct print especially if the original pages were typed with a poor typewriter ribbon or if the university sent us an inferior photocopy.

AVIS

La qualité de cette microforme dépend grandement de la qualité de la thèse soumise au microfilmage. Nous avons tout fait pour assurer une qualité supérieure de reproduction.

S'il manque des pages, veuillez communiquer avec l'université qui a conféré le grade.

La qualité d'impression de certaines pages peut laisser à désirer, surtout si les pages originales ont été dactylographiées à l'aide d'un ruban usé ou si l'université nous a fait parvenir une photocopie de qualité inférieure.

Canada

Protein Mediated Electron Transfer Reactions of Cytochrome c Peroxidase and Cytochrome c

Eddy Tsun-Cheong, Cheung

A Thesis

in

The Department

of

Chemistry and Biochemistry

Presented in Partial Fulfilment of the Requirements

for the Degree of Doctor of Philosophy at

Concordia University

Montreal, Quebec, Canada

June 1992

ISBN 0-315-80926-4

ABSTRACT

Protein Mediated Electron Transfer Reactions of

Cytochrome c Peroxidase and

Cytochrome c

Eddy Tsun-Cheong Cheung, Ph.D.

Concordia University, 1992

This thesis focuses on the redox reactions of two structurally well characterized heme proteins, cytochrome c (C) and its biological partner cytochrome c peroxidase (CCP).

The reactivity of C has been examined by comparing the emission lifetime quenching of a series of ruthenium(II) polypyridyl excited states (Ru^*L_3) by C(FeIII). The measured quenching rate constants for Ru^*L_3 complexes with neutral ligands (i.e. 2,2-bipyridine and 1,10-phenanthroline) are independent of solvent ionic strength. The lack of electrostatic effects on the quenching rate constants suggests that the charges on the ruthenium metal are insulated by the π-conducting ligands. However, the quenching of the negatively charged $Ru^*(DIPS)_3^{4-}$ [DIPS = 4,7-di(phenyl-4'-sulfonate)-1,10-phenanthroline] shows strong ionic strength dependence ($k_q = 1.9\times10^9$ $M^{-1}s^{-1}$ and 7.5×10^9 $M^{-1}s^{-1}$ at μ = 0.10 and 0.01 M, respectively). A 3-fold increase in the quenching rate of $Ru^*(bpy)_3^{2+}$ by C(FeIII) is observed on reducing the pH from 7.0 to 3.0, while rates of quenching by C(FeII) remain essentially unchanged, an observation which shows that the protein structure of C(FeII) is less sensitive to pH than of C(FeIII) over the range examined. The results obtained from steady-state quantum yield measurements on the Ru^*L_3-photosensitized

reduction of C are consistent with a reaction mechanism that involves electron transfer quenching of the excited complexes by C(FeIII) within a solvent-cage prior to the release of the redox products.

The analysis of the ionic strength dependence of the rate of CCP(FeII) oxidation by ferricyanide indicates a charge of -9 on the protein at pH 7.0. Using the Marcus cross-relationship, the electron self-exchange rate constant at $\mu = \infty$ ($k_{11}^{\infty} = 7.2 \times 10^{-5}$ $M^{-1}s^{-1}$) was calculated from the cross reaction rate constant ($k_{12}^{\infty} = 2.1 \times 10^{5}$ $M^{-1}s^{-1}$) for the oxidation of CCP(FeII) by $Fe(CN)_6^{3-}$. This k_{11}^{∞} is compared to the k_{11}^{∞} values for other heme proteins, and a correlation is observed between the self-exchange rates and the degree of exposure of the heme.

First-order rate constants were measured for the oxidation of yeast CCP(FeII) by horse and yeast C(FeIII) at μ = 0.01 to 1.0 M. Porphyrin cytochrome c fluorescence intensity quenching and fluorescence polarization in the presence of CCP(FeIII) give evidence for the formation of a CCP:C complex at $\leq$ 0.02 M but not at μ = 0.2 M. Thus, at low μ ($\leq$ 0.02 M) a reaction mechanism involving the reduction of C(FeIII) within an electrostatically-stabilized complex is proposed, while at high μ, a unimolecular rate-limiting step prior to protein association is proposed. This interpretation is supported by the observation of oxidation rates at high μ which are independent of the sequence of C used, and the large differences in the measured activation enthalpies and entropies for horse C oxidations at μ = 0.02 ($\Delta H^{\#}$ = 4.6 kcal mol^{-1} and $\Delta S^{\#}$ = -46 eu) and 0.2 M ($\Delta H^{\#}$ = 17 kcal mol^{-1} and $\Delta S^{\#}$ = -7.8 eu), clearly indicate that different rate-limiting steps are involved at low and high ionic strength.

ACKNOWLEDGEMENTS

I would like to thank my research supervisor, Dr. A.M. English, for her continuous support and active participation throughout this project. I am also indebted to Dr. J.A. Kornblatt and Dr. C.H. Langford for their valuable advise which contributed significantly to the development of my research. I would like to thank Dr. S.R. Mikkelsen and Dr. J.A. Capobianco for being on my thesis examining committee.

I would like to acknowledge the financial support from the Chemistry Department and a graduate student fellowship from Concordia University.

TABLE OF CONTENTS

LIST OF TABLES

LIST OF FIGURES

LIST OF ABBREVIATIONS

C(FeII)	- Ferrocytochrome c
C(FeIII)	- Ferricytochrome c
CCP(FeII)	- Ferrocytochrome c peroxidase
CCP(FeIII)	- Ferricytochrome c peroxidase
PorC	- porphyrin cytochrome c, the iron-free derivative of cytochrome c
bpy	- 2,2'-bipyridine
phen	- 1,10-phenanthroline
DIP	- 4,7-diphenyl-1,10-phenanthroline
DIPS	- 4,7-diphenyl-1,10-phenanthroline disulphonate
RuL_3	- Ruthenium polypyridine complex
Ru^*L_3	- excited state of Ruthenium polypyridine complex
Pi	- phosphate buffer
Mb	- Myoglobin
CpdI	- CCP(FeIV, R^+), R^+ = oxidized aminoacid residue
CpdII	- CCP(FeIV)
EDTA	- Ethylenediaminetetraacetic acid
ΔE°	- thermodyamic driving force of a reaction
$E_{1/2}$	- standard reduction potential (versus NHE)
ε	- extinction coefficient
A	- absorbance

k_o - natural decay rate constant

k_q - bimolecular quenching rate constant

k_b - thermal back electron transfer rate constant

k_{cr} - cage release rate constant

k_g - germinate pair recombination rate constant

k_{en} - energy transfer rate constant

k_{el} - electron transfer rate constant

k_{obs} - experimental observed rate constant

k_d - diffusion controlled rate constant

k_s - slow phase rate constant

k_f - fast phase rate constant

k_{11} - self-exchange rate constant of the protein

k_{12} - bimolecular cross-reactions rate constant

k_{22} - self-exchange rate constant of the inorganic redox reagent

K_d - dissociation constant

K_a - association constant

μ - ionic strength

τ - emission lifetime

Φ - quantum yield

ß - fraction of reaction going via the fast component in the biphasic reaction

P - polarization value

λ_{max} - wavelength at the absorption maximum

η^* - efficiency of $Ru^*L_3^{2+}$ formation by photoexcitation

η_r - reduction efficiency of $Ru^*L_3^{2+}$ by EDTA

η_{cr} - cage release efficiency of the redox products in competition with the germinate pair recombination

η_q - efficiency of the quenching of excited states

φ - number of moles of Fe^{2+} ions formed in ferrioxalate actinometry

$\Delta S^{\#}$ - activation entropy

$\Delta H^{\#}$ - activation enthalpy

T - Temperature

Chapter 1

GENERAL INTRODUCTION

1.1 Biological Electron Transfer:

The transfer of an electron from one molecule to another is one of the most fundamental processes in all living organisms. In both photosynthesis and respiration, the energy liberated on electron flow down an electron transport chain is conserved in the high energy phosphate bond of adenosine triphosphate (1). The electron transport assembly found in the inner mitochrondrial membrane consists of an array of asymmetrically organized electron carriers that promote efficient flow of electrons from the matrix side to the cytosolic side (1). Electron carriers such as flavins, quinones, iron-sulfur and heme proteins, are involved in the transport of electrons from NADH to O_2 (2):

$$\text{NADH} \xrightarrow{\quad} \underset{\text{reductase}}{\text{NADH-Q}} \xrightarrow{\quad} \text{Coenzyme Q} \xrightarrow{\quad} \text{Cyt. b} \xrightarrow{\quad}$$

$$\text{Cyt. c} \xrightarrow{\quad} \text{Cyt. c oxidase} \xrightarrow{\quad} O_2$$

Due to the complexity of electron transport chains, little is known of the intimate details of their electron transfer reactions. However, the obvious importance of such reactions has led researchers from various disciplines to devote much of their attention

to determine the factors that control electron transfer reactions. Factors such as the separation and the relative orientations of the donor-acceptor, the nature of the intervening medium, the thermodynamic driving force ($\Delta E°$) of the reaction, and the effects of protein-protein recognition on the reaction kinetics, are frequently addressed topics (3).

The research reported in this thesis involves studies on protein-mediated electron transfer reactions. The investigations are centered on two structurally well-characterized, and readily-isolated heme proteins, cytochrome c (C) and its biological partner, cytochrome c peroxidase (CCP).

C and CCP were selected for the present studies for a number of reasons. Cytochromes are long recognized for their role in the electron transfer chains (1). Unlike most of the membrane-bound, multisubunit protein complexes, C and CCP can be separated from mitochrondrial membranes by gentle treatment (4,20). The isolation (20,39,51) and crystallization (4,52) of the two proteins are facilitated by their water-solubility; thus, their amino acid sequences (5,6), and structures (7-9) have been examined in detail. Based on the crystal structures of C (7) and CCP (8,9), a hypothetical model of their electron transfer complex has been proposed (10,11), and evidence supporting this model has been obtained from a number of independent studies (12-17,38). The model provides a donor-acceptor system with a well defined heme separation and relative orientation; thus, kinetic measurements of electron transfer within this protein-protein complex are of considerable interest. Furthermore, the heterolysis of H_2O_2 to water catalyzed by CCP (Section 1.3) involves a pathway highly akin to the reduction of dioxygen to water catalyzed by mitochondrial cytochrome c oxidase. Peroxidatic activity of cytochrome

oxidase has also been demonstrated (18); using hydrogen peroxide as an oxidizing substrate, C(FeII) was oxidized by cytochrome oxidase under anaerobic conditions. Thus, it is conceivable that the reduction of dioxygen by the oxidase might share intermediates similar to those found in the peroxidase reaction cycle. Another interesting observation is the ability of ferrous horseradish peroxidase, HRP(FeII), to reduce dioxygen to water (37). Evidence for the activation of dioxygen by HRP was obtained by resonance Raman studies (36), which clearly indicated the weakening of the O=O bond in the oxyperoxidase complex, HRP(FeII):O_2. Since a prominent property of the oxyperoxidase complex is its ability to oxidize dithionite, it was referred to by the authors as "a prototype of a terminal oxidase" (37). These interesting observations highlight possible mechanistic similarities between oxidases and peroxidases. However, owing to the relative structural simplicity of peroxidases, and for the other reasons mentioned above, CCP and C were selected for the present studies as models to probe the nature of biological electron transfer reactions.

1.2 Current Research on Protein-Mediated Electron Transfer:

Redox reactions of small ions and inorganic complexes have been extensively studied to provide a basis for theoretical models (reviews 28,47). Some electron transfer theories have been extended to protein-mediated electron transfer reactions (29,45,56,57). In particular, analysis of reaction rates between inorganic redox reagents and metalloproteins at different ionic strengths and pH's have been used to evaluate physical properties, such as surface charges (49), and topologies of the redox sites of the proteins (48).

Current theoretical treatments of the dependence of electron transfer rates on the

thermodynamic driving force ($\Delta E°$) are summarized by Sutin (46) and Marcus (47), and will not be elaborated here. However, experimental studies on the correlation between observed rates and $\Delta E°$ have benefited significantly from recent advances in experimental techniques. Initially, experiments were carried out with ground-state inorganic redox reagents which provided a limited range of $\Delta E°$ (< 1 V NHE). Electronically excited states of inorganic complexes, and radicals generated by flash photolysis and pulse radiolysis have provided attractive methods for measuring electron transfer rate over a wide range of $\Delta E°$. Bimolecular electron transfer rates between C and a number of photoreduced flavins increase rapidly with $\Delta E°$ and reaches a maximum at $\Delta E° > 0.6$ V (vs. NHE) (22).

The distance dependence of electron transfer rates has also been the focus of both theoretical and experimental studies. One of the prominent features of biological redox reactions is the large distance between donor and acceptor which are separated by the protein matrix. An experimental approach used by two independent research groups, led by Gray and Isied, involves the covalent attachment of $Ru(NH_3)_5^{3+}$ to surface histidine residues of structurally well-characterized metalloproteins such as myoglobin (43), C (30a,b,44,53). More recently, the same approach was succussfully used in our lab to study electron transfer in ruthenium modified CCP (59). These reactions are initiated by flash photolysis or by pulse radiolysis, and electron transfer kinetics are followed spectrophotometrically. A rate of 3.2 s^{-1} was reported for the transfer of electron from the $Ru(NH_3)_5^{2+}$ centre (on His-60) to the ferryl(FeIV) heme of CCP (59). In the case of C, the redox sites are separated by 12 Å (distance between the edge of Ru-bound His-33 and

heme-linked His-18) and rates of 30 s^{-1} and 53 s^{-1} were observed using flash photolysis (30b) and pulse radiolysis (53), respectively, for electron transfer from Ru(II) to heme center. Sykes et al. have also measured intramolecular electron transfer rates in $Ru(NH_3)_5^{3+}$-modified metalloproteins (54,55). In bacterial C_{551}, a rate of 13 s^{-1} was observed for electron transfer from Ru(II) to the Fe(III) heme at a donor-acceptor separation of 7.9 Å (55) measured between the γ-C atom of the modified His-47 to the S atom of the axial Met-61.

By replacing the native heme with zinc mesoporphyrin IX to form a semi-artificial (Zn,Fe) hybrid hemoglobin, Hoffman and colleagues (31,32) have demonstrated electron transfer ($k = 100\ s^{-1}$) from the Zn-porphyrin triplet state to the FeIII-heme, at a donor-acceptor separation of 20 Å. A similar approach has been used in studies on intracomplex electron transfer in protein-protein complexes including: cytochrome b_5(FeIII):C(Zn), $k = 5x10^5\ s^{-1}$ (32); cytochrome b_5(FeIII):Hb(Zn), $k = 8x10^3\ s^{-1}$ (34); and CCP(Zn):C(FeIII), $k = 140\ s^{-1}$ (35), with donor-acceptor separation of 8, 10 and 17 Å, respectively. More recently, photoinduced intramolecular electron transfer rates in Zn and Ru modified myoglobin were reported (43). Four of the solvent-accessible histidine residues were individually modified by $Ru(NH_3)_5^{3+}$ and the heme was substituted by zinc mesoporphyrin IX. The distances between the N(3) of the modified histidine residues and the edge of the porphyrin range from 12 to 22 Å, and the electron transfer rates range from $7.0x10^4$ to $8.5x10^3\ s^{-1}$.

For a system with weak donor-acceptor electronic coupling, the electron transfer rate should fall-off exponentially with the separation distance, R (46,47):

$$k = k_o \exp(-\alpha R)$$

where α reflects the extent of electronic coupling through the protein medium. In general, a relatively small α value (0.7 to 0.9 $Å^{-1}$) is obtained for electron transfer in proteins (42,43), suggesting that the electronic coupling might be propagated through the intervening amino acid residues.

From computer modelling of the CCP:C complex (10,11), an intracomplex electron transfer pathway involving the π-conducting aromatic amino acid residues that bridge the hemes across a distance of 17 Å (heme edge-to-edge) is proposed. However, the exact pathway the electron takes in travelling from one center to another is not defined. Thus, ongoing research efforts probe the regulation of electron transfer by key amino acid residues. For example, rate measurements were carried out between Zn-substituted CCP and mutant yeast C's where Phe-82 of C was modified by site-directed mutagenesis (50). In every variant with an aliphatic residue at position 82 of C (e.g. Gly-82) the intra-complex electron transfer rate from C(FeII) to CCP(ZnP)$^+$, the zinc porphyrin π-cation radical, was reduced by a factor of approximately 10^4. The control of electron transfer kinetics by protein-protein interactions has also been investigated using native C and CCP (26) and by single amino acid replacements (27). By replacing the conserved Arg or Lys residues on yeast C, which are supposedly involved in binding of CCP, with neutral amino acids (i.e. Ile), the intracomplex electron transfer rate from C(FeII) to CCP(FeIV) increased from 260 s^{-1} to 1000 s^{-1} for the wild type iso-1 yeast C and the Ile-13 mutant, respectively. The authors concluded that the electrostatically stabilized C/CCP complex

is not optimized for electron transfer, and that ionic interactions between the proteins can be partially masked by increasing ionic strength or by neutralization of key positively charged residues, allowing the two proteins to orient themselves to form a more efficient electron transfer complex (27).

Mutants of CCP have also been prepared by site-directed mutagenesis (40). The heme environment of these CCP mutants has been examined by resonance Raman spectroscopy (41a,b) and the catalytic activity of CCP was found to be highly dependent on Trp-191 (58), a key amino acid residue which forms H-bonding and π-π interactions with the iron coordinated proximal His-175 (11). The rate of the CCP-catalyzed C(FeII) oxidation decreased by 3000-fold upon replacing Trp-191 with Phe (58). However, it is not possible to determine whether the drop in catalytic activity is due to the steric constraints on the relaxation of the iron center to the resting ferric state in the Phe-191 mutant, or to the interruption of the interprotein electron transfer pathway between CCP and C. In this thesis, studies on the reactivities of the two native proteins with no structural modificaction are reported.

1.3 Structures and Functions of C and CCP:

C is a single electron carrier which serves as an electron donating substrate for its oxidase and peroxidase. It is a monomeric protein with a molecular weight of $\approx$ 13 kD (14). The prosthetic group is an iron-protoporphyrin IX, which is covalently attached to the protein by thioether linkages on the vinyl groups of the heme. The axial ligands to the iron atom are the sulfur atom of a methionine residue (Met-80) and the nitrogen atom of

a histidine residue (His-18). The heme group is surrounded by many tightly packed hydrophobic side chains and most of the heme is buried in this hydrophobic interior except for the heme edge of the pyrole rings 2 and 3.

Analysis of the amino acid sequence of C's from various species reveals a number of conserved residues that have remained essentially unchanged during years of evolution (5). These invariants include: the methionine and histidine that are coordinated to the iron, the cysteines that are covalently bonded to the heme, and the positively-charged lysine and arginine residues that are located on the surface of the molecule near the heme crevice (5,19). A complementary ring of negatively-charged aspartate residues are found on the surface of CCP (14). Independent studies using chemical modification (12), cross-linking (13) and computer graphic modelling (14), indicate the formation of a 1:1 noncovalent complex between C and CCP. Results indicate that the binding site on C for CCP spans the heme edge, and stresses the importance of the spatial distribution of complementary surface charges in the binding of the two proteins.

CCP is a monomeric enzyme with a molecular weight of 35 kD (11). The protein consists of a single polypeptide of 293 amino acid residues folded into two clearly defined domains with a single heme sandwiched between the two domains (8). The heme group is held in place by hydrogen bonding between one of the heme propionates and a threonine from the peptide backbone. The iron atom is coordinated to the N(1) atom of the imidazole side chain of His-175, and the sixth coordination position is vacant (21). Unlike C, the heme of CCP is buried below the protein surface. Only an edge of pyrrole ring IV is accessible to the external milieu (8).

CCP catalyses the heterolysis of hydrogen peroxide using ferrocytochrome c [C(FeII)] as an electron source (20). The scheme for the catalytic reaction is as follows (11):

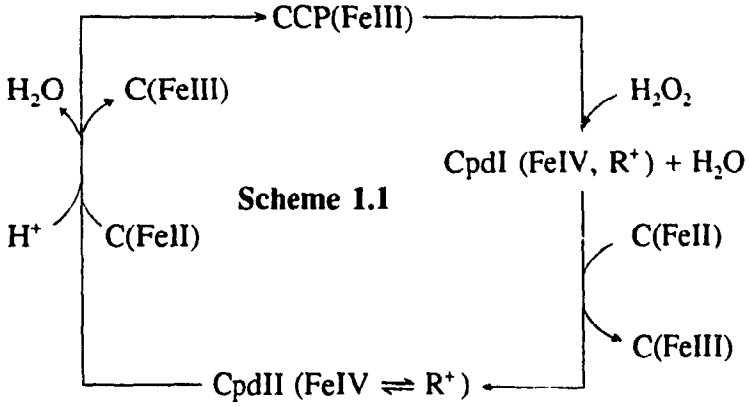

Scheme 1.1

The cleavage of the peroxy O-O bond results in the removal of two electrons from native CCP(FeIII) to produce compound I (CpdI) in which the ferric heme is oxidized to the ferryl (FeIV) state, and an amino acid residue is reversibly oxidized (R^+). A single electron is transferred from C(FeII) to CpdI forming CpdII, which at neutral pH, is an equilibrium mixture of FeIV and R^+ (11). Native CCP(FeIII) is regenerated following the reduction of CpdII by another molecule of C(FeII).

1.4 Overview of Thesis:

In Chapter 2, a comparative study on the emission lifetime quenching by C of a series of ruthenium polypyridyl complexes with ligands of different sizes and hydrophobicities is reported. The aim of these studies is to probe the reactivity of C(FeII) and C(FeIII) using small inorganic complexes and to examine the photochemical

processes involved in the quenching of Ru^*L_3 by C. The ionic interactions between C and Ru^*L_3 complexes are examined by comparing the quenching rate constants obtained at high (μ = 0.1 M) and low (μ = 0.01 M) ionic strengths. The observed rates are compared to the calculated diffusion-controlled rates, and the correlation between the observed rate constants and the degree of heme exposure is discussed.

Saturation kinetics are reported here for the quenching of $Ru(DIPS)_3^{4-}$ [DIPS = 4,7-di(phenyl-4'-sulfonate)-1,10-phenanthroline] by C(FeIII). This is the first time that saturation kinetics have been clearly observed for the reaction of C with a nonphysiological reagent. This raises the possibility that electron transfer may occur via an intramolecular pathway within a precursor complex formed between the protein and the inorganic reagent. However, emission lifetime quenching can also occur by other competing processes such as energy transfer (25). Therefore, it is necessary to determine if electron transfer is indeed involved in the quenching process, and to address this question, steady-state quantum yield measurements on the Ru^*L_3-photosensitized reduction of C were carried out. The combined data from emission lifetime quenching and quantum yield measurements are used to rationalize the photochemical processes. These experimental results are also given in Chapter 2.

The oxidation of CCP(FeII) to its resting state (FeIII) involves the transfer of one electron, thus, providing a relatively simple reaction that can be used to characterize the redox reactivity of CCP. Kinetic studies on the bimolecular reactions between CCP(FeII) and $Fe(CN)_6^{3-}$ are reported in Chapter 3. Using $Fe(CN)_6^{3-}$ as an oxidant, a comparison of the redox reactivity of CCP and other heme proteins, such as C (28) and myoglobin (29)

that also undergo one-electron transfer reactions is possible. This allows the rationalization of heme reactivity based on the known structures and biological functions of these proteins.

Little is known about the control of electron transfer between two biological molecules. Unlike the redox reactions of small inorganic complexes, where the two reactants can approach each other to within their van der Waals radii, the redox-active metal centers in proteins are usually separated by 10-20 Å by the protein matrix. In spite of the fact that semiartifical electron donor-acceptor metalloproteins are powerful tools in the study of long-range electron transfer, these systems do not permit us to examine the control of electron transfer kinetics by protein-protein complex formation. In Chapter 4, the results of investigations on electron transfer between CCP(FeII) and C(FeIII) are given. The reaction between C(FeIII) and CCP(FeII) serves as a model for the study of long-range electron transfer between two biological partners. The data included in Chapter 4 are: rates of oxidation of CCP(FeII) by C(FeIII), studies on the sequence-dependence of the reaction rates using C's from different organisms, the temperature-dependence of the rates and steady-state fluorescence intensity quenching and polarization measurements of the equilibrium binding of horse porphyrin C and CCP.

1.5 **References**:

1 Giese, A.C., "Cell Physiology", Fifth edition, 1979, W.B. Saunders Co., Philadelphia.

2 Stryer, L., "Biochemistry", Second edition, 1981, W.H.Freeman & Co., San Francisco.

3 Lever, A.B.P., Coord. Chem. Review , 1985, Vol. 64, Elsevier Science Publishers B.V., Amsterdam.

4 Dickerson, R.E., Timkovich, R., "The Enzymes", 1975, Vol XI, part A, p.397, P.D. Boyer ed., Academic Press, New York.

5 Dickerson, R.E., Scientific American, 1980, 242, 136.

6 Takio, K., Titani, K., Eriksson, L.H., and Yonetani, T., Arch. Biochem. Biophys., 1980, 203, 615.

7 Swanson, F., Trus, B.L., Mandel, N., Mandel, G., Kallai, O.B., Dickerson, R.E., J. Biol. Chem., 1977, 252, 759.

8 Poulos, T.L., Freer, S.T., Alden, R.A., Edwards, S.L., Skoglund, U., Takio, K., Erikson, B., Xuong, N.H., Yonetani, T., Kraut, J., J. Biol. Chem., 1980, 255, 575.

9 Finzel, B.C., Poulos, T.L., Kraut, J., J. Biol. Chem., 1984, 259, 13027.

10 Poulos, T.L., Kraut, J., J. Biol. Chem., 1980, 255, 10322.

11 Poulos, T.L., Finzel, B.C., Protein Peptide Rev., 1984, 4, 115.

12 Bechtold, R., Bosshard, H.R., J. Biol. Chem., 1985, 260, 5191.

13 Waldmeyer, B., Bosshard, H.R., J. Biol. Chem., 1985, 260, 5184.

14 Waldmeyer, B., Bechtold, R., Bosshard, H.R., Poulos, T.L., J. Biol. Chem., 1982, 257, 6073.

15 Leonard, J.J., Yonetani, T., Biochemistry, 1974, 13, 1465.

16 Kornblatt, J.A., English, A.M., Eur. J. Biochem., 1986, 155, 505.

17 Erman, J.E., Vitello, L.B., J. Biol. Chem., 1984, 255, 6224.

18 Orii, Y., J. Biol. Chem., 1982, 257, 9246.

19 Bosshard, H.R., Zurrer, M., J. Biol. Chem., 1980, 255, 6694.

20 Yonetani, T, Ray, G.S., J. Biol. Chem., 1965, 240, 4503.

21 Hashimoto, S., Tereoka, J., Inubushi, T., Yonetani, T., Kilagawa, T., J. Biol. Chem. 1986, 261, 11110.

22 Meyer, T.E., Przysiecki, C.T., Watkins, J.A., Bhattacharyya, A., Simondsen, R.P., Cusanovich, M.A., Tollin, G., Proc. Natl. Acad. Sci. USA, 1983, 80, 6740.

23 Cho, K.C., Che, C.M., Cheng, F.C., Choy, C.L., J. Am. Chem. Soc., 1984, 106, 6844.

24 English, A.M., Lum, V.R., Delaive, P.J., Gray, H.B., J. Am. Chem. Soc., 1982, 104, 870.

25 Scandola, F., Balzani, V., J. Biol. Ed., 1983, 60, 814.

26 Hazzard, J.T., Poulos, T.L., Tollin, G., Biochemistry, 1987, 26, 2836.

27 Hazzard, J.T., McLendon, G., Cusanovich, M.A., Das, G.m Sherman, F. and Tollin, G., Biochem. 1988, 27, 4445.

28 Wherland, S., Gray, H.B., "Biological Aspects of Inorganic Chemistry", Addison, A.W., Cullen,W., James, B.R., Dollphin, D., Eds., Wiley, New York, 1977, p.289.

29 Wherland, S., Gray, H.B., Proc. Natl. Acad. Sci. USA, 1978, 73, 2950.

30a Nocera, D.G., Winkler, J.R., Yocom. K.M., Bordignon, E., Gray, H.B., J. Am. Chem. Soc., 1982, 104, 5145.

30b Nocera, D.G., Winkler, J.R., Yocom. K.M., Bordignon, E., Gray, H.B., J. Am. Chem. Soc., 1984, 106, 5145

31 McGourty, J.L., Blough, N.V., Hoffman, B.M., J. Am. Chem. Soc., 1983, 105, 4470.

32 Peterson-Kennedy, S.E., McGourty, J.L., Hoffman, B.M., J. Am. Chem. Soc., 1984, 106, 5010.

33 McLendon, G.L., Miller, J.R., J. Am. Chem. Soc., 1985, 107, 7811.

34 Simolo, K.P., McLendon, G.L., Mauk, M.R., Mauk, A.G., J. Am. Chem. Soc., 1984, 106, 5012.

35 Ho, P.S., Sutoris, C., Liang, N., Margoliash, E., Hoffman, B.M., J. Am. Chem. Soc., 1985, 107, 1070.

36 Van Wart, H.E. and Zimmer, J., J. Biol. Chem., 1985, 260, 8372.

37 Wittenberg, J.B., Noble R.W., Wittenberg, B.A., Antioini, E., Brunori, M. and Wyman, J., J. Biol. Chem., 1967, 242, 626.

38 Vitello, L.B. and Erman, J.E., Arch. Biochem. Biophys., 1987, 258, 621.

39 Margoliash, E. Biochem. J. 1954, 56, 535.

40 Fishel, L.A., Villafranca, J.E., Mauro, J.M., and Kraut, J., Biochem., 1987, 26, 351.

41a Smulevich, G., Mauro, J.M., Fishel, L.A., English, A.M., Kraut, J., and Spiro, T.G., Biochem., 1988, 27, 5477.

41b Smulevich, G., Mauro, J.M., Fishel, L.A., English, A.M., Kraut, J., and Spiro, T.G., Biochem., 1988, 27, 5486.

42 Mayo, S.L., Ellis, W.R., Crutchley, R.J., and Gray, H.B., Science, 1986, 233, 948.

43 Axup, A.W., Albin, M., Mayo, S.L., Crutchley, R.J. and Gray, H.B. J. Am. Chem. Soc., 1988, 110, 435.

44 Isied, S.S., Worosila, G., Atherton, S. J. Am. Chem. Soc., 1982, 104, 7659

45 Miller, J.R. and Beitz, J.V., "Tunnelling in Biological Systems", Academic Press, New York, 1979, p.269.

46 Sutin, N. and Creulz, C., J. Chem. Ed., 1983, 60, 809.

47 Marcus, R.A. and Sutin, N., Bioch. Biophys. Acta., 1985, 811, 263.

48 Tollin, G., Cheddar, G., Watkins, J.A., Meyer, T.E. and Cusanovich, M.A., Biochem., 1984, 23, 6345.

49 Goldkorn, T. and Schejter, A., J. Boil. Chem., 1979, 254, 12562.

50 Liang, N., Mauk, G., Pielak, G.J., Johnson, J.A., Smith, M. and Hoffman, B.M., Science, 1988, 240, 311.

51 English, A.M., Laberge, M., Walsh, M., Inorg. Chim. Acta. 1986, 123, 113.

52 Yonetani, T., Chance, B., and Kajiwara, S., J. Biol. Chem. 1966, 41, 2981.

53 Isied, S.S., Kuehn, C., Worosila, G., J. Am. Chem. Soc. 1984, 106, 1722.

54 Jackman, M.P., McGinnis, J., Powls, R., Salmonm G.A., Sykes, A.G., J. Am. Chem. Soc. 1988, 110, 5880.

55 Osvath, P., Salmon, A., Sykes, A.G., J. Am. Chem. Soc. 1988, 110, 7114.

56 Mauk, A.G., Scott, R.A., and Gray, H.B., J. Am. Chem. Soc. 1980, 102, 4360.

57 Mauk, A.G. and Gray, H.B., Biochem. Biophys. Res. Com. 1979, 86, 206.

58 Mauro. J.M., Fishel, L.A., Hazzard, J.T., Meyer, T.E., Tollin, G., Cusanovich, M.A. and Kraut, J., Biochem. 1988, 27, 6243.

59 Fox, T., Hazzard, J.T., Edwards, S.L., English, A.M., Poulos, T.L. and Tollin, G., J. Am. Chem. Soc. 1990, 112, 7426.

Chapter 2

QUENCHING OF THE ELECTRONIC EXCITED STATES OF RUTHENIUM POLYPYRIDINE COMPLEXES BY CYTOCHROME C

2.1 Introduction:

The quenching of the luminescent excited state of ruthenium polypyridyl complexes (Ru^*L_3) by metalloproteins is used extensively to probe the kinetics and mechanisms of electron transfer reactions (1-6). The observed rates are dependent on the properties of the ruthenium complex and the protein under study. The surface of cytochrome c (C) possesses both hydrophobic and hydrophilic amino acid residues; thus, electrostatic and hydrophobic interactions between RuL_3 and C are probed in a comparative study on the emission lifetime quenching of a series of Ru^*L_3 of various charges and ligand hydrophobicities by C(FeIII).

It is also of interest to examine the reactivity of C in its oxidized and reduced states. A number of independent studies indicate that certain properties of C may be significantly different in its FeIII and FeII forms. Brosshard et al. (7) demonstrated that some surface lysine residues of C(FeII) are protected from modification but are accessible in the ferric state. From differential scanning calorimetry (8), C(FeII) was found to be more resistant towards thermal denaturation; and both the solution structure (29) and the crystal structure (9) of C reveal subtle but significant structural differences between the oxidized and

reduced states. Therefore, the quenching of Ru^*L_3 by C(FeIII) and C(FeII) was investigated to determine if the structural differences between the two oxidation states result in a change in their quenching efficiencies.

The control of reactivity by structural factors can also be probed using low pH forms of C. Studies (10-13) have shown that C(FeIII) undergoes a heme crevice opening in acidic (pH $\leq$ 4) medium. Such structural change is expected to increase the heme exposure and thereby, increase the reactivity of C towards external redox reagents (10-12). If C(FeII) is structurally more compact and rigid (14) and less sensitive to pH changes, then the lowering of pH should have a more profound effect on the reactivity of C(FeIII) than on C(FeII). Thus, the reactivities of C(FeIII) and C(FeII) with $Ru^*(bpy)_3^{2+}$ are compared at pH 7.0, 4.0 and 3.0 .

The ability of the excited states of ruthenium complexes to participate in both oxidation and reduction processes provide us with a tool for the study of redox reactions. However, the interpretation of the emission quenching data is often complicated by the fact that deactivation of excited states may occur via both electron transfer and energy transfer mechanisms. Therefore, quenching by C(FeIII) is also examined by steady-state photolysis, and the results are combined with emission life-time quenching data to determine quantum yields for C(FeII) production.

2.2 Theoretical Considerations:

Depending on the system under study, the quenching of Ru^*L_3 by a quencher, Q, may either be oxidative (eq.2.1) or reductive (eq.2.2); moreover, energy transfer may also

provide a decay pathway for excited Ru^*L_3 (eq.2.3).

$$Ru^*L_3^{2+} + Q \longrightarrow RuL_3^{3+} + Q^- \qquad \text{(eq.2.1)}$$

$$Ru^*L_3^{2+} + Q \longrightarrow Ru^+L_3^{1+} + Q^+ \qquad \text{(eq.2.2)}$$

$$Ru^*L_3^{2+} + Q \longrightarrow RuL_3^{2+} + Q^* \qquad \text{(eq.2.3)}$$

If Ru^*L_3 is oxidatively quenched by Q, the processes involved are the following:

$$RuL_3^{2+} \xrightarrow{h\nu} Ru^*L_3^{2+} \qquad \text{(eq.2.4)}$$

$$Ru^*L_3^{2+} \xrightarrow{k_o} RuL_3^{2+} + h\nu \qquad \text{(eq.2.5)}$$

$$Ru^*L_3^{2+} + Q \xrightarrow{k_q} RuL_3^{3+} + Q^- \qquad \text{(eq.2.6)}$$

$$RuL_3^{3+} + Q^- \xrightarrow{k_b} RuL_3^{2+} + Q \qquad \text{(eq.2.7)}$$

where k_o is the natural decay rate constant, k_q is the bimolecular quenching rate constant, and k_b is the thermal back electron transfer rate constant. After photoexcitation (eq.2.4), $Ru^*L_3^{2+}$ returns to the ground state by a radiative pathway (eq.2.5), where $1/k_o$ is the natural decay lifetime (τ_o), or in the presence of an electron acceptor, Q, $Ru^*L_3^{2+}$ is oxidatively quenched (eq.2.6). Because of thermal back electron transfer between RuL_3^{3+} and Q^- (eq.2.7), there is no net accumulation of electron transfer products. Back electron transfer can be prevented by the addition of an electron donor such as ethylenediaminetetraacetic acid (EDTA). RuL_3^{3+} is efficiently reduced by EDTA (27) but not Ru^*L_3 (31)

and ground state RuL_3^{2+} is regenerated (eq.2.8), "trapping" the reduced quencher, Q^-. In the process, EDTA is converted to an organic cation radical ($EDTA^+$) which is irreversibly oxidized by Q (eq.2.9) to give carbon dioxide, formaldehyde, ethylenediaminetriacetic acid ($EDTA_{ox}$) and Q^- (5):

$$RuL_3^{3+} + EDTA \xrightarrow{k_r} RuL_3^{2+} + EDTA^+ \qquad \text{(eq.2.8)}$$

$$EDTA^+ + Q \longrightarrow Q^- + EDTA_{ox} + CO_2 + CH_2O \qquad \text{(eq.2.9)}$$

where k_r is the rate constant for the reduction of $Ru^*L_3^{3+}$ by EDTA.

For a bimolecular reaction in solution, the quenching reaction (eq.2.6) can be divided into a number of steps: generation of the redox products within a solvent cage (eq.2.10), release of the redox products from the solvent cage by diffusion (eq.2.11), and geminate pair back electron transfer (eq.2.12).

$$Ru^*L_3^{2+} + Q \xrightarrow{k_q} [RuL_3^{3+}:Q^-] \qquad \text{(eq.2.10)}$$

$$[RuL_3^{3+}:Q^-] \xrightarrow{k_{cr}} RuL_3^{3+} + Q^- \qquad \text{(eq.2.11)}$$

$$[RuL_3^{3+}:Q^-] \xrightarrow{k_g} RuL_3^{2+} + Q \qquad \text{(eq.2.12)}$$

where k_{cr} is the cage release rate constant, and k_g is the geminate pair recombination rate constant.

Steady-state treatment of the rate equations gives a final expression for the quantum yield, Φ, for Q^- production (28):

$$\Phi = 2\eta^*\eta_{el}\eta_r\eta_{cr} \qquad \text{(eq.2.13)}$$

where $\eta^* = 1$ (19,30)

$$\eta_{el} = k_{el}[Q]/\{k_o + k_q[Q]\}$$

$$\eta_r = k_r[EDTA]/\{k_b[Q^-] + k_r[EDTA]\}$$

$$\eta_{cr} = k_{cr}/(k_{cr} + k_g)$$

η^* is the efficiency of $Ru^*L_3^{2+}$ formation on photoexcitation, η_{el} is the efficiency of the bimolecular electron transfer step, η_r is the efficiency of RuL_3^{3+} reduction by EDTA, and η_{cr} is the cage-release efficiency of the redox products from the solvent cage. For every equivalent of C(FeII) generated by the quenching of Ru^*L_3, a second equivalent of C(FeIII) is reduced by $EDTA^+$, thus a multiplication factor of 2 is included in the expression for Φ. If $k_r[EDTA] >> k_b[Q^-]$, η_r approaches unity, a condition readily achieved by using high EDTA concentrations (10 mM) (32). Hence $\Phi/[Q]$ vs. Φ is given by:

$$\frac{\Phi}{[Q]} = 2\eta_{cr}\frac{k_{el}}{k_o} - \frac{k_q\Phi}{k_o} \qquad \text{(eq.2.14)}$$

At high quencher concentration ($\Phi/[Q] \rightarrow 0$), the maximum quantum yield, Φ_{max}, can

be determined from the x-intercept ($2\eta_{cr}(k_e/k_o)$) in the plot of $\Phi/[Q]$ vs. Φ (eq.2.14). Thus, from the steady-state quantum yield data, it is possible to determine the Φ_{max} for photoreduction, and the ratio k_q/k_o. If energy transfer (eq.2.3) is a competing quenching process, then $k_q = k_{en} + k_{el}$, where k_{en} and k_{el} are the rate constants for energy and electron transfer, respectively. The comparison of k_q/k_o values obtained from steady-state quantum yield vs. emission lifetime quenching experiments would also indicate if the two rate constants obtained from the two approaches are in agreement.

2.3 **Experimental**:

2.3.1 Materials:

Potassium ferrioxalate was purchased from Pfaltz and Bauer Chemical Company. Tris(1,10-phenanthroline)ruthenium(II) chloride [$Ru(phen)_3^{2+}$] and hydrated ruthenium trichloride ($RuCl_3.3H_2O$) were purchased from Alfa. Tris(2,2'-bipyridine)ruthenium(II) chloride.$6H_2O$ [$Ru(bpy)_3^{2+}$]; 4,7-diphenyl-1,10-phenanthroline.H_2O (DIP); 4,7-diphenyl-1,10-phenanthroline disulfonic acid disodium salt (DIPS); 1,10-phenanthroline (phen) and 2,2'-bipyridine (bpy) are products of GFS Chemicals. $Ru(phen)_2(CN)_2$, $Ru(bpy)_2(CN)_2$, $Ru(DIP)_3^{2+}$ and $Ru(DIPS)_3^{4-}$ were previously prepared in this laboratory using literature procedures (15). Horse heart cytochrome c (type VI) from Sigma was used as received. Sodium phosphate (Pi) and potassium biphthalate (KPH) buffers were used at neutral and acidic pH's, respectively. The anaerobic sample cells used in emission lifetime measurements were constructed from 3 mm square glass tubing (Richland Glass Co., New Jersey) with a 7-mm OD neck. A sealed Ace-Thread connector with an O-ring (7 mm; Ace Glass Inc., New Jersey) was used to form a greaseless, air-tight seal with the neck

of each cell (Figure 2.1).

2.3.2 Protein sample preparation:

A stock solution of 20 μM RuL_3 in buffer was divided into two aliquots and C(FeIII) was added to one to give ≈1 mM protein concentration. Oxygen was removed by passing purified argon gas through the solutions for 1 hr. In a glove box under a nitrogen atmosphere, 20 μM RuL_3 solutions with different protein concentrations were prepared by mixing suitable aliquots of the two stock solutions to give a final sample volume of 100 μl.

Protein samples for the quenching of Ru^*L_3 by C(FeII) were prepared following the same procedure except that C(FeIII) was reduced with sodium dithionite. Excess dithionite was removed by dialysing 2 ml of the stock solution against 2 l of buffer under a nitrogen atmosphere for at least 4 hr before use.

2.3.3 Emission lifetime measurements:

The emission lifetimes of the Ru^*L_3 complexes were measured by monitoring the decay of the emission intensity at 610 nm. A degassed sample of RuL_3 was excited at 337 nm by a 300-ps 60-μJ pulse from a nitrogen laser (PRA Nitromite LN-100) and the emission intensity was detected at right angles by a photomultiplier (EMI model 978513). Since the discharge time of the detection system is determined by the product of the resistance and capacitance (R.C. constant), a variable resistor was used to optimize the

Figure 2.1

Diagram of the sample cell used in emission lifetime measurements.

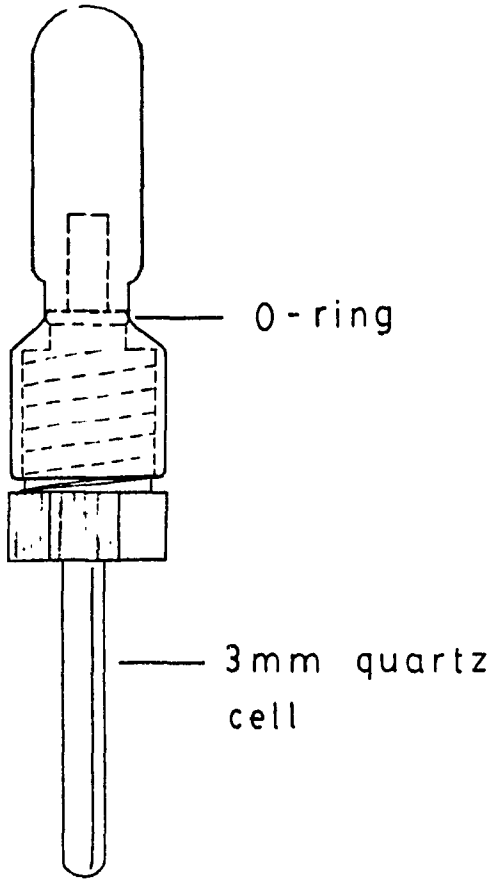

signal (in volts) and control the R.C. constant of the detection system. Signals were displayed and photographed on a Tektronix 7633 oscilloscope equipped with a Tektronix 7B80 time base and a 7A15 amplifier. A block diagram of the instrumental set up is presented in Figure 2.2. The emission intensity at time t, I(t), was read from the voltage scale on the photograph. The emission lifetime was obtained from the slope of the semi-log plot of I(t) vs. time, and the bimolecular quenching rate constant (k_q) was determined from the slope of the Stern-Volmer (eq.2.15) plot of $1/\tau$ vs. [Q] (16).

$$1/\tau = 1/\tau_o + k_q[Q] \qquad \text{(eq.2.15)}$$

2.3.4 Actinometry for continuous photolysis:

The excitation light source was a 100 W high-pressure Hg arc lamp (Osram) installed in a lamp housing connected to a d.c. power supply (Ealing). The collimated light beam was passed through a double-grating monochromator (Bausch and Lomb) and the excitation wavelength was 436 ± 2 nm since this is the most intense mercury line in the visible region. The intensity of the incident beam was determined by ferrioxalate actinometry following the procedures of Park and Hatchard (17). A 6.0 mM actinometric solution was prepared by dissolving 3.0 g of potassium ferrioxalate ($K_3[Fe(C_2O_4)_3]\,3H_2O$, FW = 491.25) crystals in 1.0 l of 0.1 N H_2SO_4. The solution was stored in a brown bottle in the dark to avoid photodecomposition. Irradiation of a ferrioxalate solution causes reduction of Fe(III) and oxidation of oxalate:

Figure 2.2

Diagram of the instrumental setup for emission lifetime measurements. Abbreviation used: F = 500-nm cut-off filter, L = focusing lenses (focal length = 5.0 cm), M = monochromator, PMT = photomultiplier tube, R = variable resistor.

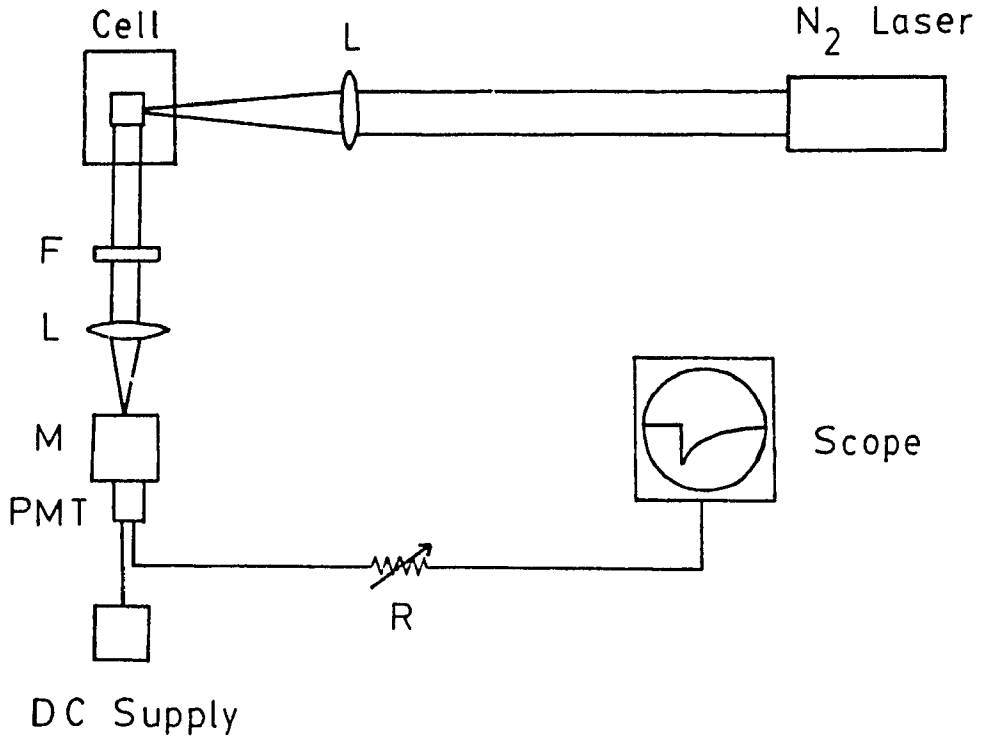

$$Fe(III)(C_2O_4)_3^{3-} \xrightarrow{h\nu} Fe(II) + C_2O_4^{\cdot-} + 2\ C_2O_4^{2-} \qquad \text{(eq.2.16)}$$

$$Fe(III)(C_2O_4)_3^{3-} + C_2O_4^{\cdot-} \longrightarrow Fe(II) + 3\ C_2O_4^{2-} + 2\ CO_2 \qquad \text{(eq.2.17)}$$

The free ferrous ion is subsequently complexed with 1,10-phenanthroline (phen) and the concentration of $Fe(phen)_3^{2+}$ is determined spectrophotometrically. To determine the incident light intensity (I_o) on a photoreaction cell upon irradiation at 436 nm, a 3.0 ml solution of 6.0 mM ferrioxalate was added to a 1-cm quartz cell and irradiated for the desired length of time. During irradiation, the solution was continuously stirred by a micro-magnetic stirrer. The irradiated solution (2.0 ml) was added to a 25-ml volumetric flask containing 2.0 ml of 1.0 mM phen solution. The solution was diluted to 25 ml with water and allowed to stand in dark for 30 min. A blank solution was prepared simultaneously in a similar manner using 2.0 ml of non-irradiated ferrioxalate solution. The absorbance of the phen solutions containing irradiated and non-irradiated ferrioxalate were recorded at 510 nm. The procedure was repeated for various irradiation times (t). The amount of ferrous ions formed during photolysis, φ (mol s^{-1}) was calculated using eq.2.18, where 0.0375 is the dilution factor ($3/2 \times 25\times10^{-3}$) for the ferrioxalate solution, d (cm) is the pathlength of the reaction cell, and ε (= 1.11×10^4 $M^{-1}cm^{-1}$) is the molar extinction coefficient of $Fe(phen)_3^{2+}$ at 510 nm.

$$\varphi = \frac{0.0375\ \Delta A_{510}}{d\ \varepsilon\ \Delta t}\ (\text{mole s}^{-1}) \qquad \text{(eq.2.18)}$$

The absorbance (A) of 6.0 mM ferrioxalate at 436 nm is 0.279. From Beer's law ($I_a/I_o = 1 - 10^{-A}$), the ratio of I_o to the absorbed light intensity (I_a) is 2.11. Thus, I_o, was calculated from eq.2.19 using the reported quantum yield for Fe(II) production at 436 nm [Φ = 1.1 (17)] and the irradiation time (t). I_o used in these experiments ranged between $1x10^{-9}$ to $3x10^{-9}$ einstein s^{-1}.

$$I_o = 2.11\ \varphi/\Phi t \quad \text{(einstein } s^{-1}\text{)} \qquad \text{(eq.2.19)}$$

2.3.5 Steady-state quantum yield measurements:

The $Ru^{*}L_3$ photosensitized reduction of C(FeIII) was carried out in 3.0 ml of phosphate buffer, pH 7.0, containing 10 mM Na_2EDTA, 60-100 µM RuL_3, and 3-170 µM C(FeIII). Due to the absorption of C (ε_{436} = 21.5 $mM^{-1}cm^{-1}$), the maximum C concentration used was limited to 170 µM. The samples were deoxygenated prior to use, the rate of photoreduction of C (mole s^{-1}) was determined by measuring the absorbance change at 550 nm as a function of time ($\Delta A_{550}/\Delta t$), and dividing this by the difference molar extinction coefficient of C, $\Delta\varepsilon$ ($=\varepsilon_{red} - \varepsilon_{ox}$ = 18.5 $mM^{-1}cm^{-1}$). The quantum yield was determined by dividing the rate of C reduction by the intensity of the light absorbed by RuL_3 (I_a) only (eq.2.20).

$$\Phi_{obs} = \frac{3.0x10^{-3}\Delta A_{550}}{I_a \Delta\varepsilon \Delta t} \qquad \text{(eq.2.20)}$$

I_a is given by $I_o[1-10^{-A(T)}]A(RuL_3)/A(T)$, where I_o is the intensity of the incident light, and

$A(RuL_3)$ and A(T) are the absorbance of RuL_3 and the total absorbance (RuL_3 + C) at 436 nm, respectively.

2.4 **Results**:

2.4.1 Natural decay lifetimes:

The excitation and emission spectra of $Ru(bpy)_3^{2+}$ are presented in Figure 2.3. The decay in emission intensity at 610 nm vs. time and a semi-log plot of the decay curve are presented in Figure 2.4. The observed τ_o (620 ± 20 ns) is in good agreement with literature values (18,19). The semi-log plots of all Ru^*L_3 emission decays are linear with correlation coefficients ≥ 0.998. The measured τ_o's for all the Ru^*L_3 complexes along with their reduction potentials are presented in Table 2.1.

2.4.2 Quenching by ferricytochrome c at pH 7.0:

The bimolecular quenching rate constants for the quenching of Ru^*L_3 by C(FeIII) at μ = 0.1 and 0.01 M are presented in Table 2.2. The quenching of $Ru^*(bpy)_3^{2+}$ and $Ru^*(DIPS)_3^{4-}$ by C(FeIII) has been studied previously (3) and the reported quenching rate constants ($2x10^8$ and $1.2x10^9$ $M^{-1}s^{-1}$, respectively) are lower than the present values (k_q = $8.6x10^8$ and $1.9x10^9$ $M^{-1}s^{-1}$ for $Ru(bpy)_3^{2+}$ and $Ru(DIPS)_3^{4}$, respectively). This discrepancy may be due to the difference in the excitation wavelengths used, 532 nm vs. 337 nm in the present work. Photoreduction of C(FeIII) on UV-irradiation was observed in the absence of any photosensitizer (33). The photochemical process involves electron transfer to the Fe(III) atom from the sulfur atom of Met-80 which is coordinated to the

Figure 2.3

The excitation and emission spectra of $Ru(bpy)_3^{2+}$ in phosphate buffer at pH 7.0, μ = 0.1 M and 24 °C.

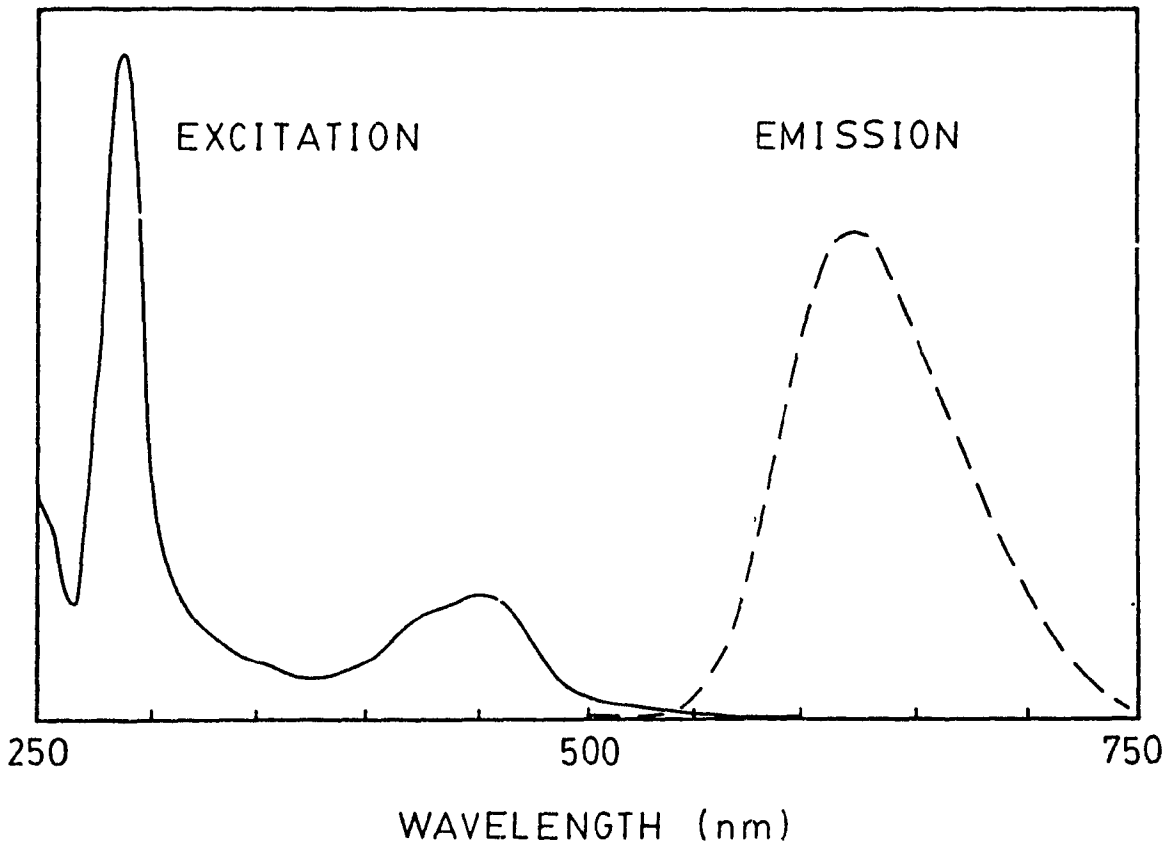

Figure 2.4

The natural decay profile of $Ru^{*}(bpy)_3^{2+}$ emission intensity at 610 nm (I) in deoxygenated phosphate buffer at pH 7.0, μ = 0.1 M and 24°C. Excitation wavelength = 337 nm and emission wavelength = 610 nm. Inset: Plot of ln I vs. time.

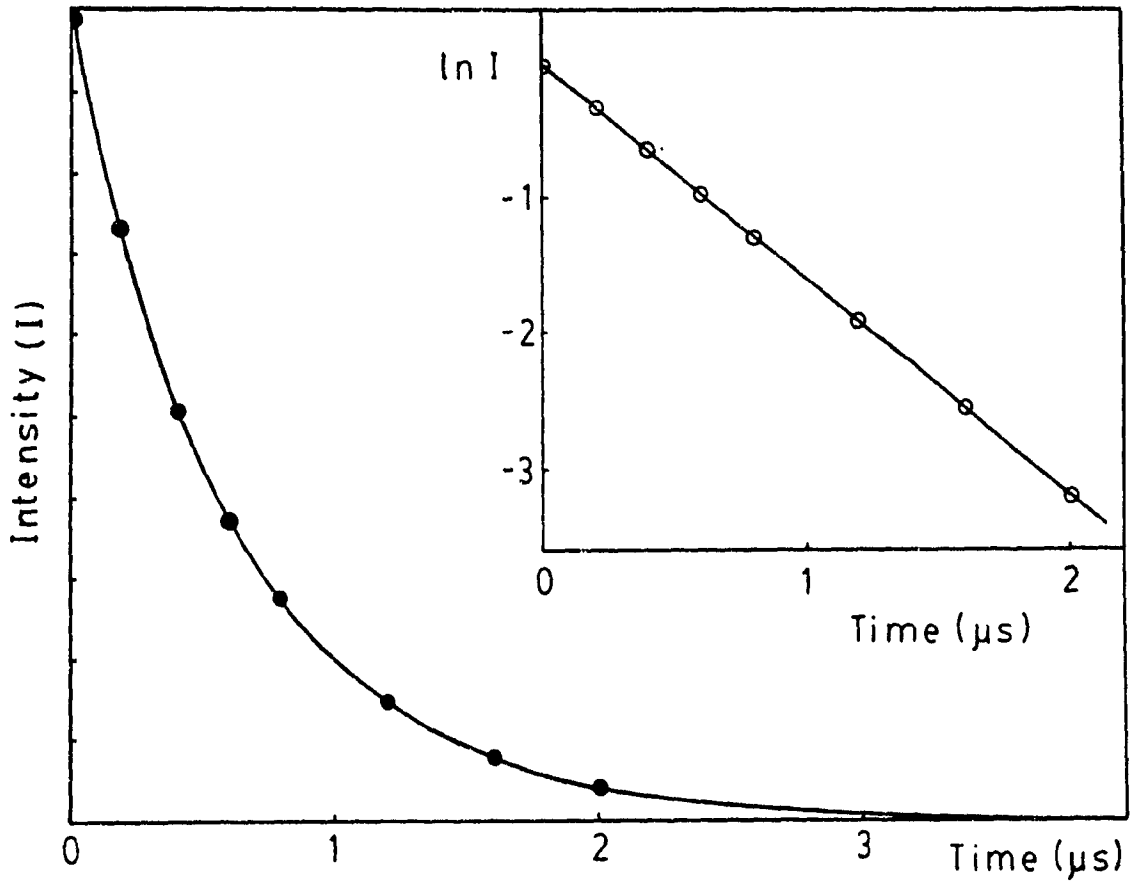

Table 2.1 Observed Emission Lifetimes (τ_o) and Standard Reduction Potentials of The Excited State of Ruthenium Polypyridine Complexes

Complex[a]	τ_o[b] (μs)	E°(V)[d] $Ru^{2+/+}$	E°(V)[d] $Ru^{3+/2+}$
$Ru(bpy)_3^{2+}$	0.62 (0.02)[c]	0.83	-0.84
$Ru(bpy)_2(CN)_2$	0.27 (0.05)	0.60	-0.87
$Ru(phen)_3^{2+}$	0.98 (0.02)	0.81	-0.87
$Ru(phen)_2(CN)_2$	0.70 (0.03)	--	--
$Ru(DIP)_3^{2+}$	3.4 (0.1)	0.85	-0.90
$Ru(DIPS)_3^{4-}$	3.8 (0.1)	0.85	-0.90

[a]bpy = 2,2'-bipyridine; phen = 1,10-phenanthroline; DIP = 4,7-diphenyl-1,10-phenanthroline; DIPS = 4,7-(diphenyl-4'-disulfonate)-1,10-phenanthroline.

[b]Measured emission lifetime using excitation and emission wavelengths at 337 and 610 nm, respectively. Experimental conditions: deoxygenated phosphate buffer, μ = 0.1 M, pH 7.0, 24°C,

[c]Standard error in parentheses.

[d]Reduction potentials (vs. NHE) from Refs. 3, 18 and 19.

heme. The higher quenching rate constants observed in the present work may be caused by similar photochemical effects induced by excitation at 337 nm.

Within experimental error (± 10%), the k_q's for the positively charged complexes such as $Ru(bpy)_3^{2+}$ and $Ru(phen)_3^{2+}$ are independent of ionic strength (μ = 0.1 and 0.01 M). The same is observed for the quenching of the uncharged $Ru(phen)_2(CN)_2$ complex. The k_q's for $Ru(bpy)_2(CN)_2$ are less reliable due to the short emission lifetime and poor aqueous solubility of this complex at low ionic strength. The lack of ionic strength dependence of these reactions suggests that the charge on the Ru metal center is insulated by the polypyridyl ligand. The emission intensity of $Ru(DIP)_3^{2+}$ is strongly quenched by C(FeIII). However, no change in the emission lifetime was observed even at the emission detection limit. This is a strong indication that the quenching mechanism in this instance is not a dynamic bimolecular process but a static one; thus, binding between C and ground state $Ru(DIP)_3^{2+}$ is expected.

Electrostatic effects are clearly apparent in the quenching of the sulfonated complex which has a highly negatively charged surface. The observed k_q's for $Ru(DIPS)_3^{4-}$ are 1.9×10^9 and 7.5×10^9 $M^{-1}s^{-1}$ at 0.1 and 0.01 M ionic strength, respectively (Table 2.2); this is the trend expected in the quenching of $Ru(DIPS)_3^{4-}$ by a positively charged protein. Furthermore, at 0.01 M ionic strength, the emission lifetime levels-off at ≈0.35 μs, and the on-set of rate saturation is observed at ≈0.3 mM protein (Figure 2.5). By comparison, no rate saturation was observed for $Ru(bpy)_3^{2+}$ (Figure 2.5) or $Ru(phen)_3^{2+}$ (Figure 2.6) up to 1 mM protein.

Table 2.2 Rate Constants for the Quenching of Excited Ruthenium Polypyridine Complexes by Ferricytochrome c [a,e]

Complexes [b]	$k_q x 10^{-8}$ ($M^{-1}s^{-1}$) μ = 0.1 M	$k_q x 10^{-8}$ ($M^{-1}s^{-1}$) μ = 0.01 M
$Ru(bpy)_3^{2+}$	8.6 (0.4)[c]	9.0 (0.5)
$Ru(bpy)_2(CN)_2$	14 (1)	---
$Ru(phen)_3^{2+}$	12.0 (0.4)	14.0 (0.3)
$Ru(phen)_2(CN)_2$	13.0 (0.4)	13.0 (0.5)
$Ru(DIP)_3^{2+}$	[d]	[d]
$Ru(DIPS)_3^{4-}$	19.0 (0.8)	75 (6)

[a]Deoxygenated phosphate buffer, pH 7.0, at 24 ± 1 °C, cytochrome c concentration ranged 0-1.2 mM, 20 µM Ruthenium polypyridine complex, experimental procedure as described in text (Sections 2.3.1 to 2.3.3).

[b]abbreviations as listed in Table 2.1.

[c]Standard deviation of slope of Stern-Volmer plot in parentheses.

[d]Only static quenching of emission observed.

[e]Data used for Stern-Volmer plots are given in Appendix A.

Figure 2.5

Stern-Volmer plots of emission quenching of $Ru^*(bpy)_3^{2+}$ and $Ru^*(DIPS)_3^{4-}$ by ferricytochrome c at pH 7.0 , and 24 °C. The natural emission lifetimes of $Ru(bpy)_3^{2+}$ and $Ru(DIPS)_3^{4-}$ are 0.62 and 3.70 μs, respectively. In order to compare the quenching of the two ruthenium complexes with different τ_o values, emission lifetime data, τ_o/τ, are plotted.

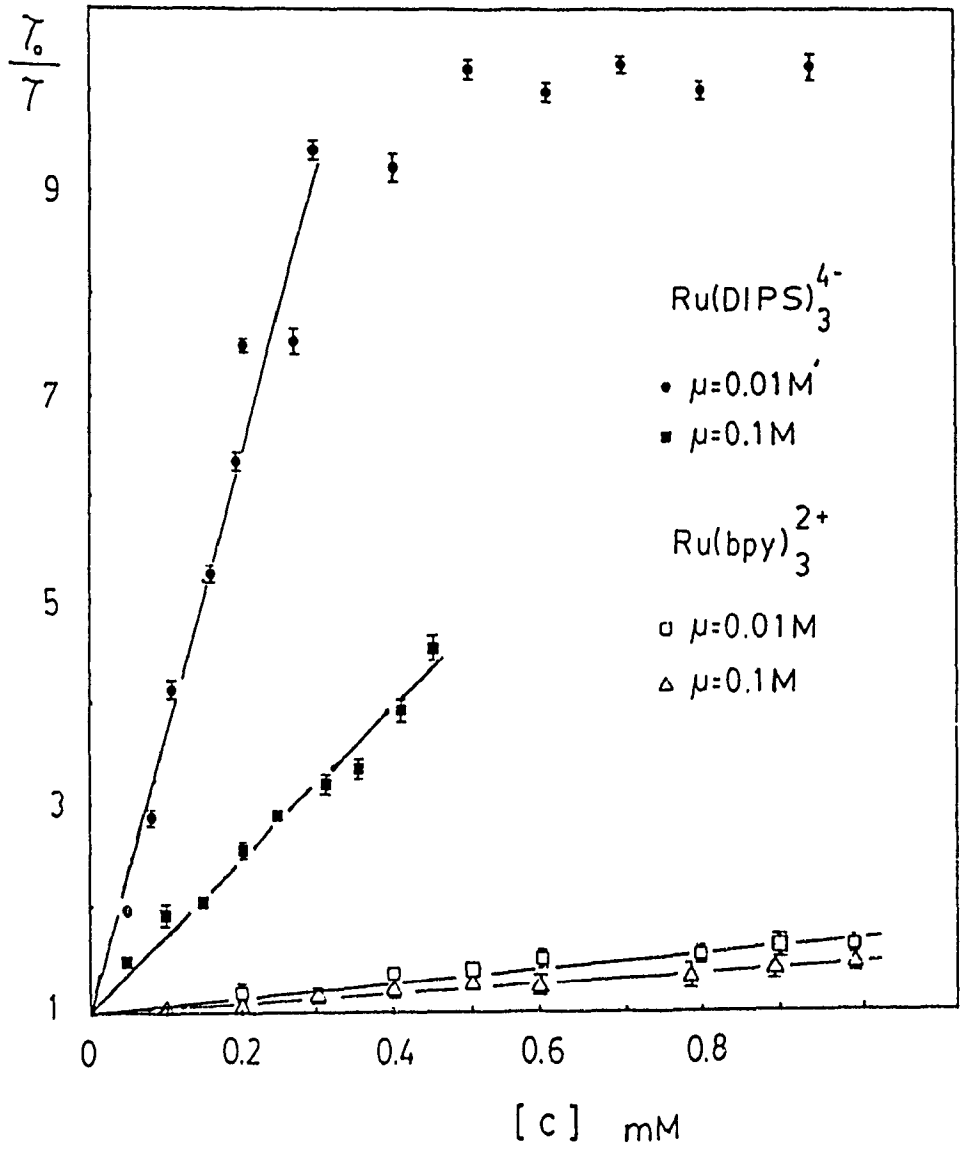

Figure 2.6

Stern-Volmer plots of the emission quenching of $Ru^{*}(phen)_3^{2+}$ by ferro- and ferricytochrome c in phosphate buffer at pH 7.0, and at 24 °C. Circles (○) and (●) denote the quenching by C(FeIII) at μ = 0.1 and 0.01 M, respectively; triangles (△) and (▲) denote the quenching by C(FeII) at μ = 0.01 and 0.1 M, respectively.

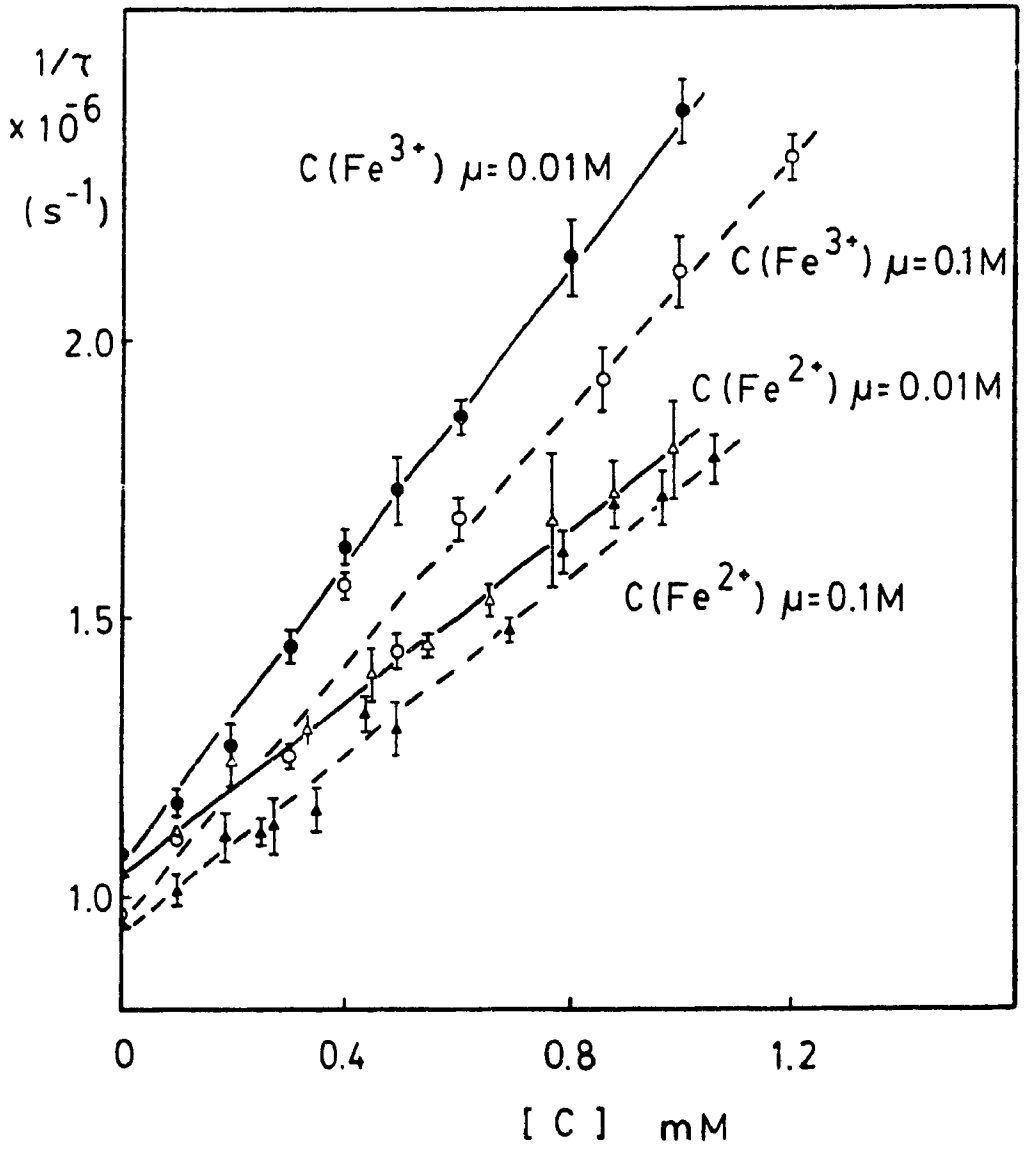

2.4.3 Quenching by ferrocytochrome c:

The quenching rate constants by C(FeII) at μ = 0.01 and 0.1 M Pi are presented in Table 2.3. The general trends observed in quenching by C(FeIII) are also observed here. Again, quenching of $Ru(bpy)_3^{2+}$ and $Ru(phen)_3^{2+}$ by C(FeII) appear to be independent of μ. The negatively charged $Ru(DIPS)_3^{4-}$ shows electrostatic effects. The observed k_q's are, on average, ≈30% lower than those for C(FeIII) quenching.

2.4.4 pH dependence of the quenching reactions:

The k_q's for the quenching of $Ru(bpy)_3^{2+}$ by C(FeII) and C(FeIII) at pH 3.0, 4.0 and 7.0 (μ = 0.1 M) are presented in Table 2.4 and Figure 2.7. On reducing the pH from 7.0 to 3.0, the k_q for C(FeII) quenching increases only slightly from 5.6×10^8 to 6.6×10^8 $M^{-1}s^{-1}$. On the other hand, the k_q for C(FeIII) quenching increases from 8.6×10^8 to 2.3×10^9 $M^{-1}s^{-1}$.

2.4.5 Actinometry:

The incident light intensity for continuous photolysis was determined before every set of experiments. The difference in absorbance of irradiated and non-irradiated (control) ferrioxalate solutions was measured after the addition of phen to form $Fe(phen)_3^{2+}$, which was determined spectrophotometrically at 510 nm. The measured absorbance increases linearly with irradiation time, and a typical set of experimentally measured ΔA_{510} values vs. irradiation time are given in Table 2.5 and plotted in Figure 2.8. A standard error of 9.4% was calculated for the slope (linear-least squares fit). Using equation 2.18, the

Table 2.3 Rate Constants for the Quenching of Excited Ruthenium Polypyridine Complexes by Ferrocytochrome c [a,e]

Complexes [b]	$k_q x 10^{-8}$ ($M^{-1}s^{-1}$) μ = 0.1 M	$k_q x 10^{-8}$ ($M^{-1}s^{-1}$) μ = 0.01 M
$Ru(bpy)_3^{2+}$	5.6 (0.1) [c]	7.1 (0.2)
$Ru(bpy)_2(CN)_2$	16 (1)	---
$Ru(phen)_3^{2+}$	8.0 (0.4)	7.8 (0.4)
$Ru(phen)_2(CN)_2$	7.6 (0.3)	16.0 (0.5)
$Ru(DIP)_3^{2+}$	d	d
$Ru(DIPS)_3^{4-}$	11.0 (0.6)	51 (1)

[a-c]Refer to Table 2.2

Table 2.4 pH Dependence of Rate Constants for the Quenching of $Ru^*(bpy)_3^{2+}$ by Ferri- and Ferrocytochrome c[a]

pH	C(FeIII) $k_q x 10^{-8}$ ($M^{-1}s^{-1}$)	C(FeII) $k_q x 10^{-8}$ ($M^{-1}s^{-1}$)
7	8.6 (0.4)	5.6 (0.1)
4	13.0 (0.6)	6.0 (0.4)
3	23 (1)	6.6 (0.3)

[a]Experimental conditions: 20 μM $Ru(bpy)_3^{2+}$, 0 to 1.2 mM cytochrome c in deoxygenated phosphate buffer, pH 7.0 or biphthalate buffer, pH 3.0 and 4.0, μ = 0.1 M, 24°C.

Standard deviation of slope of Stern-Volmer plots in parentheses. Emission lifetime quenching data used to determine k_q's are given in Appendix A.

Table 2.5 Ferrioxalate Actinometry: Measured Absorbance Change at 510 nm vs. Irradiation Time, t[a]

t (min)	ΔA_{510}
0	0.000
2.0	0.045
4.0	0.075
6.0	0.103
8.0	0.128
10.0	0.186
12.0	0.201

[a]Concentration of Fe^{2+} formed by the photolysis of ferrioxalate was determined spectrophotometrically by measuring the absorption of $Fe(phen)_3^{2+}$ at 510 nm as a function of irradiation time (t). The radiation source was a 100 W high pressure mercury arc lamp and the excitation wavelength was 436 nm. Experimental conditions and procedures are given in Section 2.3.4.

Figure 2.7

Stern-Volmer plots of emission quenching of $Ru^{*}(bpy)_3^{2+}$ by ferro- and ferri-cytochrome c at different pH's. The reactions were carried out in phosphate buffer at pH 7.0 and in biphthalate buffer at pH 3.0 and 4.0, and μ = 0.1 M for all solutions. Circles (o) and (•) denote the quenching by C(FeII) at pH 7.0 and 3.0, respectively. Triangles (▲), (▼) and (▽) denote quenching by C(FeIII) at pH = 3.0, 4.0 and 7.0, respectively.

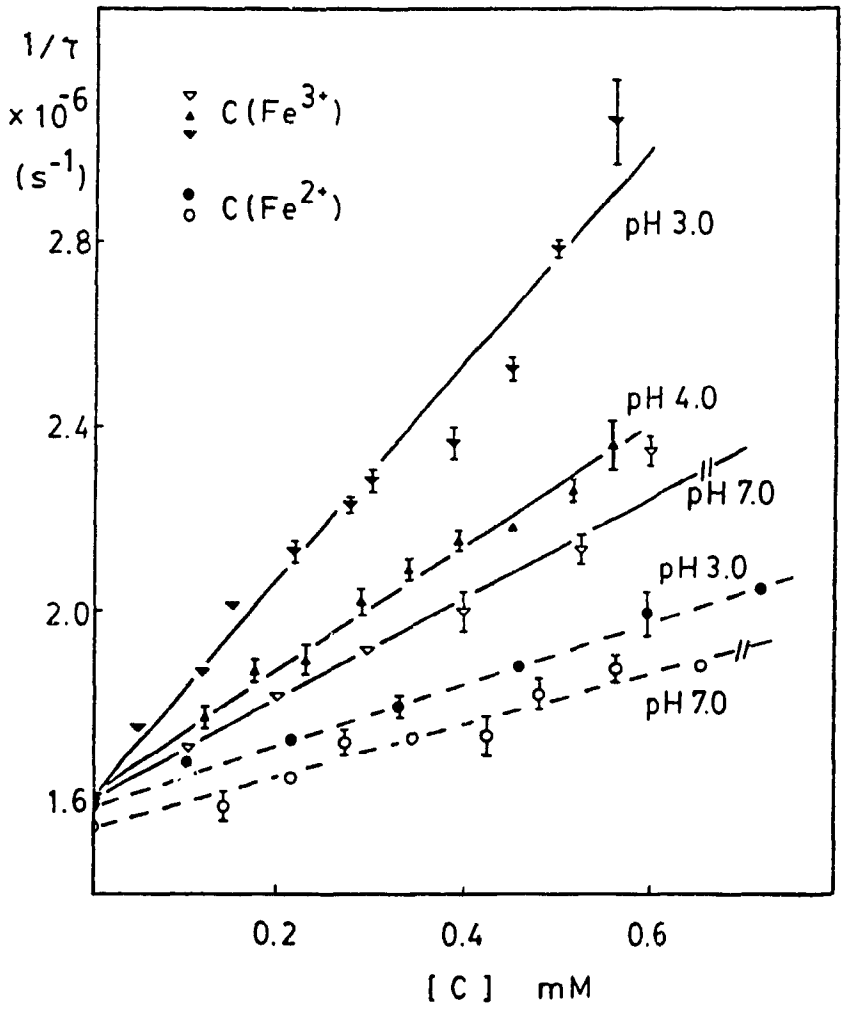

Figure 2.8

Ferrioxalate actinometry: Absorbance change at 510 nm vs. irradiation time. Plot of data given in Table 2.5.

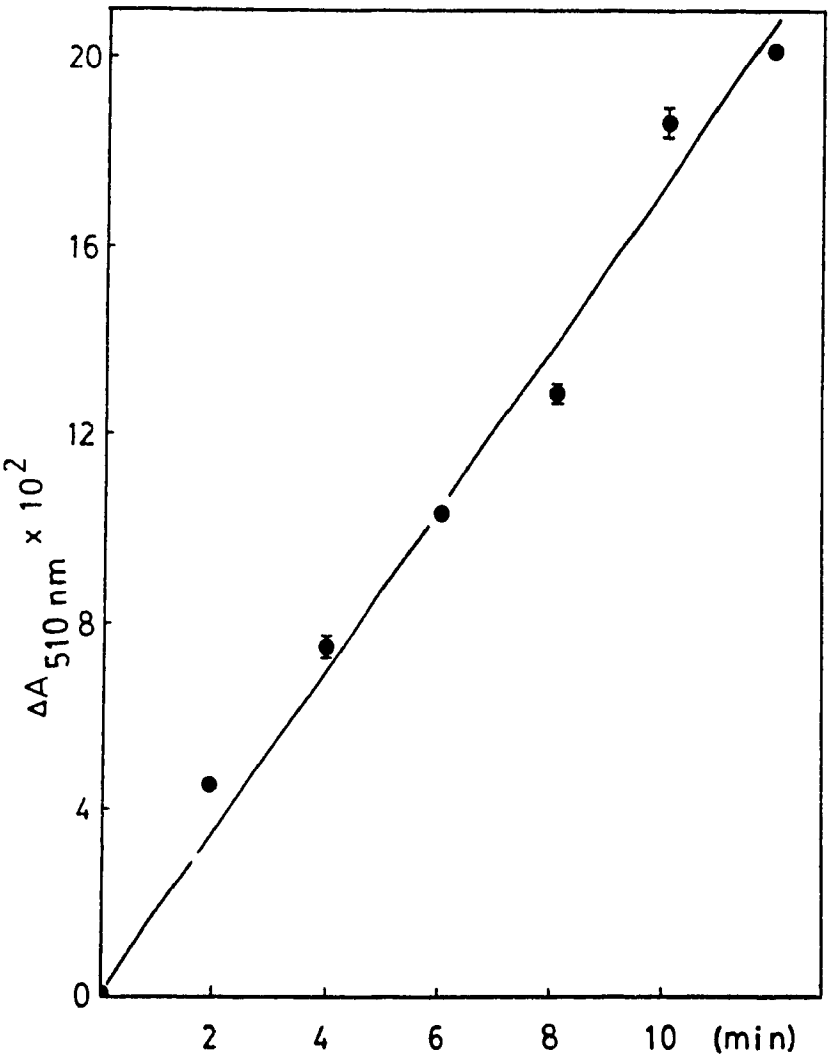

number of moles of Fe^{2+} ion calculated from the slope ($2.8x10^{-4}$) was $9.6x10^{-10}$ mole s^{-1} and the corresponding light intensity was calculated to be $1.9x10^{-9}$ einstein s^{-1} (eq.2.19).

2.4.6 Steady-state quantum yields for C(FeIII) photoreduction:

Under continuous irradiation, the absorbance at 550 nm of a solution of RuL_3, C(FeIII) and EDTA increases linearly at least for the first 100 s. This indicates that the light intensity used in the experiment permits a steady-state to be reached without significantly decreasing the C(FeIII) concentration. The characteristic C(FeII) spectrum was clearly observed after 5 min irradiation, and the observed rates ($\Delta A_{550}/\Delta t$ s^{-1}) and quantum yields for C(FeIII) reduction (Φ_{obs}) are tabulated as a function of C concentration in Table 2.6. The relative efficiency of $Ru(DIPS)_3^{4-}$ as a sensitizer at $\mu = 0.16$ M and the marked dependence of its Φ_{obs} on ionic strength are apparent from Figure 2.9. By comparison, Φ_{obs} for $Ru(bpy)_3^{2+}$ and $Ru(phen)_3^{2+}$ are significantly lower than those for $Ru(DIPS)_3^{4-}$ at $\mu = 0.16$ M, and relatively insensitive to ionic strength (Table 2.6 and Figure 2.9). These observations mirror the ionic strength effects observed in emission lifetime quenching experiments.

The quantum yield data given in Table 2.6 are plotted as $\Phi_{obs}/[Q]$ vs. Φ_{obs} [Q = C(FeIII)] in Figure 2.10. The plots are linear as expected from eq.2.14, and the slopes ($k_q/k_o = K_{sv}$) vary between $6.7x10^3$ to $4.1x10^4$ M^{-1} with standard errors between 10 to 30%. In Table 2.7, these Stern-Volmer constants (K_{sv}) are compared to those calculated

Figure 2.9

Plots of observed quantum yield (Φ_{obs}) vs. concentration of ferricytochrome c [C(FeIII)] for Ru^*L_3-photosensitized cytochrome c reduction by $Ru(phen)_3^{2+}$ and $Ru(DIPS)_3^{4-}$, in 5 (μ = 0.07 M) or 50 (μ = 0.16 M) mM phosphate buffer containing 10 mM EDTA, at pH 7.0, and 24°C. Excitation wavelength was 436 nm, and C(FeII) production was monitored at 550 nm. C(FeIII) concentrations and corresponding Φ_{obs} are from Table 2.6.

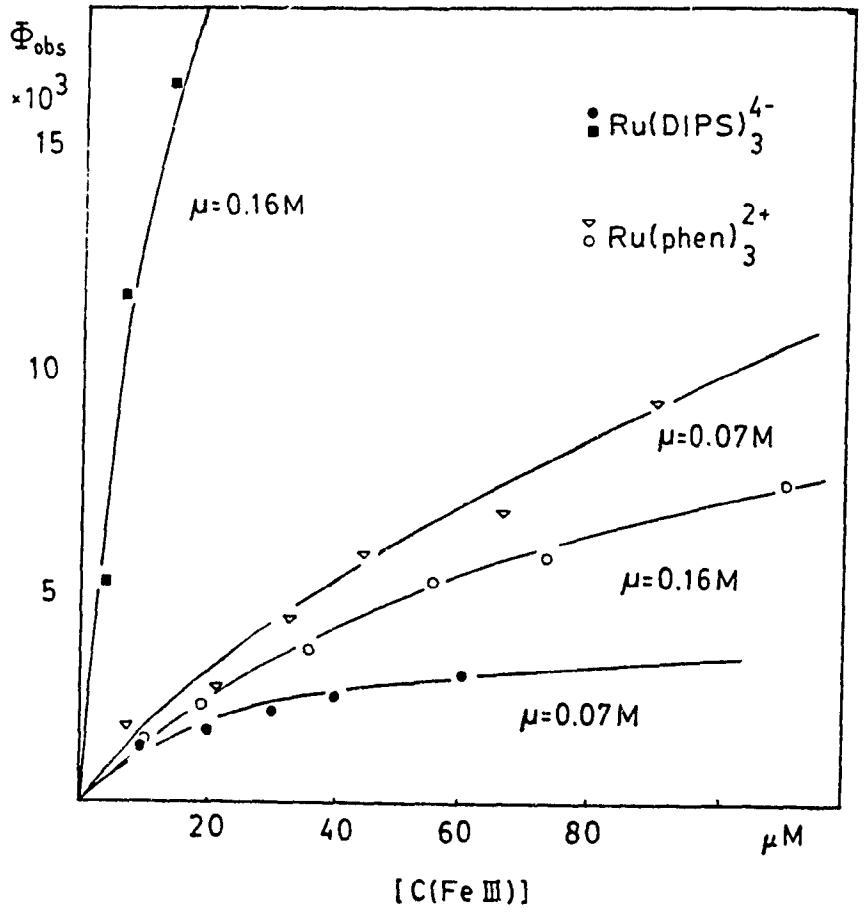

Figure 2.10

Plots of $\Phi_{obs}/[Q]$ vs. Φ_{obs} (eq.2.14) for $Ru^{*}L_3$ photo-sensitized cytochrome c reduction. [Q], the concentration of C(FeIII), and Φ_{obs} are from Table 2.6 and the experimental conditions are given in the caption to Figure 2.9. Notation used: $Ru^{*}(bpy)_3^{2+}$ (△), $Ru^{*}(phen)_3^{2+}$ (□), $Ru^{*}(DIPS)_3^{4-}$ (○) at μ = 0.16 M; $Ru^{*}(bpy)3^{2+}$ (▲), $Ru^{*}(phen)_3^{2+}$ (■), $Ru^{*}(DIPS)_3^{4-}$ (●) at μ = 0.07 M.

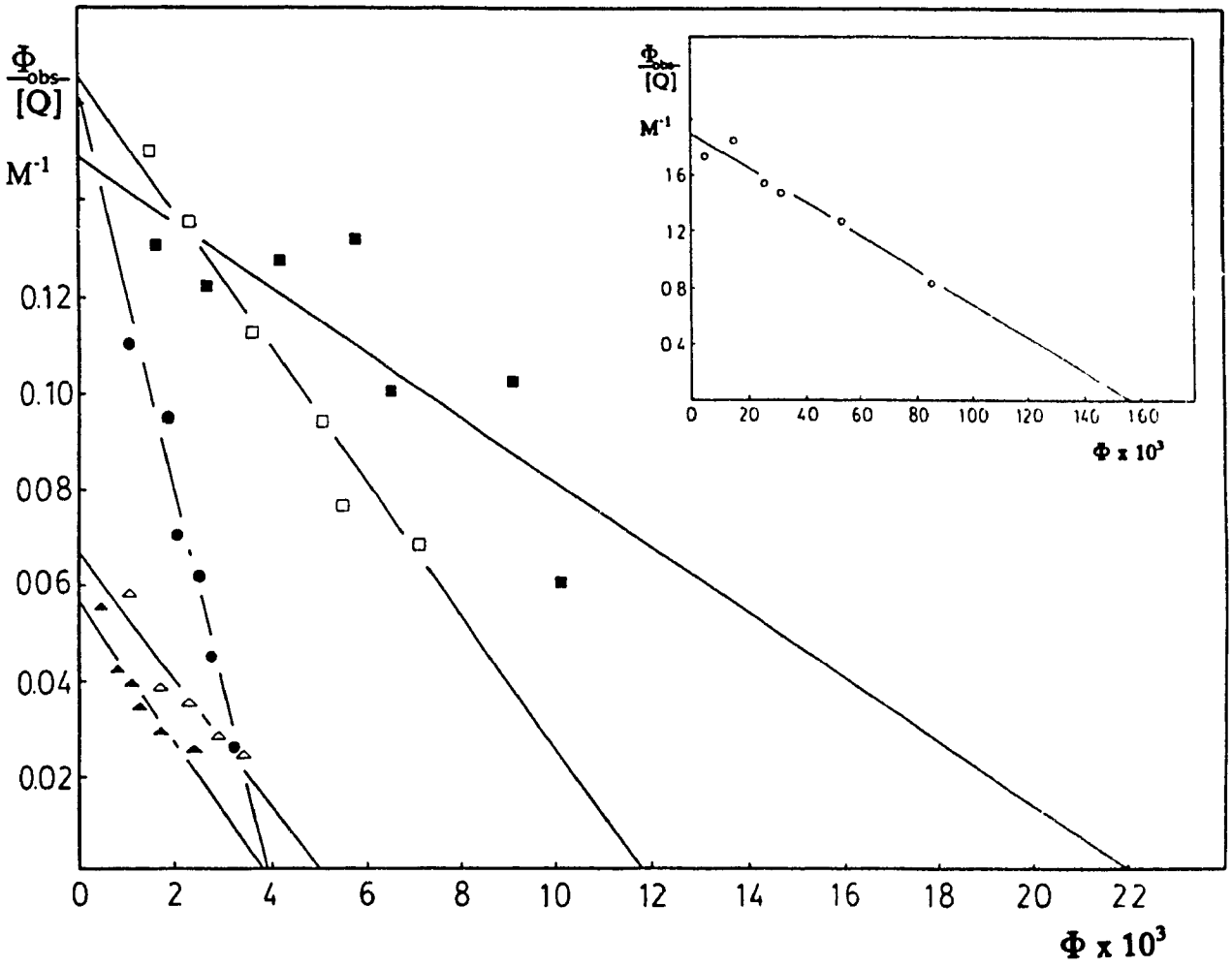

Table 2.6 Observed Rates and Quantum Yields for the Ru^*L_3-photosensitized Reduction of Ferricytochrome c

	μ = 0.07 M[a]			μ = 0.16 M[b]		
COMPLEX	[C] (μM)	Rate[c] ($\Delta A_{550}/\Delta t$ s^{-1}) x10^5	Φ_{obs}[d] x10^3	[C] (μM)	Rate[c] ($\Delta A_{550}/\Delta t$ s^{-1}) x10^5	Φ_{obs}[d] x10^3
$Ru(phen)_3^{2+}$	13	1.4	1.7	10	1.3	1.5
	22	2.0	2.7	17	1.8	2.3
	33	2.8	4.2	32	2.4	3.6
	44	3.4	5.8	54	2.7	5.1
	66	3.1	6.6	72	2.5	5.5
	89	3.6	9.1	111	2.6	7.6
	166	2.5	10.1			
$Ru(bpy)_3^{2+}$	9	4.0	0.5	19	0.8	1.1
	19	6.0	0.8	44	1.0	1.7
	28	7.0	1.1	66	1.1	2.3
	38	8.0	1.3	101	1.0	2.9
	57	8.0	1.7	139	0.9	3.4
	95	9.0	2.4			
$Ru(DIPS)_3^{4}$	10	9.0	1.1	3	5.2	5.2
	20	14.0	1.9	8	13.8	14.8
	30	14.0	2.1	17	21.4	26.1
	40	15.0	2.5	22	24.7	32.2
	60	13.0	2.7	42	32.5	53.5
	121	10.0	3.2	102	31.6	86.2

[a,b]Estimated ionic strength of solutions containing 10 mM EDTA and 5 mM or 50 mM phosphate at pH 7.0.

[c]Measured rate of increase in absorbance at 550 nm due to the reduction of C on 436 nm excitation. I_o = 1.9x10^{-9} einstein s^{-1}. Other experimental conditions as stated in Section 2.3.5.

[d]Φ_{obs} values calculated using Equation 2.20

using the emission lifetime data ($K'_{sv} = \tau_o k_q$) reported in Table 2.1 and 2.2. The K_{sv} values obtained from the slopes are ≈1.5 to 26-fold higher than the K'_{sv} calculated from the lifetime data. Except for $Ru(DIPS)_3^{4-}$ at μ = 0.16 M, these differences are too large to be accounted for by the experimental errors in K_{sv} and K'_{sv}.

Included in Table 2.7 are the maximum quantum yields, Φ_{max}, obtained by extrapolating to infinite C(FeIII) concentration. The experimental Φ_{max} values for $Ru(DIPS)_3^{4-}$ are highly dependent on ionic strength, showing a 40-fold increase on increasing the ionic strength from 0.07 M to 0.16 M. The Φ_{max} values for $Ru(bpy)_3^{2+}$ and $Ru(phen)_3^{2+}$ show little or no ionic strength dependence.

2.5 **Discussion**:

2.5.1 Excited-state quenching mechanism:

The increase in Φ_{max} at high ionic strength for $Ru(DIPS)_3^{4-}$ corroborates a reaction scheme which involves the formation of an electron-transfer pair in a solvent cage (eq.2.10-2.12), since increasing ionic strength decreases electrostatic attraction between the two oppositely-charged redox products. Ionic strength has minimal effect on the quenching rate constants for both $Ru(bpy)_3^{2+}$ and $Ru(phen)_3^{2+}$ (Table 2.2), and the lack of ionic strength dependence of the Φ_{obs} values for these two complexes is as expected if the charges on the metal center are insulated by the ligands.

The large increase in some of the K_{sv} values obtained from the steady-state experiments compared to lifetime experiments implies change in the interaction between the excited complexes and C(FeIII). For example, the presence of negatively-charged

Table 2.7 Experimental Φ_{max} Values for Ru^*L_3-photosensitized Reduction of Ferricytochrome c and Stern-Volmer Constants

	μ = 0.07 M[a]			μ = 0.16 M[b]		
COMPLEX[c]	Φ_{max}[d] x10^3	K_{sv}[e] x10^{-3} (M^{-1})	K'_{sv}[f] x10^{-3} (M^{-1})	Φ_{max}[d] x10^3	K_{sv}[e] x10^{-3} (M^{-1})	K'_{sv}[f] x10^{-3} (M^{-1})
$Ru(phen)_3^{2+}$	22(2)	8(2)	1.37(3)	11.8(6)	14(2)	1.18(4)
$Ru(bpy)_3^{2+}$	3.8(3)	15(3)	0.56(3)	5.0(3)	13(3)	0.53(2)
$Ru(DIPS)_3^{4-}$	3.9(2)	41(5)	28(2)	158(7)	12(1)	7.2(3)

[a,b]Estimated ionic strength of 5 or 50 mM phosphate buffer containing 10 mM EDTA, at pH 7.0 and 24 ± 1 °C.

[c]Concentrations of RuL_3 used; 60 µM $Ru(DIPS)_3^{4-}$, 100 µM $Ru(bpy)_3^{2+}$ and 100 µM $Ru(phen)_3^{2+}$; other experimental conditions given in Section 2.3.5.

[d]Maximum quantum yield determined by extrapolation to [Q] = ∞ in plots of $\Phi_{obs}/[Q]$ vs. Φ_{obs} (eq.2.14) where Q = C(FeIII). Standard errors in units of the last digit are given in parentheses.

[e]Stern-Volmer constants obtained from slopes of $\Phi_{obs}/[Q]$ vs. Φ_{obs} (eq.2.14).

[f]Stern-Volmer constants calculated from the τ_o and k_q values listed in Tables 2.1 and 2.2, respectively, and were obtained at μ = 0.01 and 0.1 M.

EDTA molecules could alter quenching rates by ion-pair formation with $Ru(bpy)_3^{2+}$ and $Ru(phen)_3^{2+}$. Such ion-pairing is expected to increase the quenching rate constants and reduce the cage release efficiencies by increasing the attraction between RuL_3 and C(FeIII). No ion-pairing is expected between $Ru(DIPS)_3^{4-}$ and EDTA, which is supported by the relatively small (< 1.7-fold) increases in the K_{sv} values relative to K'_{sv}. Since the EDTA concentration was kept at 10 mM, the marked increases in the Φ_{max} value for $Ru(DIPS)_3^{4-}$ at μ = 0.16 M mainly reflects the ionic strength dependence of the cage release efficiency for $Ru(DIPS)_3^{4-}$.

The present experiments do not allow the determination of the k_e/k_q ratio; nevertheless, the variation in the experimental Φ_{max} values corroborates a reaction scheme in which the deactivation of Ru^*L_3 by C(FeIII) involves electron transfer quenching, and the formation of electron transfer pairs is an integral part of the reaction mechanism.

2.5.2 Emission lifetime quenching by ferricyctochome c:

Results show that ionic strength has minimal effect on the quenching rates of $Ru^*(phen)_3^{2+}$ and $Ru^*(bpy)_3^{2+}$ by C(FeIII). Thus, if every encounter of the reactants resulted in quenching, the observed k_q's would reflect the limiting reaction rates in the presence of steric effects caused by the protein matrix. Indeed, when the bulk of the protein matrix is removed, the quenching of $Ru^*(bpy)_3^{2+}$ by the heme-octapeptide isolated from C has a rate of $5x10^{10}$ $M^{-1}s^{-1}$ (1), indicating that the quenching of $Ru^*(bpy)_3^{2+}$ by the heme is diffusion-controlled. Hence, the ratio of k_q/k_d, where k_d is the theoretical

diffusion-limited rate, should give an estimate of the steric factor caused by the protein matrix which reduces the accessibly of the heme. The observed rate of $Ru(bpy)_3^{2+}$ quenching by C ($8.6x10^8$ $M^{-1}s^{-1}$) is 10% of the calculated diffusion-controlled rate[1] ($8.6x10^9$ $M^{-1}s^{-1}$). If it is assumed that quenching occurs via the exposed heme edge only, then the steric factor (k_q/k_d) is the ratio of the area of the exposed heme edge divided by the total surface area of the C molecule. Using solvent perturbation, Schlauder et al. (22) have determined that about 30% of the heme of C(FeIII) is exposed to solvent, which translates to about 4% of the total protein surface area (23). The observed rates for $Ru(bpy)_3^{2+}$ and $Ru(phen)_3^{2+}$ show higher reactivities than expected, indicating that ≈10% of the protein surface can deactivate the exited complexes. This high steric value could be due to the dynamic nature of the protein structure, which makes the heme more accessible to hydrophobic ligands.

If quenching follows bimolecular kinetics, the excited state lifetime should decrease linearly with quencher concentration. As seen from Figure 2.5, at μ = 0.01 M, $Ru^*(DIPS)_3^{4-}$ is no longer quenched by a bimolecular mechanism at [Q] > 0.5 mM, since

---

[1]Diffusion-control rates for non-ionic reactions can be calculated using eq.2.21 (20);

$$k_d = 4\pi(D_1 + D_2)(R_1 + R_2)N/1000$$

where R_1 and R_2 are the radii of the reagents, N is Avogadro's number, D_1 and D_2 are the diffusion coefficients which can be estimated from the Einstein-Sutherland equation:

$$D = kT/6\pi\eta R$$

where k is the Boltzmann constant, T is temperature in K, η is solvent viscosity and R is the radius of the molecule.

τ levels off. Therefore, it is necessary to consider a quenching scheme which gives rise to saturation kinetics. One such scheme is the following:

$$RuL_3 \overset{h\nu}{\underset{k_o}{\rightleftharpoons}} Ru^*L_3$$

$$Ru^*L_3 + Q \overset{k_1}{\underset{k_{-1}}{\rightleftharpoons}} Ru^*L_3{:}Q \xrightarrow{k_2} \text{products}$$

where $k_2 = k_{et} + k_{en}$, and products are $Ru^+L_3{:}Q^-$ for electron transfer (k_{et}) and $RuL_3{:}Q$ for energy transfer (k_{en}) (see page 129).

Saturation kinetics are observed when binding between Ru^*L_3 and the quencher becomes significant as proposed previously (6). For the above scheme, the apparent association constant K can be calculated by the following equation (See Appendix C for the derivation of equations 2.21 and 2.22):

$$k_q = k_2 K \qquad \text{(low [Q])} \qquad \text{(eq.2.21)}$$

$$k_2 = 1/\tau_s - 1/\tau_o \qquad \text{(high [Q])} \qquad \text{(eq.2.22)}$$

Here k_q is the observed bimolecular quenching rate constant (7.5×10^9 $M^{-1}s^{-1}$), τ_s is the saturation lifetime for Ru^*L_3 at high [Q], and k_2 is 3×10^6 s^{-1}; thus $K = 2.5 \times 10^3$ M^{-1}. Substitution of these k_2 and K values into eq.2.23 below (derived in Appendix C for the above scheme), gives a plot that is compared to the experimental data in Figure 2.11.

Figure 2.11

Stern-Volmer plot of emission quenching of $Ru^{*}(DIPS)_3^{4-}$ by ferricytochrome c at μ = 0.01 M, pH 7.0 and 24 °C. Broken line (--o--) shows values calculated according to the precursor complex model for the quenching of $Ru(DIPS)_3^{4-}$.

$$\frac{\tau_o}{\tau} = \frac{1 + \tau_o k_2 K[C(FeIII)]}{1 + K[C(FeIII)]}$$ where $k_2 = 3 \times 10^6\ s^{-1}$ and $K = 2.5 \times 10^3\ M^{-1}$

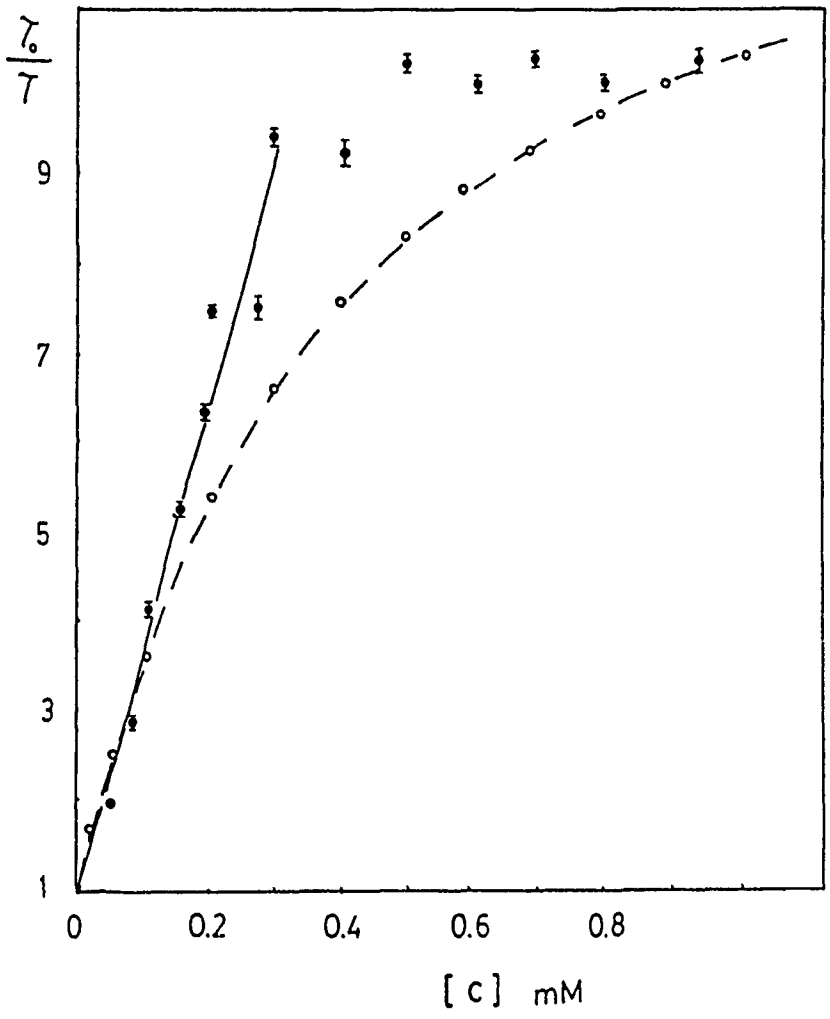

$$\frac{\tau_o}{\tau} = \frac{1 + \tau_o k_r K[C(FeIII)]}{1 + K[C(FeIII)]} \qquad \text{(eq.2.23)}$$

However, the above reaction model is not the only one that gives saturation kinetics. In fact, the sharp levelling off of the experimental τ_o/τ values in Figure 2.11 suggests a mechanism which involves a 2:1 complex with $Ru(DIPS)_3^{4-}$ sandwiched between two cytochrome c molecules. A similar 2:1 complex was proposed previously in the quenching of $Ru(bpy)_3^{2+}$ by blue copper proteins (6).

2.5.3 Emission lifetime quenching by ferrocytochome c:

In general, the quenching rates by C(FeII) (Table 2.2) are ≈30 % slower than those observed here by C(FeIII) (Table 2.3). There are a number of possible explanations for this observation: since there is no evidence that the quenching by C(FeII) involves electron transfer, it is possible that the quenching mechanism of C(FeII) involves only energy transfer. However, this is unlikely because the broad absorption band of C in the Ru^*L_3 emission region (600-680 nm) is significantly less intense upon reduction; thus, the rate of energy transfer, which is proportional to the spectral overlap of the donor and acceptor, should be reduced. The driving force for reductive quenching ($\Delta E \approx 0.6$ V) is about 0.5 V lower than that for oxidative quenching ($\Delta E \approx 1.1$ V), which could account for the differences observed in the quenching rate constants. However, the lower rate constants for the quenching by C(FeII) may be due to structural differences between the

two oxidation states. If the quenching rate constants reflect the degree of heme-edge exposure, a comparison of the diffusion limited rate constant[1] ($k_d = 8.6x10^9\ M^{-1}s^{-1}$) and the observed rate of $Ru^*(bpy)_3^{2+}$ quenching by C(FeII), indicates 6% heme exposure for C(FeII) vs. 10% for C(FeIII). Although it is not possible, at this stage, to conclude whether the lower reactivity of C(FeII) with Ru^*L_3 is due to a less accessible heme or to lower driving forces for electron transfer, evidence for the control of reactivity by structural factors, rather than by thermodynamic factors, is obtained from the dependence of k_q on pH.

2.5.4 pH dependence studies:

The acid-induced breakage of the Met-80 S-Fe bond in C(FeIII) and an associated heme crevice opening was observed by Wilting et al. (25). Similar results were observed in the urea denaturation of C (1,26). A concurrent lowering of the reduction potential of C was observed when the urea concentration was increased to 7.0 M (26). The exposure of the heme to the aqueous environment destabilizes the ferrous state and results in the lowering of E° from 0.26 V to about 0.1 V. Based on the decrease in the E° on acid denaturation, a drop in the C(FeIII) oxidative quenching rate constants may be expected. Furthermore, the total charge of C at pH 3.0 is more positive than at pH 7.0; hence, the rate of $Ru^*(bpy)_3^{2+}$ quenching should be reduced at pH 3.0. However, the results show a 3-fold increase (Table 2.4) in C(FeIII) quenching rates, whereas the rates for C(FeII) quenching are insensitive to the change in pH. The 3-fold increase in reactivity of C(FeIII) at pH 3.0 indicates the importance of heme exposure in controlling the efficiency

of quenching, while the lack of pH effects on k_q for C(FeII) shows the absence of conformational change for C(FeII). Since C(FeII) is more positively charged at low pH than at neutral pH, the absence of electrostatic effects on the quenching of $Ru^*(bpy)_3^{2+}$ by C is shown again here by the pH-independence of the k_q values.

2.6 **References:**

1 McLendon, G., Smith, M., J. Biol. Chem., 1978, 253, 4004.

2 Cho, K.C., Che, C.M., Cheng, F.C., Choy, C.L., J. Am. Chem. Soc., 1984, 106, 6843.

3 Sutin, N., Adv. Chem. Ser., 1977, 162, 156.

4 English, A.M., Lum, V.R., Delaive, P.J., Gray, H.B., J. Am. Chem. Soc., 1982, 104, 870.

5 Winkler, J.R., Nocera, D.G., Yocom, K.M., Bordignon, E., Gray, H.B., J. Am. Chem. Soc., 1982, 104, 5798.

6 Brunchwig, B.S., Delaive, P.J., English, A.E., Goldberg, M., Gray, H.B., Mayo, S., Sutin, N., Inorg. Chem., 1985, 24, 3743.

7 Bosshard, H.R., Zurrer, M., J. Biol. Chem., 1980, 255, 6694.

8 Yu, C., Steidl, J., Yu, L., J. Biol. Chem., 1978, 253, 404.

9 Takono and Dickerson "Electron Transport and Oxygen Utilization", Elsevier North-Holland Inc. Chien Ho (ed). 1982, Session I, p.17.

10 Xandell, J.K., Fay, D.P., Sutin, N., J. Am. Chem. Soc., 1973, 95, 1131.

11 Przystas, T.J., Sutin, N., Inorg. Chem., 1975, 14, 2103.

12 Brunschwig, B., Sutin, N., Inorg. Chem., 1976, 15, 631.

13 Grimes, C.J., Piezkiewicz, D., Fleischer, E B., Proc. Natl. Acad. Sci., 1974, 71, 1408.

14 Eden, D., Mathew, J.B., Rosa, J.J., Richards, F.M., Proc. Natl. Acad. Sci., 1982, 79, 815.

15 Hauenstein, B.L., Dressick, W.J., Buell, S.L., Demas, J.N., DeGraff, B.A., J. Am. Chem. Soc., 1983, 105, 4251.

16 Turro, N.J., "Modern Molecular Photochemistry", The Benjamin Cummings Publishing Company, Inc., Menlo Park, California 1978.

17 Calvert, J.G., Pitts, J.N. Jr., "Photochemistry", J. Wiley and Son, New York, N.Y. 1966.

18 Lin, C.T., Bottcher, W., Chou, M., Creutz, C., Sutin, N., J. Am. Chem. Soc., 1976, 98, 6536.

19 Bolletta, F., Maestri, M., Balzani, N., J. Phys. Chem., 1076, 80, 2499.

20 Radius (R) of cytochrome c was calculated from its molecular weight (13 kD) using the equation from Ref. (21), $R = 0.717\ M.W.^{1/3}$

R_1 = 17 Å for cytochrome c and R_2 = 7 Å for RuL_3

The diffusion coefficients (D) were calculated by the Einstein-Sutherland equation:

$D_1 = 1.3 \times 10^{-6}\ cm^2 s^{-1}$ for cytochrome c; $D_2 = 3.5 \times 10^{-6}\ cm^2 s^{-1}$ for RuL_3

21 Wherland, S., Gray, H.B., "Biological Aspects of Inorganic Chemistry", A.W. Addison, W. Culler, B.R. James, D. Dollphin Eds., Wiley, New York 1977.

22 Schlauder, G.G., Kassner, R.J., J. Biol. Chem., 1979, 254, 4110.

23 Stellwagen, E., Nature, 1987, 275, 74.

24 Meyer, T.E., Przysiecki, C.T., Watkins, J.A., Bhattacharyya, A., Simonsdon, R.P., Cusanovich, M.A., Tollin, G., Proc. Natl. Acad. Sci., 1983, 80, 6740.

25 Wilting, J., Van Buuren, K.J.H., Braams, R., Van Gelder, B.F., Biochim, Biophys. Acta., 1975, 376, 285.

26 Myer, Y.P., Saturno, A.F., Vrma, B.C., Pande, A., J. Biol. Chem., 1979, 254, 11202.

27 Gaines, G.L., J. Phys. Chem., 1979, 83, 3088.

28 Kalyanasundaram, K., Kiwi, J., Gratzel, M., Helvetica Chimica Acta, 1978, 61, 2720.

29 Trewhwlla, J., Carlson, V.A.P., Curtis, E.H., Heidorn, D.B., Biochem., 1988, 27, 1121.

30 Demas, J.N., Taylor, D.G., Inorg. Chem., 1979, 3177.

31 Prasad, D.R., Mandal, K., Hoffman, M.Z., Coordination Chem. Rev., 1985, 65, 175.

32 With $k_r \approx 10^6$ $M^{-1}s^{-1}$ (31) and $k_b \approx 10^8$ $M^{-1}s^{-1}$ (2), the rate of reduction of $Ru(bpy)_3^{3+}$ by 10 mM EDTA is much greater than its reduction by the C(FeII) produced during photolysis (<<0.1 mM).

33 Bartocci, C., Maldotti, A., Carassiti, V., Traverso, O., and Ferri, A., Inorg. Chim. Acta, 1985, 107, 5.

Chapter 3

KINETICS OF FERROCYTOCHROME c PEROXIDASE OXIDATION BY HEXACYANOFERRATE(III)

3.1 Introduction:

In this study, the kinetics of oxidation of ferrocytochrome c peroxidase, CCP(FeII), by ferricyanide were examined:

$$CCP(FeII) + Fe(CN)_6^{3-} \rightleftharpoons CCP(FeIII) + Fe(CN)_6^{4} \qquad \Delta E^\circ = 0.603\ V \qquad (I)$$

Ferricyanide was used extensively in the study of redox reactions of other mononuclear heme proteins such as cytochrome c (C) (4) and myoglobin (Mb) (5). Since these heme proteins all undergo one-electron transfer reactions with ferricyanide, and their crystal structures are available (6-9), it is possible to rationalize the redox reactivity of the FeIII/II couple based on the structure of the protein. The data obtained also serve to compare and contrast the mechanisms of oxidation of CCP(FeII) by an inorganic redox reagant and by its biological redox partner C(FeIII), which is reported in the next chapter. As discussed in Section 1.3, the CCP-catalyzed reduction of H_2O_2 involves two intermediates, Compound I (CpdI) and Compound II (CpdII) of CCP, which both possess a ferryl(FeIV) heme. The rates of reduction of the FeIV heme of CpdII by ferrocyanide

have been measured by Erman and coworkers (2,11a,b):

$$CpdII(FeIV) + Fe(CN)_6^{4-} \rightleftharpoons CCP(FeIII) + Fe(CN)_6^{3-} \qquad \Delta E^\circ = 0.678\ V \quad (II)$$

therefore, it is of interest to compare the reactivity of the FeIV/III and FeIII/II couples of CCP with $Fe(CN)_6^{4-/3-}$. Since the protein structures of CpdI of CCP and the native enzyme remain essentially the same (12), the reactivity of the different couples should not depend on differences in the accessibility of the heme. Thus, the effects of heme ligation on the redox reactivity of the FeIV/III and FeII/III couples of the CCP heme can be evaluated.

Electron transfer reactions between metalloproteins and inorganic complexes have been examined by using the Marcus relationship, an empirical equation that relates the cross reaction rate, k_{12}, to the electron self-exchange rates, k_{11} and k_{22}, of the two reactants (1-4). One of the most important observations is that the variation in the calculated self-exchange rates of metalloproteins parallels the degree to which the metal site is buried. However, this relationship is not rigorously followed; the order of reactivity for a series of proteins determined using one reagent may vary considerably from that determined using another (3,4).

In order to examine the correlation between the self-exchange rate and the accessibility of the redox site, it is necessary to reduce the number of variables involved in the cross reactions. This is accomplished by comparing redox reactivities of proteins containing the same prosthetic group towards a common redox reagent so that the

dependence of electron transfer rates on the structures of different metal centers can be eliminated. The ionic strength dependence of electron transfer rates should also be determined so that electrostatic effects can be evaluated. Since the kinetic accessibility of the redox site is expected to be highly dependent on the steric constraints imposed by the protein matrix, it is of interest to compare data obtained for proteins with well-characterized structures.

3.2 **Experimental**:

3.2.1 Materials:

CCP was isolated from baker's yeast according to the published procedure (13) and its purity index (A_{408}/A_{280}) was 1.3. Potassium ferricyanide (Sigma, grade I) solutions were prepared by weight using reagent grade material. Acetophenone (Aldrich) was used directly as received and reagent grade isopropanol (Aldrich) was glass distilled before use.

3.2.2 Methodology:

CCP concentrations were determined spectrophotometrically using an extinction coefficient of 93 $mM^{-1}cm^{-1}$ at 408 nm (11a). CCP solutions, 3.0 μM, were prepared in phosphate buffer, pH 7.0, containing 0.008% acetophenone and 2% isopropyl alcohol. Samples were deoxygenated in 1-cm cuvettes under purified argon for 30 min. In-situ UV-photoreduction of CCP(FeIII) to CCP(FeII) was performed following the procedure of Ward (14). Reducing organic radicals were photogenerated using a 150 W xenon lamp

(Osram), and in general, the reduction of CCP was completed within 10-20 s of continuous irradiation. An aliquot (10-100 µl) of ferricyanide was transferred to the cuvette by a gas-tight syringe, and the solution was rapidly mixed. The mixing time was typically 2-3 s and the rate of disappearance of CCP(FeII) was monitored by following the absorbance decrease at 440 nm on a HP 8451A rapid scan spectrophotometer. A 400 nm cut-off filter was used to eliminate UV-photoreduction by the spectrophotometer beam. The phosphate concentration of the buffer was varied between 5 to 200 mM, and all reactions were carried out at pH 7.0 and 24 ± 1 °C.

3.2.3 Data Treatment:

The bimolecular rate constant for the oxidation of CCP(FeII) by ferricyanide was determined at a 1:1 molar ratio of the two reagents. The absorbance change at 440 nm was plotted as $(A_t - A_\infty)^{-1}$ vs. t, where A_t and A_∞ are the absorbances at t s after mixing and after complete oxidation (t ≈ 180 s), respectively. The bimolecular rate constant (k_{12}) was determined by multiplying the slope by $\Delta\varepsilon_{440}$ (68 $mM^{-1}cm^{-1}$) for CCP(FeII) and CCP(FeIII) (see Appendix D for details).

The effective electrostatic charge on CCP was determined by the analysis of the ionic strength dependence of Reaction I. Following Debye-Hückel treatment, the observed rate constant, k_{obs}, can be related to the rate constant at zero ionic strength, $k_{12}°$, by the following equation:

$$\ln k_{obs} = \ln k_{12}° - \frac{Z_1^2 a\mu^{1/2}}{1+bR_1\mu^{1/2}} - \frac{Z_2^2 a\mu^{1/2}}{1+bR_2\mu^{1/2}} + \frac{(Z_1+Z_2)^2 a\mu^{1/2}}{1+bR^{\#}\mu^{1/2}} \qquad \text{(eq.3.1)}$$

where a=1.17 and b=0.329 for water at 25 °C, μ is the ionic strength, $R^{\#}$ is the radius of the activated complex, Z_1, Z_2 and R_1, R_2 are the charges and radii of CCP [23.2 Å (15)] and ferricyanide [4.5 Å (16)], respectively. Since $R_1 > R_2$, it is assumed that $R_1 = R^{\#}$ and eq.3.1 reduces to eq.3.2:

$$\ln k_{obs} = \ln k_{12}^{\circ} + \frac{(2Z_1Z_2+Z_2^2)a\mu^{1/2}}{1+bR_1\mu^{1/2}} - \frac{Z_2^2a\mu^{1/2}}{1+bR_2\mu^{1/2}} \qquad \text{(eq.3.2)}$$

A plot of $\ln k_{obs} + \frac{Z_2^2a\mu^{1/2}}{1 + bR_2\mu^{1/2}}$ vs. $\frac{a\mu^{1/2}}{1 + bR_1\mu^{1/2}}$

has a slope = $2Z_1Z_2 + Z_2^2$ and y-intercept = $\ln k_{12}^{\circ}$.

The rate constant at infinite ionic strength, k_{12}^{∞}, can be determined by correcting for electrostatic interactions using Marcus-type work terms:

$$\ln k_{obs} = \ln k_{12}^{\infty} - 3.576\left(\frac{e^{-\tau R_2}}{1+\tau R_1} + \frac{e^{-\tau R_2}}{1+\tau R_2}\right)\frac{Z_1Z_2}{(R_1+R_2)} \qquad \text{(eq.3.3)}$$

where; $\tau = 0.329\mu^{1/2}$, R and Z are defined as before. A plot of

$$\ln k_{obs} \quad \text{vs.} \quad \frac{e^{-\tau R_2}}{1+\tau R_1} + \frac{e^{-\tau R_1}}{1+\tau R_2}$$

has a slope = $-3.576\, Z_1 Z_2/(R_1+R_2)$ and y-intercept = $\ln k_{12}^{\infty}$.

The self-exchange rate constant of ferricyanide, k_{22}, and the driving force of the reaction, ΔE°_{12}, are also corrected to infinite buffer ionic strength using eq.3.4 and eq.3.5, respectively (3):

$$\ln k_{22}^{\infty} = \ln k_{22} + 3.576 \left[\frac{2\, e^{-\tau R_2}}{1+kR_2}\right] \frac{Z_1' Z_2'}{2R_2} \qquad \text{(eq.3.4)}$$

$$\Delta E_{12}^{\infty} = \Delta E^{\circ}_{12} + 0.0982 \left[\frac{e^{-\tau R_1}}{1+kR_2} + \frac{e^{-\tau R_2}}{1+kR_1}\right] \frac{(Z_1 Z_2 - Z_1' Z_2')}{R_1 + R_2} \qquad \text{(eq.3.5)}$$

where Z_1' and Z_2' are the charges on the products.

The protein self-exchange rate constant, k_{11}, is determined form the Marcus equation:

$$k_{11} = (k_{12})^2/k_{22}K_{12}f \qquad \text{(eq.3.6)}$$

where f is given by:

$$\ln f = (\ln K_{12})^2/[4\ln(k_{11}k_{22}/Z^2)] \qquad \text{(eq.3.7)}$$

In eq.3.7, Z is the collision frequency (10^{11} $M^{-1}s^{-1}$) and K_{12} is the equilibrium constant for the cross reaction which can be calculated using the following equation:

$$K_{12} = nF\Delta E_{12}/(RT) \qquad \text{(eq.3.8)}$$

where n is the number of electrons transferred, F and R are Faraday's constant and the gas constant, respectively, and T is the absolute temperature. If all the parameters in eq.3.6 are corrected to $\mu = \infty$, then $k_{11} = k_{11}^{\infty}$.

3.3 **Results**:

Upon photoreduction the absorption maximum of CCP shifts from 408 nm to 440 nm, with an isosbestic point at 420 nm (Figure 3.1). The molar absorbtivities of CCP(FeIII) and CCP(FeII) at 440 nm are 87 ± 2 and 19 ± 2 $mM^{-1}cm^{-1}$, respectively; hence, $\Delta\varepsilon$ at 440 nm is 68 ± 2 $mM^{-1}cm^{-1}$. Figure 3.2A shows the absorbance decrease at 440 nm vs. time when 1:1 and 1:3 ratios of protein to oxidant were mixed in 200 mM phosphate. Clearly the rate depends on the ferricyanide concentration. Figure 3.2B shows the second-order kinetic fit, $(A_t - A^{\infty})^{-1}$ vs. t, for the 1:1 case at 200 mM phosphate. The reaction follows second order kinetics at all ionic strengths used here. The ΔA_{440} (= 0.003) due to the reduction of a 3 μM ferricyanide solution was neglected since it is less than 2% of the calculated ΔA_{440} (= 0.2) for the oxidation of a 3 μM CCP(FeII) solution. However, due to the time required for mixing of the two reagents (2-3 s), the ΔA_{440} observed for reactions carried out in 5 mM phosphate was ≈75% of the expected values, and ≈30%

Figure 3.1

Photoreduction of CCP(FeIII) to CCP(FeII) in 100 mM phosphate buffer, pH 7.0 at 24 ± 1 °C. Absorption maxmium is at 408 nm (ϵ = 93 $mM^{-1}cm^{-1}$) for CCP(FeIII) and 440 nm (ϵ = 87 $mM^{-1}cm^{-1}$) for CCP(FeII) with an isosbestic point at 420 nm.

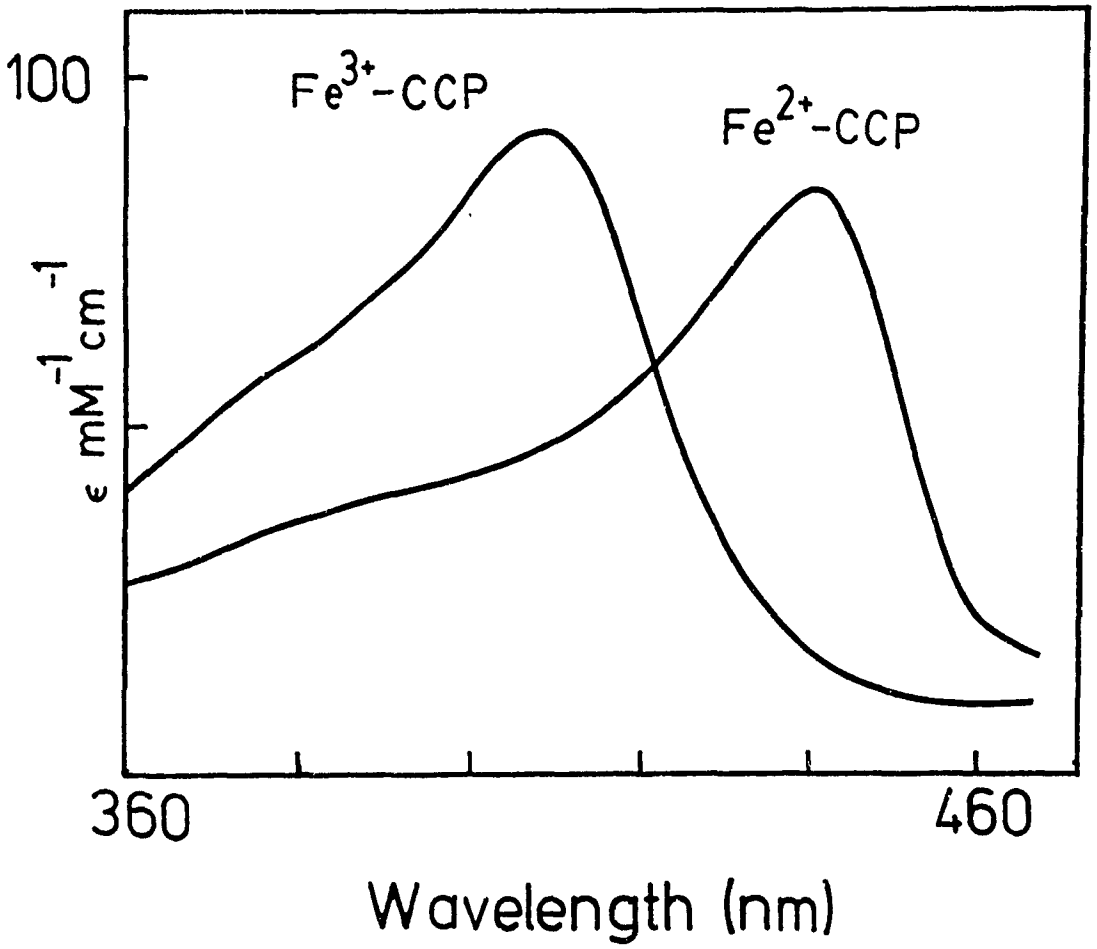

Figure 3.2

Oxidation of CCP(FeII) by ferricyanide in 200 mM Phosphate, ($\mu \approx 0.37$ M), pH 7.0, 24 ± 1 °C. (A) The upper curve shows the absorbance change at 440 nm for CCP:ferricyanide = 1:1, and the lower curve for CCP:ferricyanide = 1:3. The CCP concentration is 3 μM in each case. (B) Fit of the 1:1 reaction to second order kinetics. A_t and A_∞ are the absorbances at 440 nm at t s and after the reaction ($t \approx 180$ s).

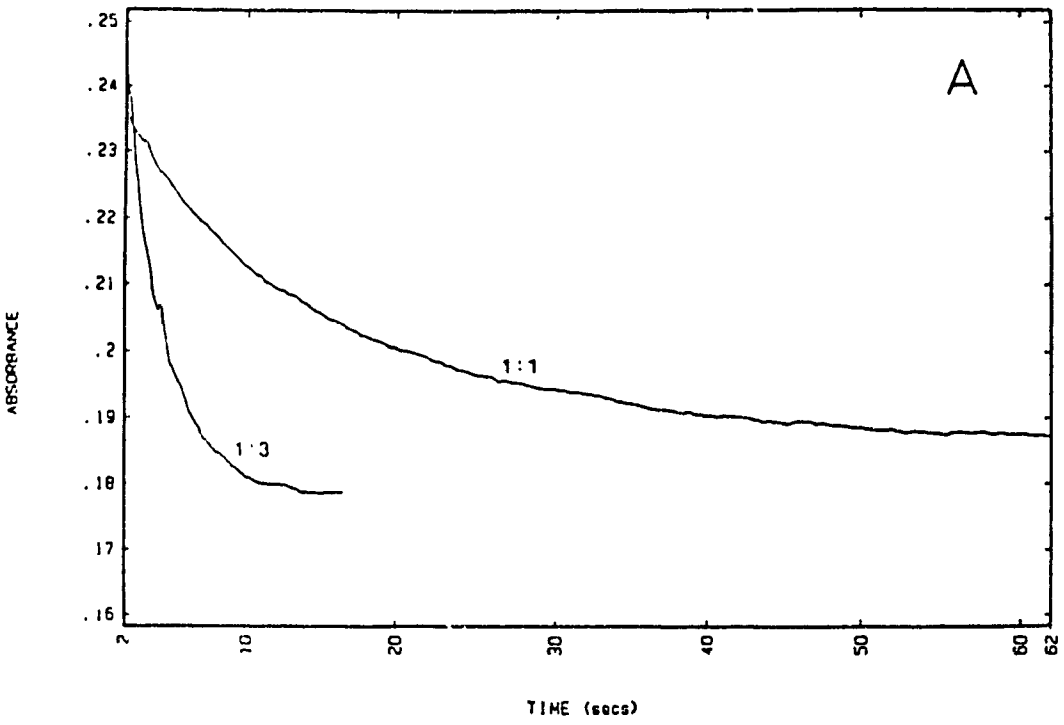
A
ABSORBANCE
.25
.24
.23
.22
.21
.2
.19
.18
.17
.16
1:1
1:3
2
10
20
30
40
50
60
62
TIME (secs)

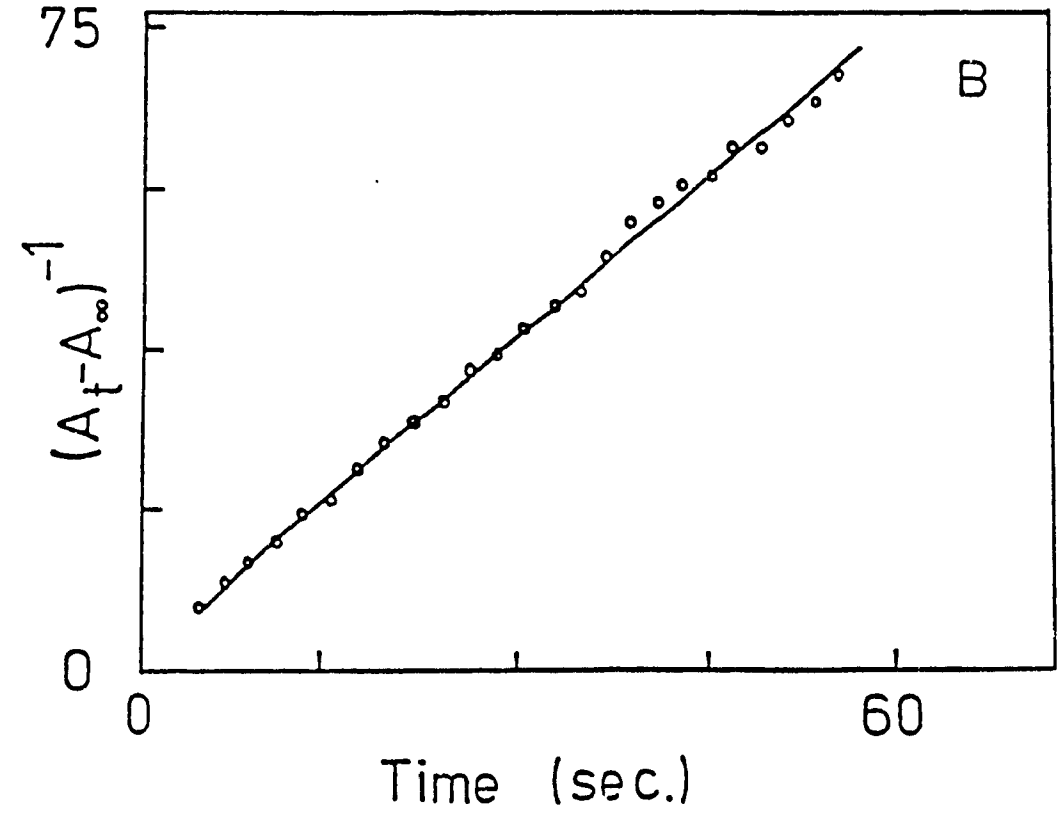
B
75
0
$(A_t-A_\infty)^{-1}$
0
60
Time (sec.)

for reactions at >50 mM phosphate. Table 3.1 lists the k_{obs} at different phosphate concentrations. The k_{obs} values decrease from 8.7×10^4 $M^{-1}s^{-1}$ at 200 mM phosphate to 2.1×10^4 $M^{-1}s^{-1}$ at 5 mM phosphate. The final spectrum measured at t = 180 s is characteristic of CCP(FeIII) with λ_{max} at 408 nm, while ferrocyanide has negligible absorbance at $\lambda > 350$ nm.

Figure 3.3A shows the fit of the rate constants to eq.3.2 (Debye-Hückel) for μ = 0.009 - 0.37 M. The rate constants demonstrate Debye-Hückel behaviour over the range of ionic strengths investigated. Extrapolation to $\mu = 0$ gives $k_{12}^{\circ} = 1.0 \times 10^3$ $M^{-1}s^{-1}$; and assuming $Z_2 = -3$, the slope of the plot yields $Z_1 = -9$ for CCP(FeII). Figure 3.3B shows the fit of the experimental data to eq.3.3 over the ionic strength range investigated. The curvature of the plot at low ionic strength significantly affected the k_{12}^{∞} estimated from the y-intercept. In order to obtain a better estimate of k_{12}^{∞}, the data point at the lowest ionic strength was not included in the regression. The slope in this instance yields Z_1 = -3 for CCP(FeII), and extrapolation to infinite ionic strength gives $k_{12}^{\infty} = 2.1 \times 10^5$ $M^{-1}s^{-1}$.

To eliminate the effects of electrostatic interactions on the reactivity of proteins with small inorganic reagents, it is customary to extrapolate k_{obs} and k_{22} to their values at infinite ionic strength (3), and to use these values in the Marcus relationship (eq.3.6) to determine k_{11}^{∞}. Since $k_{12}^{\infty} = 2.1 \times 10^5$ $M^{-1}s^{-1}$, and the k_{22}^{∞} for the FeIII/II couple of ferricyanide is calculated to be 8.7×10^5 $M^{-1}s^{-1}$ using eq.3.4 and its reported self-exchange rate constant [$k_{22} = 1.5 \times 10^4$ $M^{-1}s^{-1}$ in phosphate buffer, pH 7.0, μ = 0.1 M (4)], a value of 7.2×10^5 $M^{-1}s^{-1}$ is calculated for k_{11}^{∞} for CCP(FeII/III).

Table 3.1. Observed Rate Constants for Oxidation of CCP by $Fe(CN)_6^{3-}$ in Phosphate Buffers, pH 7.0 at 24 ± 1 °C.

Pi concentration (mM)	Ionic Strength[a] (mM)	$k_{obs} \times 10^{4}$ [b] ($M^{-1}s^{-1}$)
5	9	2.1
10	19	4.2
15	28	5.1
25	46	6.6
50	93	7.6
100	190	8.4
200	370	8.7

[a]Calculated ionic strength.

[b]Average value of at least 4 independent runs, and the standard errors are within 10 % of the average value. The $Fe(CN)_6^{3-}$ and CCP concentrations used were 3.0 μM in each case.

Figure 3.3

Ionic strength (μ) dependence of the oxidation of CCP(FeII) by ferricyanide in Phosphate buffer, pH 7.0. Plots of experimental data k_{obs} vs. μ using eq.3.2 (panel A) and 3.3 (panel B) in the text.

(A) $$f(k) = \ln k_{obs} + \frac{Z_c^2 a\mu^{1/2}}{1 + bR_2\mu^{1/2}} \quad \text{vs.} \quad f(\mu) = \frac{a\mu^{1/2}}{1 + bR_1\mu^{1/2}}$$

(B) $$f'(k) = \ln k_{obs} \quad \text{vs.} \quad f'(\mu) = \frac{e^{-\tau R_2}}{1+\tau R_1} + \frac{e^{-\tau R_1}}{1+\tau R_2}$$

The parameters given in these expression are explained in Section 3.2.3 of the text.

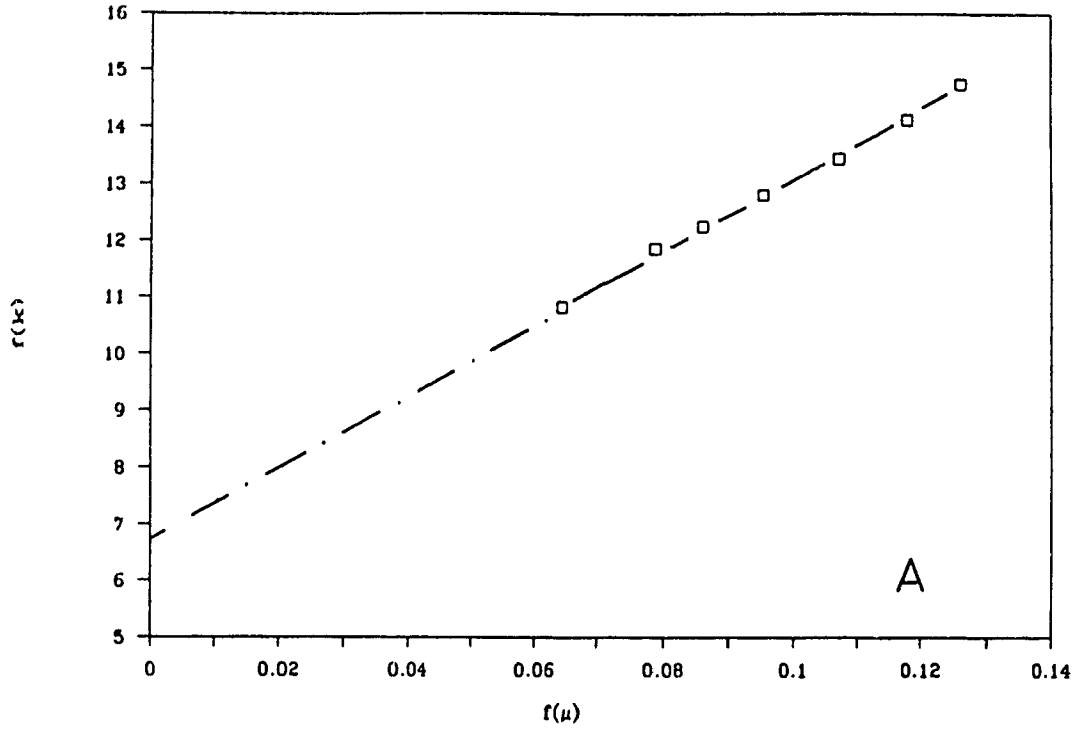
16
15
14
13
12
11
10
9
8
7
6
5
f(k)
0
0.02
0.04
0.06
0.08
0.1
0.12
0.14
f(μ)
A

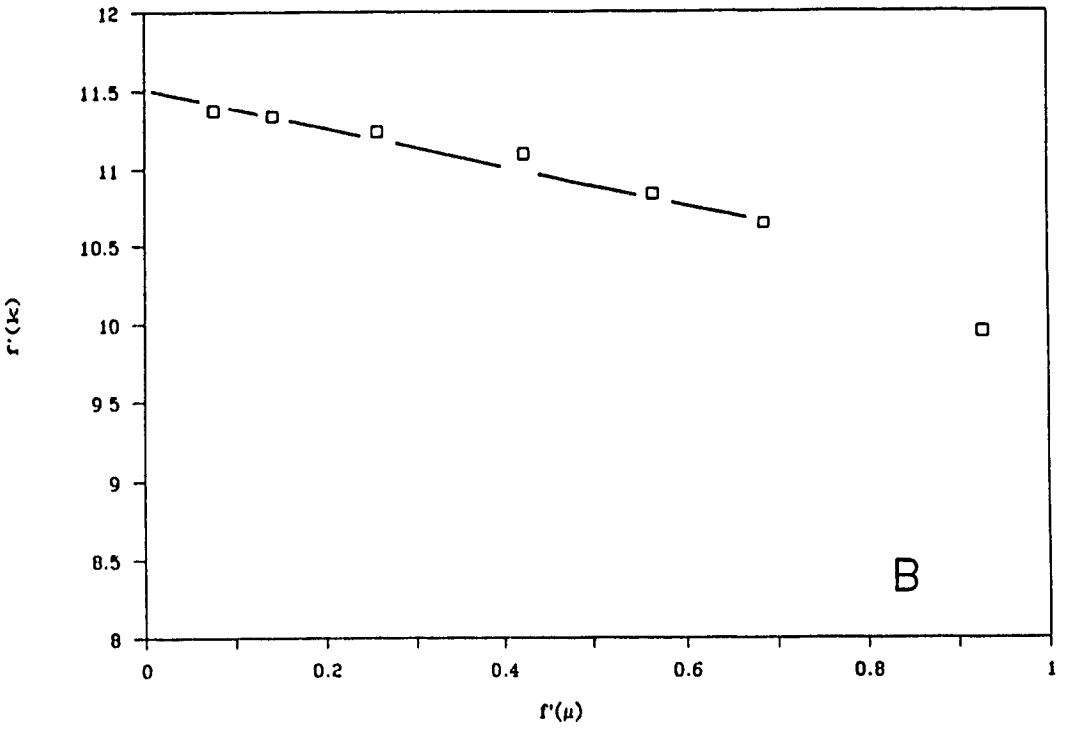
12
11.5
11
10.5
10
9.5
9
8.5
8
f'(k)
0
0.2
0.4
0.6
0.8
1
f'(μ)
B

3.4 **Discussion**:

The oxidation of CCP(FeII) by ferricyanide shows different reaction kinetics and ionic strength dependency compared to its oxidation by C(FeIII) (Chapter 4). Bimolecular kinetics are observed under the present experimental conditions for the oxidation of CCP(FeII) by the non-physiological redox reagent, ferricyanide.

The ionic strength dependence of the reaction rate is consistent with that expected for reaction between two like-charged particles. An effective charge of -9 is obtained for CCP(FeII) [= -8 for CCP(FeIII)] when the experimental data are subjected to the Debye-Hückel analysis, where reactions between charged ions are rationalized by changes in the activity coefficients of the reactants. This is in good agreement with the value of -9.5 obtained by acid-base titration of CCP(FeIII) at pH 7.0 (11a) and the value of -9 for CCP(FeIII) from the Debye-Hückel analysis of the reported data (11a) for the oxidation of ferrocyanide by CpdII. Using the procedure in (3), a value of -11 was calculated for CCP(FeII) from the reported amino acid content of the protein (10). Thus, it would appear that the overall charge of the protein determines its reactivity with ferricyanide. This was shown to be the case previously for the reduction of ferricyanide by Euglena gracilis cytochrome c_{552} (C_{552}) which carries a charge of -9 at pH 7.0 (17).

Electrostatic effects can also be examined by the Marcus treatment, where the expression of the cross-reaction rate involves consideration of the free energy required to bring the two reactants from infinite separation to the separation in the activated complex. The Marcus treatment of the observed rate data gives a charge of -3 for CCP(FeII). The analysis of the data reported by Erman et al. (11a) on the oxidation of ferrocyanide by

CpdII also gives a low charge of -4 on CCP(FeIV). The lower value obtained by the Marcus treatment cannot be explained; however, the k_{12}^{∞} value (2.1×10^5 $M^{-1}s^{-1}$) obtained by extrapolation of eq.3.3 to $\mu = \infty$ for the oxidation of CCP(FeII) by ferricyanide is reasonable, since $k_{obs} = 8.7 \times 10^4$ $M^{-1}s^{-1}$ at 200 mM Pi.

To ascertain the effects of heme accessibility on the relative reactivity of heme proteins, it is of interest to compare the k_{11}^{∞} values for the FeIII/II couples of CCP, Mb, C and C_{552}. CCP possesses a high-spin, 5-coordinate heme in both oxidation states (23, 25), yet the k_{11}^{∞} (7.2×10^{-5} $M^{-1}s^{-1}$) for CCP(FeII/III) couple is low compared to the k_{11}^{∞} (4.4 $M^{-1}s^{-1}$) for Mb, which remains high spin in both oxidation states but changes from 5-coordinate to 6-coordinate upon oxidation due to the uptake of a Fe-bound water molecule (24). The heme group in Mb is embedded in a cleft near the surface of the molecule (19), and about 18% of the heme surface is exposed (21). The CCP heme is ~10 Å below the protein surface (9), and this structural difference manifests itself in the calculated k_{11}^{∞} values for the two proteins.

The heme of C is low spin, 6-coordinate in both oxidation states and about 30% of the heme is solvent accessible (21). It is expected that both the exposure and the coordination of the heme should facilitate electron exchange, and indeed, the oxidation of C by ferricyanide gives a large calculated $k_{11}^{\infty} = 2.4 \times 10^4$ $M^{-1}s^{-1}$ (4). C_{552} has a similar charge [-9 (17)] to CCP, yet it has a k_{11}^{∞} value of 5.9×10^3 $M^{-1}s^{-1}$ which is about 8 orders of magnitude higher than CCP. Therefore, the relative magnitude of the k_{11}^{∞} constants for CCP, Mb, C and C_{552} demonstrates that the reactivity of heme proteins towards ferricyanide depends on the degree of exposure of the heme.

It is also of interest to compare the reactivity of the ferryl and the ferrous forms of CCP towards the same inorganic reagent. Ferrocyanide rapidly reduces the ferryl heme to the ferric state. This reaction has been studied as a function of both ionic strength and pH (11a,b). The Marcus treatment of the the reported rate constants obtained at μ = 0.005 to 0.1 M gives k_{12}^{∞} = 4.5×10^{3} $M^{-1}s^{-1}$; hence, k_{11}^{∞} for the FeIV/III couple is 1.9×10^{9} $M^{-1}s^{-1}$. The crystal structures of CCP(FeIII) and CpdI do not reveal any major structural changes between the two forms of the protein (12). Only small differences at the heme were detected which implies that no major conformational change takes place on CpdI formation. This it is probably also true for CpdII; hence, the 4 orders of magnitude difference in the reactivity of CCP(FeII) and CpdII towards the FeIII/II couple of ferricyanide, as reflected in the k_{11}^{∞} values, may be due to differences in the reorganization energies of the high-spin FeII and low spin FeIV hemes. CCP(FeII/III) is high-spin, 5-coordinate in both oxidation states (23,25), while the iron atom of CpdII is low spin, 6-coordinate, with an Fe^{4+}=O bond (26). Upon reduction of CpdII, the high-spin, 5-coordinate heme of CCP(FeIII) is formed. The cleavage of the Fe^{4+}=O bond as well as the conversion of the spin states is expected to result in a larger inner sphere reorganization energy for the CpdII(FeIV)/CCP(FeIII) couple than for the CCP(FeII/III) couple.

C, C_{552}, Mb, CCP and CpdII are arranged in order of reactivity towards outer-sphere electron transfer with ferro/ferricyanide in Table 3.2. The order of reactivity can be rationalized in terms of the biological function of the various proteins. The cytochromes are designed to be simple electron transferases; hence, the protein structure around the

Table 3.2. Calculated Self-exchange Rate Constants (k_{11}^{∞}) for Heme Proteins from Their Cross Reactions with Ferri- or Ferrocyanide

Protein[a]	R_1(Å)[b]	Z_1/Z_1'[c]	Heme[d]	k_{12}[e] ($M^{-1}s^{-1}$)	k_{12}^{∞} [e] ($M^{-1}s^{-1}$)	k_{11}^{∞} [e] ($M^{-1}s^{-1}$)	ΔE_{12}[f] (mV)
CpdII	23.5	-9/-10	$Fe^{4+/3+}$,6l,5h	$1.5x10^3$	$4.5x10^3$	$1.9x10^{-9}$	648
CCP	23.5	-11/-10	$Fe^{2+/3+}$,5h,5h	$7.6x10^4$	$2.1x10^5$	$7.2x10^{-5}$	603
Mb	18.4	3.5/4.5	$Fe^{2+/3+}$,5h,6h	$1.8x10^6$	$1.1x10^6$	4.4	350
C_{552}	15.8	-9/-8	$Fe^{2+/3+}$,6l,6l	$4.0x10^4$	$1.4x10^5$	$5.9x10^3$	39
C	16.6	6.5/7.5	$Fe^{2+/3+}$,6l,6l	$9.2x10^6$	$2.9x10^6$	$2.4x10^4$	147

[a]CpdII = compound II, CCP = cytochrome c peroxidase, Mb = myoglobin, C_{552} = cytochrome c_{552} (Euglena gracilis) and C = cytochrome c (horse).

[b]Protein radii from R_1=0.717 x $M.W^{1/3}$ (15) and the following molecular weights: CCP 35,350; Mb 16,950; C_{552} 10,740; C 12,384; R_2 = 4.5 Å (16).

[c]Estimated protein charges from sequence data using the procedure outlined in (3); Z_1 and Z_1' are the calculated charges before and after the reactions.

[d]Heme-iron oxidation, coordination and spin states; 6 and 5 = 6- and 5-coordinate; h = high spin and l = low spin.

[e]k12 (uncorrected) for CpdII and Mb from Refs. 11a and 5; C552 and C from Ref. 3; and CCP(FeII/III) in 50 mM Pi from this work.k_{11}^{∞} and k_{12}^{∞} are the self-exchange rate constant for the heme protein and the cross reaction rate constant at $\mu = \infty$, respectively. The calculated self-exchange rate for $Fe(CN)_6^{3-/4-}$ at $\mu = \infty$, k_{22}^{∞}, is $8.7x10^5$ $M^{-1}s^{-1}$ based on the reported value at μ = 0.1 M [$1.5x10^4$ $M^{-1}s^{-1}$ (4)].

[f]E° for ferricyanide at μ = 0.1 M is 409 mV (3), E° for CpdII (1.087 V), CCP (-194 mV), Mb (59 mV), C_{552} (370 mV) and C (260 mV) adopted from Refs. 2, 20, 27, 28 and 29, respectively.

heme is such that the iron can be readily oxidized and reduced. Nature designed Mb to reversibly bind oxygen which it does only in the ferrous form (19), so it is important that Mb remains reduced; therefore, Mb is not expected to be as efficient as the cytochromes at transferring electrons. Finally, as mentioned above, the enzymatic cycle of CCP generates a highly oxidizing intermediate, CpdI (10). Clearly, if the oxidizing equivalents of this CpdI are not to be randomly discharged, its highly reactive heme has to be well-insulated. The reactivity of the heme in CCP may well be masked by the topology of its environment; in fact, the heme of CCP is buried ~10 Å below the protein surface and the protein structure is designed to recognize and bind to its reducing substrate, C(FeII) (22).

3.5 **References**:

1 Mauk, A., and Gray, H.B., Biochem. Biophy. Res. Comm. 1979, 86, 206.

2 Purcell, W.L., and Erman, J.E., J. Am. Chem. Soc. 1976, 98, 7033.

3 Wherland, S., Gray, H.B., "Biological Aspects of Inorganic Chemistry", A.W Addison, W. Cullen, B.R. James, D.Dollphin Eds.; Wiley, New York, 1977, p.289.

4 Wherland, S., and Gray, H.B., Proc. Natl. Acad. Sci. USA. 1978, 73, 2950.

5 Antoini, E., Brunori, M., and Wyman, J., Biochem. 1965, 4, 545.

6 Swanson, R., Trus, B.L., Mandel, N., Mandel, G., Kallai, O.B., Dickerson, R.E., J. Biol. Chem. 1977, 252, 759.

7 Poulos, T.L., Freer, S.T., Alden, R.A., Edwards, S.L., Skogland, U., Takio, K., Eriksson, B., Xuong, N., Yonetani, T., Kraut, J., J. Biol. Chem. 1980, 255, 575.

8 Nobbs, C.L., Watson, H.C., and Kendrew, J.C., Nature, 1966, 206, 339.

9 Finzel, B.C., Poulos, T.L., and Kraut, J., J. Biol. Chem. 1984, 259, 13027.

10 Yonetani, T., Adv, Enzymol. 1970, 33, 309.

11a Jordi, H., and Erman, J.E., Biochem. 1974, 13, 3734.

11b Jordi, H., and Erman, J.E., ibid. 3741.

12 Edwards, S.L., Nguyen, H.X., and Kraut, J., Biochem. 1987, 26, 1503.

13 English, A.M., Laberge, M., Walsh, M., Inorg. Chim. Acta. 1986, 123, 113.

14 Ward, B., and Chang, C.K., Photochem. Photobiol. 1982, 35, 757.

15 Cantor, C.R. and Schimmel, P.R. in "Biophysical Chemistry Part II: Techniques for the study of Biological Structure and Function", Freeman, San Francisco, 1980, p.554.

16 Swanson, B.I., and Ryan, R.R., Inorg. Chem. 1973, 12, 283.

17 Goldkorn, T., and Schejter, A., J. Biol. Chem. 1979, 254, 12562.

18 Campion, R.J., Deck, C.F., King, P. Jr., and Wahl, A.C., Inorg. Chem. 1967, 6, 672.

19 Antonini, E., and Brunori, M., "Hemoglobin and Myoglobin in Their Reactions with Ligands" Neuberger, A., and Tatum, E.L. Ed., NorthHolland (1971).

20 Conroy, C.E., Tuma, P., Daum, P.H., and Erman, J.E., Biochim. Biophys. Acta. 1978, 537, 62.

21 Stellwagen, E., Nature, 1978, 375, 73.

22 Poulos, T.L., and Finzel, B.C., Peptide and Protein Revs. 1984, 4, 115.

23 Yonetani, T., Anni, H., J. Biol. Chem., 1987, 262, 1.

24 Stryer, L., Biochemistry, 1981, 2nd Edition, Freeman and Company, San Francisco, P.52.

25 Smulevich, G., Mauro, J.M., Fishel, L.A., English, A.M., Kraut, J. and Spiro, T.G., Biochemistry, 1988, 27, 5477.

26 Reczek, C.M., Sitter, A.J., Terner, J., J. Mol. Struct. 1989, 214; Hashimoto, S., Teraoka, J., Inubushi, T., Yonetani, T., and Kitagawa, T., J. Biol. Chem., 1986, 261, 11110.

27 Crutchley, R.J., Ellis, W.R. Jr., Gray, H.B., J. Am. Chem. Soc., 1985, 107, 5002.

28 Wood, F.E., and Cucanovich, M.A., Arch. Biochem. Biophys., 1975, 168, 333.

29 Taniguchi, V.T., Ellis, W.R. Jr., Cammarata, V., Webb, J., Anson, F.C., and Gray, H.B. in "Electrochemical and Spectrochemical Studies of Biological Redox Components", Advances in Chemistry series #201, Ed. Kadish, K.M., Am. Chem. Soc., Washington, D.C., 1982, p.51-68.

Chapter 4

STUDIES ON ELECTRON TRANSFER BETWEEN CYTOCHROME C AND FERROCYTOCHROME C PEROXIDASE

4.1 Introduction:

Studies on the reactivity of cytochrome c (C) and ferrocytochrome c peroxidase [CCP(FeII)], with inorganic complexes (Chapters 2 & 3) have demonstrated the dependence of electron transfer rates on the surface charge of the reagents, and on the accessibility of the protein redox site. However, information obtained from reactions with inorganic redox reagents cannot resolve all the factors that control electron transfer between the two biological partners. The hemes of CCP and C are located off-center in the protein matrix; thus, the orientation of the two molecules relative to each other is crucial for the optimization of electron transfer. Therefore, unlike the highly symmetric inorganic complexes, structural factors such as the relative orientation of the redox partners, and the possibility of conformation changes will also play a major role in controlling electron transfer rates between proteins.

Using the atomic coordinates from the crystal structures of CCP (1) and tuna C (2), the spatial distribution of the charges on the surface of C and CCP have been analyzed by computer graphics (3,4). Optimization of the interactions between the positively-charged lysine and arginine residues located on the surface of C and the negatively-

charged aspartate residues on CCP results in a 3-dimensional model of a noncovalent complex between C and CCP. Noteworthy features of this protein-protein complex are the parallel alignment of the hemes and their nearest edge-to-edge distance of 16.5 Å. Thus, electron transfer via direct π-orbital overlap of the two redox centers can be precluded. Instead, an electron transfer pathway via interfacial amino acid residues was proposed (4). The location of aromatic amino acid residues (His-180 in CCP and Phe-82 in C) near the intermolecular interface led to the proposal of an aromatic electron-transfer bridge between the two hemes.

However, this hypothetical model does not provide information on the dependence of the electron transfer kinetics on the actual dynamics of protein-protein interaction. The objectives of the present study are: (i) to measure the electron transfer rate between CCP(FeII) and C(FeIII):

$$C(FeIII) + CCP(FeII) \rightleftharpoons CCP(FeIII) + C(FeII) \qquad \Delta E^\circ = 0.45\ V \qquad (eq.4.1)$$

and (ii) to correlate the observed reaction kinetics with the equilibrium binding of the two molecules.

4.1.1 Equilibrium binding studies:

Different approaches have been used to study the noncovalent binding between C and CCP (5-13, 16, 23). Recently, Kornblatt and English (14) have used porphyrin cytochrome c (PorC, the iron-free derivative of C) steady-state fluorescence quenching by

CCP(FeIII) to estimate binding constants. Fluorescence quenching is one of the more sensitive probes of binding between the two proteins, and is also used in the present study to determine the extent of interaction between the two molecules under the conditions the electron transfer kinetics were measured. A complementary approach used here takes advantage of the polarized emission from the covalently-bound porphyrin ring of PorC. Since the degree of polarization depends on the rotational lifetime of the fluorophore (27,28), it reflects the mobility of the fluorophore. Upon formation of a PorC:CCP complex, the effective molecular weight of the PorC will increase by about 4-fold. The mobility of this large protein-protein complex will be much lower than that of the free PorC molecule; thus, a significant change in fluorescence polarization is expected on complexation. This approach has an advantage over fluorescence intensity quenching in that polarization measurements are independent of inner-filter effects because the parallel and perpendicular emission intensities are subjected to the same attenuating factors, thus eliminating the need for intensity corrections.

4.1.2 Electron transfer studies

The electron transfer between CCP(FeII) and C(FeIII) is not physiologically relevant, but it serves as an informative model for the study of long-range electron transfer between heme proteins. Steady-state enzyme kinetic studies have shown that the oxidation of C(FeII) by CCP(FeIV) is highly dependent on both the amino acid sequence of C and the ionic strength of the medium (24). Thus, it is of interest to study the oxidation of CCP(FeII) by C(FeIII) (eq.4.1) as a function of buffer ionic strength, using C's from

horse, tuna, yeast, and bacteria.

4.2 **Experimental**:

4.2.1 Materials:

Yeast CCP was obtained as described in Chapter 3. Horse heart (type VI), yeast (Candida krusei, type VII and Saccharomyces cerevisiae, type VIII), tuna heart (type XI) cytochromes c were obtained from Sigma, and Pseudomonas aeruginosa cytochrome c_{551} was a generous gift from Professor H.B.Gray (Caltech). All cytochromes were used as obtained.

Horse heart PorC, which was prepared using the literature procedure (14), was a generous gift from Professor J.A. Kornblatt (Concordia). Since PorC polarization varies with age, the stock PorC solution (100 μM) was stored at -20 °C and used within 3 days after it was prepared.

4.2.2 Steady-state fluorescence intensity quenching:

3.0 μM PorC solutions in 0.01 - 0.5 M phosphate buffer pH 7.0, and in distilled water, were prepared using ε_{403} = 160 $mM^{-1}cm^{-1}$ (26). The fluorescence data were obtained on a Perkin Elmer MPF44B spectrofluorimeter. The excitation wavelength was 538 nm and the fluorescence intensity was monitored at 620 and 680 nm. At each phosphate concentration, readings were recorded before and after a stoichiometric amount (<0.1 ml) of CCP(FeIII) was added to 3.0 ml of PorC. The emission intensity was corrected for inner filter effects due to the absorption of CCP at both the excitation and

emission wavelengths using the correction factor, $F_{corr} = F_{obs}\text{antilog}[(A_{ex} + A_{em})/2]$. The molar absorbtivities of CCP(FeIII) at these wavelengths are $\varepsilon_{538} = 8.6\ mM^{-1}cm^{-1}$, $\varepsilon_{520} = 2.6\ mM^{-1}cm^{-1}$ and $\varepsilon_{680} = 1.3\ mM^{-1}cm^{-1}$.

4.2.3 Fluorescence polarization:

3.0 μM PorC solutions were prepared in 0.01 and 0.1 M phosphate buffer ($\mu \approx 0.02$ and 0.20 M). Fluorescence polarization measurements were also carried out on the Perkin Elmer MPF44B spectrofluorimeter using HNP'B polarizers (Polaroid Corporation). Measurements were performed as previously described (15). The emission grating factor (G factor) was 0.48 at the emission wavelength (620 nm). The polarization was recorded using two different excitation wavelengths (505 and 515 nm), after aliquots (10 μl) of CCP(FeIII) were added to give CCP to PorC molar ratios from 0 to 3.

4.2.4 Electron transfer kinetics:

In situ photoreduction of a 3 μM CCP(FeIII) solution was carried out as described in Chapter 3. An aliquot (30 - 100 μl) of a deoxygenated C(FeIII) solution (0.3 mM) was added to the cuvette with a gas-tight syringe. After mixing by inverting the cuvette, absorbance changes were measured by a rapid response (0.1 s) spectrophotometer (HP 8451A). The reduction of C(FeIII) to C(FeII) was followed at the isosbestic point for CCP(FeIII) and CCP(FeII) (420 nm), and the oxidation of CCP(FeII) was followed by the absorbance decay at 440 nm (Figure 3.1). Absorbance readings (300 points) were recorded for at least 10-15 half-lives of the reaction, and data were analyzed using the computer program

given in Appendix E. Rate constants for biphasic reactions were obtained by fitting the experimental data to a sum of two exponential growth curves, where the rate expression in terms of an absorbance growth is given by:

$$\ln \Delta A_t = \ln \{\Delta A_{f\infty} [1-\exp(-k_f t)] + \Delta A_{s\infty} [1-\exp(-k_s t)]\} \qquad \text{(eq.4.2)}$$

where ΔA_t (= A_∞ - A_t) is the total absorbance change at time t; k_f, k_s, and $\Delta A_{f\infty}$, $\Delta A_{s\infty}$ are the first order rate constants and absorbance changes at $t = \infty$ for the fast and slow phases, respectively. Since the overall absorbance change (ΔA_∞) at $t = \infty$ is the sum of the absorbance changes due to the fast and slow phases, the fraction of the reaction going via the fast phase (ß) is as follows:

$$\Delta A_\infty = \Delta A_{f\infty} + \Delta A_{s\infty}$$

$$\Delta A_\infty = ß\, \Delta A_\infty + \Delta A_{s\infty} \qquad \text{(eq.4.3)}$$

The reactions with horse and yeast C's (S. cerevisiae) were carried out in 0.05 to 0.5 M phosphate buffer at pH 7.0. The reaction temperature was controlled by circulating thermostatic fluid through the cell holder from a refrigerated water bath (MGW Lauda T-2). After photoreduction, the CCP(FeII) solution was equilibrated to the proper temperature for 5 min prior to the addition of C. The temperature dependence of the reaction using horse C was examined at T = 0 to 26 °C.

4.3 **Results**:

4.3.1 Fluorescence quenching:

The excitation and emission spectra of horse PorC are shown in Figure 4.1. After correcting for inner filter effects, I_o/I' values at different ionic strengths are tabulated in Table 4.1 and plotted in Figure 4.2. I_o is the PorC fluorescence intensity in the absence of CCP, I is the measured fluorescence intensity of PorC after a stoichiometric amount of CCP(FeIII) was added, and I' is the corrected fluorescence intensity. Noticeable differences are observed when comparing the fluorescence intensities of solutions containing 1:1 PorC to CCP at various ionic strengths, but at $\mu > 0.05$ M, I_o/I' levels off at ~1.1, and remains unchanged to $\mu = 1.0$ M. Assuming a bimolecular quenching mechanism at high μ, a quenching rate constant of about 10^{12} $M^{-1}s^{-1}$ is estimated from the Stern-Volmer equation (eq.2.15) using a fluorescence lifetime of 9.5 ns for PorC (28). This rate is at least 100-fold higher than the diffusion-controlled limit. Thus, the residual quenching at $\mu > 0.05$ M cannot be due to a bimolecular quenching process. Possible explanations are: (i) long range dipole-dipole energy transfer, or (ii) the inner-filter effects are underestimated by the correction factors (Section 2.3.5).

However, in distilled water, and at $\mu < 0.05$ M the I_o/I' is greater than 1.1 (Table 4.1). Since the absorption spectrum of CCP and the emission spectrum of PorC are independent of ionic strength, underestimation of inner-filter effects cannot explain this increase in quenching efficiency. Thus, the quenching at low ionic strength must be due to static quenching of PorC by CCP, which implies binding between PorC and CCP.

Figure 4.1

Emission and excitation spectra of 10 μM porphyrin cytochrome c in 0.1 M phosphate buffer, pH 7.0. The excitation wavelength used to record the emission spectrum was 535 nm, and the excitation spectrum was recorded by monitorining the emission intensity at 622 nm. The emission maxima are at 620 and 680 nm, and the excitation maxima are at 404, 504, 540 and 565 nm.

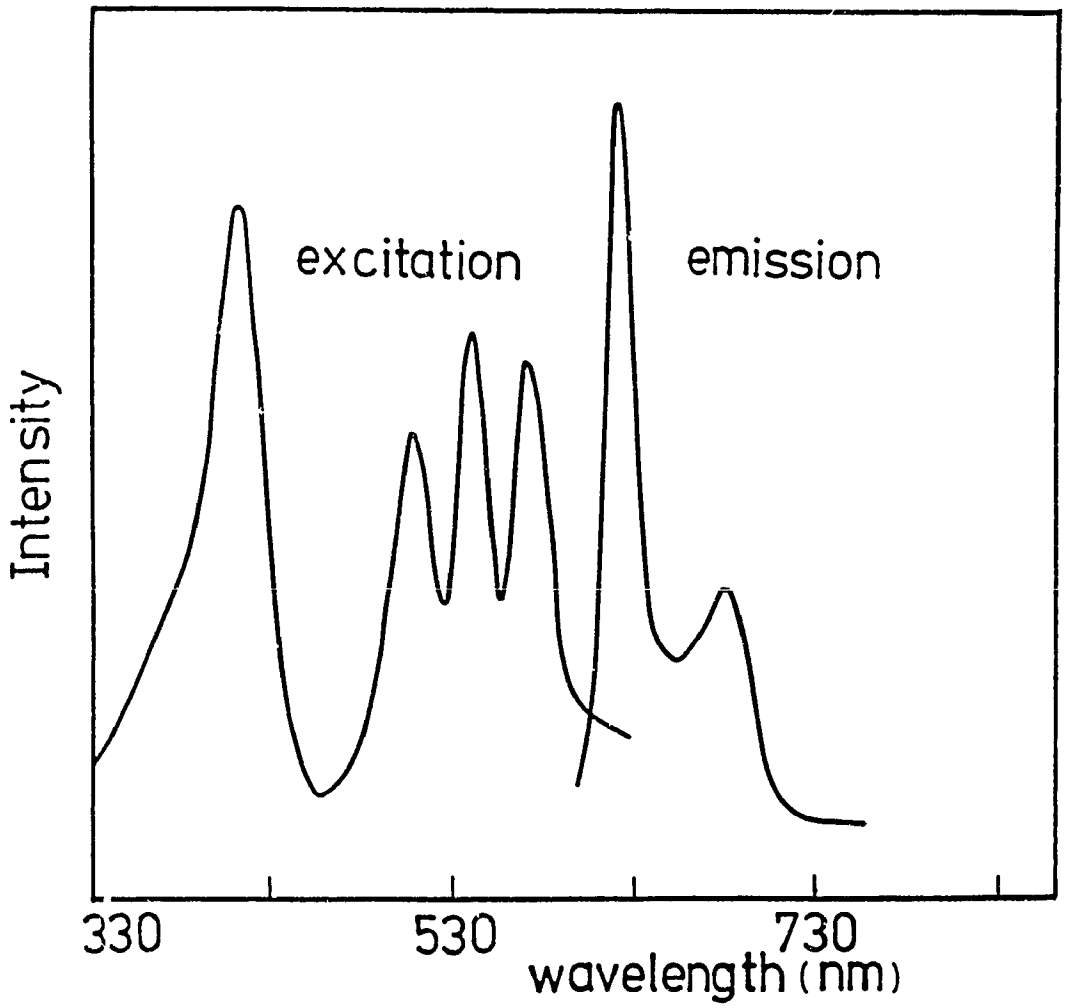

Table 4.1 Fluorescence Intensity Quenching (I_o/I') of Porphyrin Cytochrome c[b] by Ferricytochrome c Peroxidase[b] at Various Ionic Strengths[a]

Pi	μ[a]	I_o[d]	I[d]	I'[e]	I_o/I'[f]	I_o[d]	I[d]	I'[e]	I_o/I'[f]
(M)	(M)	λ_{em} = 620 nm				λ_{em} = 680 nm			
0.0	0 [c]	92	64	67	1.38	33	20	21	1.56
0.010	0.02	87	68	71	1.22	32	25	26	1.24
0.025	0.05	91	78	81	1.13	33	29	30	1.10
0.05	0.10	90	78	81	1.12	33	39	30	1.13
0.10	0.20	95	82	85	1.11	35	31	32	1.11
0.20	0.40	93	81	84	1.10	34	30	31	1.10
0.50	1.0	97	84	87	1.10	35	31	32	1.09

[a]Estimated ionic strength of phosphate buffer, pH 7.0, 24 °C.

[b]The concentrations of both PorC and CCP(FeIII) were 3 μM.

[c]distilled water, pH 7.0.

[d]I_o and I are the fluorescence intensities measured in the absence and in the presence of CCP(FeIII), respectively. λ_{ex} = 538 nm, I = fluorescence intensity before correction for inner-filter effects.

[e]Flourescence intensity after correction for inner-filter effects, the correction factors are 1.039 at 620 nm, and 1.031 at 680 nm.

[f]I_o/I' is the ratio of the corrected fluorescence intensities of PorC at the specified wavelength (nm) in the absence and presence of CCP(FeIII).

Figure 4.2

Fluorescence quenching of porphyrin cytochrome c by ferricytochrome c peroxidase in phosphate buffers, pH 7.0 vs. ionic strength. I_o and I' are the emission intensities in the absence and prescence of cytochrome c peroxidase, respectively. All I' values were corrected for inner-filter effects (Section 4.2.2) at both the excitation (538 nm) and emission wavelengths (620 and 680 nm).

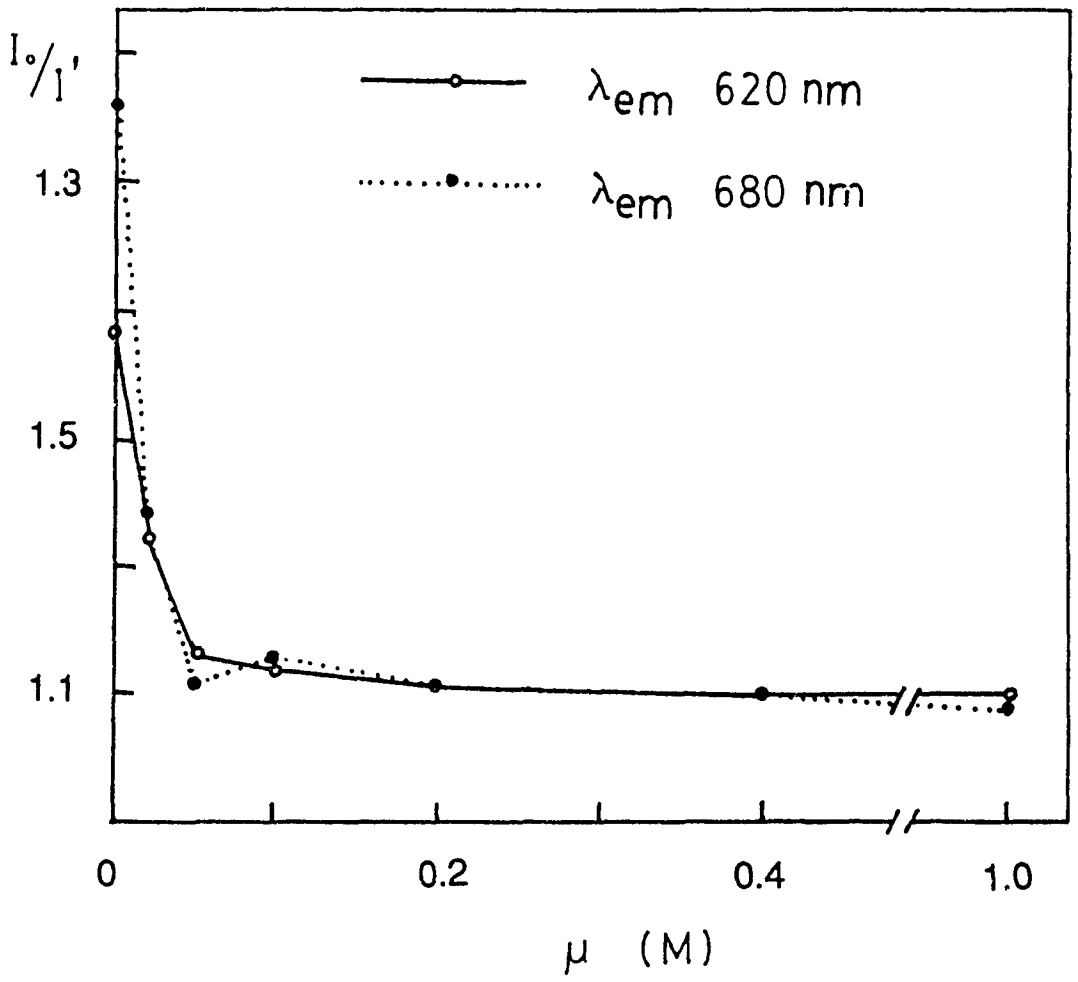

4.3.2 Fluorescence polarization:

Further evidence for complex formation between CCP and PorC, is obtained from the results of the fluorescence polarization titration of PorC by CCP at 0.01 and 0.1 M phosphate. The polarization (P) values at 505 and 515 nm for PorC vs. CCP(FeIII) are listed in Table 4.2 and plotted in Figures 4.3 A and B. In 0.01 M phosphate the P values for PorC in the absence of CCP are 0.104 (±0.006) and 0.144 (±0.006) at 505 and 515 nm, respectively. The addition of CCP results in an increase in P, and limiting values of P [= 0.147 (±0.006) and 0.200 (±0.008) at 505 and 515 nm, respectively] are observed at [CCP]/[PorC] ≥ 1. On the other hand, the P values at 0.1 M phosphate remain unchanged up to a [CCP]/[PorC] ratio of 2.4 (Table 4.2).

4.3.3 Oxidation of CCP(FeII) by horse C:

Following rapid mixing of CCP(FeII) and C(FeIII) at μ = 0.02 M, the decay at 440 nm and the growth at 420 nm are both exponential (Figure 4.4), and give rise to first order rate constants of 0.22 ± 0.02 s^{-1}. The kinetics are independent of the initial C to CCP ratio used (C:CCP = 1:1, 2:1 and 3:1), and yielded rate constants of 0.22 ± 0.02, 0.24 ± 0.01 and 0.21 ± 0.02 s^{-1}, respectively. After the reaction was complete, the absorption spectrum of the products was examined. When the CCP(FeIII) spectrum is subtracted from the product spectrum at different C/CCP ratios, only a 1:1 stoichiometric amount of C(FeII) is present; at C/CCP ratios higher than 1:1, excess C remains in the oxidized form. Thus, CCP(FeII) is the only reductant in the reaction.

Table 4.2 Fluorescence Polarization (P) of Porphyrin Cytochrome c in the Presence of Ferricytochrome c Peroxidase[a,c]

[CCP]/[PorC][b]	0.01 M Pi		0.10 M Pi	
	P (505 nm)	P (515 nm)	P (505 nm)	P (515 nm)
0.00	0.104	0.144	0.099	0.130
0.16	0.105	0.146	0.099	0.130
0.32	0.124	0.161	0.096	0.131
0.48	0.123	0.172	0.092	0.132
0.64	0.132	0.186	0.096	0.130
0.80	0.135	0.188	0.093	0.130
0.96	0.137	0.192	0.091	0.135
1.12	0.142	0.193	0.095	0.135
1.28	0.136	0.196	0.102	0.132
1.44	0.141	0.195	0.096	0.132
1.60	0.143	0.197	0.097	0.131
1.76	0.139	0.191	0.097	0.130
1.92	0.140	0.201	0.102	0.135
2.08	0.147	0.204	0.099	0.128
2.24	0.144	0.202	0.097	0.142
2.40	0.147	0.200	0.099	0.132

[a]In 0.01 and 0.1 M phosphate buffer, pH 7.0, 24°C.

[b]The concentration of porphyrin cytochrome c (PorC) was 3.0 μM, and the ferricytochrome c peroxidase (CCP) concentration was varied between 0 - 7.2 μM.

[c]λ_{ex} = 505 and 515 nm, λ_{em} = 620 nm, emission grating correction factor G = 0.48, standard error of P values < ± 4%.

Figure 4.3

Fluorescence polarization of porphyrin cytochrome c (3.0 μM) vs. the ratio of ferricytochrome c peroxidase to porphyrin cytochrome c. (A) Polarization measured at 505 nm in phosphate buffer, pH 7.0, μ = 0.02 and 0.2 M. (B) Polarization measured at 515 nm under the same conditions as in (A).

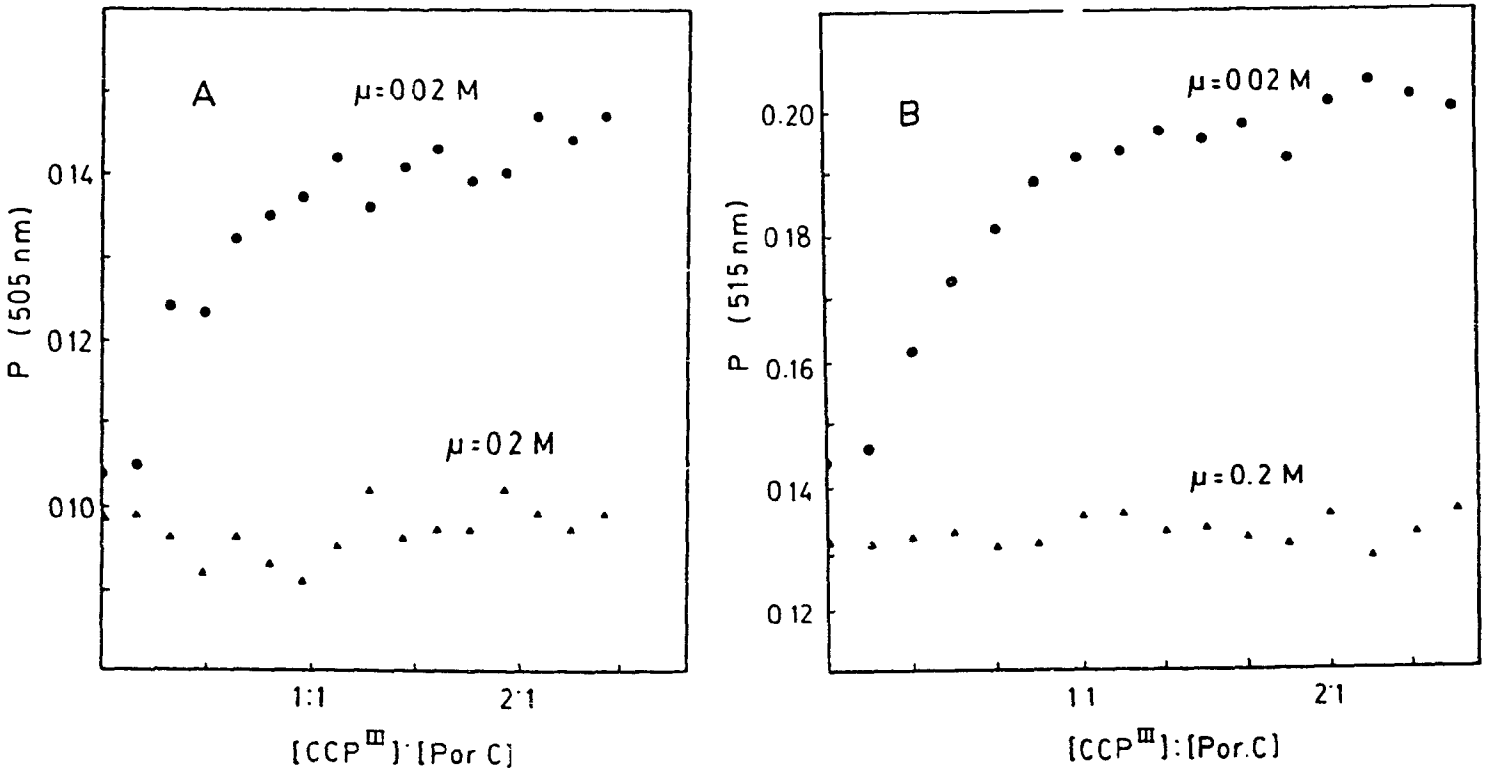

Figure 4.4

The oxidation of 3.0 μM CCP(FeII) by 3.0 μM horse C(FeIII) at 0.02 M ionic strength. Change in absorbance (Δ_{Abs}) due to C(FeII) accumulation (420 nm) and CCP(FeII) decay (440 nm) vs. time following rapid mixing of the reagents in 0.01 M phosphate buffer, pH 7.0, 24 ± 1 °C.

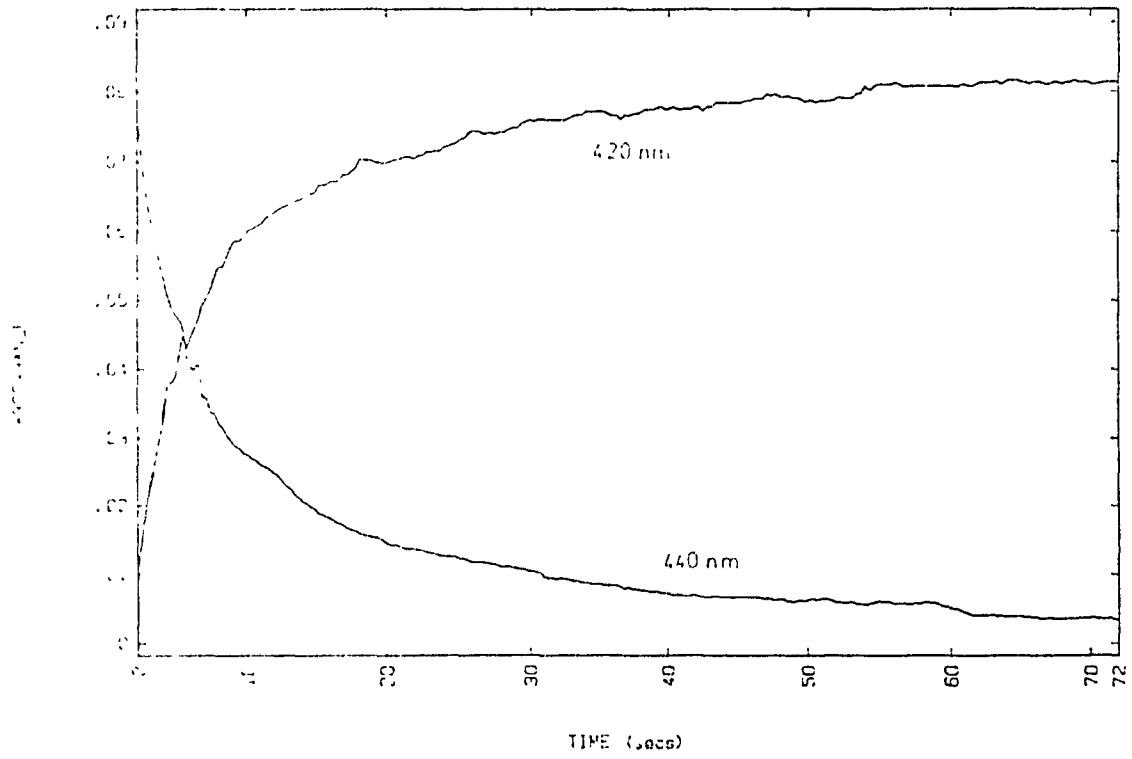

At μ = 0.20 M, the observed rate is reduced to 0.02 ± 0.002 s^{-1}. Again, the kinetics are strictly first order and the measured rate constants are independent of the C/CCP ratios between 1:1 and 3:1. This is unexpected since the binding studies (Sections 4.3.1 and 4.3.2) indicate that the CCP:C complex is essentially dissociated at high ionic strength which should give rise to bimolecular kinetics. The observation of unimolecular kinetics at high ionic strength suggests that a rate-limiting process may precede the bimolecular electron transfer steps.

The reaction at μ = 0.05 M cannot be fitted by first- or second-order kinetics, but a detailed analysis of these data using eq.4.2 and eq.4.3 reveals biphasic kinetics with two first-order rate constants of 0.2 s^{-1} and 0.02 s^{-1} (Figure 4.5). The ß value (the fraction of the fast component of the biphasic reaction) at μ = 0.05 M is determined to be 0.5 ± 0.1. Values of ß, k_f and k_s for the reduction of horse C(FeIII) at different ionic strengths are collected in Table 4.3.

4.3.4 Dependence of oxidation kinetics on the sequence of C:

When the CCP(FeII) oxidation (eq.4.1) is carried out using yeast C (S. cerevisiae) instead of horse C, biphasic kinetics are observed up to μ = 0.20 M. The absorbance data were also analyzed by eq.4.3, and the results are given in Table 4.4. In this instance, k_f decreases from 1.6 ± 0.5 s^{-1} to 0.6 ± 0.1 s^{-1} when the ionic strength is increased from 0.02 to 0.20 M, while k_s remains constant at ≈ 0.03 ± 0.01 s^{-1}, which is similar to the k_s obtained using horse C. ß is much less sensitive to the salt concentration than in the horse

Figure 4.5

Kinetic analysis of the oxidation of yeast CP(FeII) by horse C(FeIII) at μ = 0.05 M. Plot of ln ΔA_t vs. time for the absorbance data at 420 nm (black dots), and fit of these data to two first-order processes (solid line). The reaction was carried out using 3.0 μM horse C(FeIII) and 3.0 μM CCP(II) in 0.025 M phosphate buffer, pH 7.0, 24 ± 1 °C.

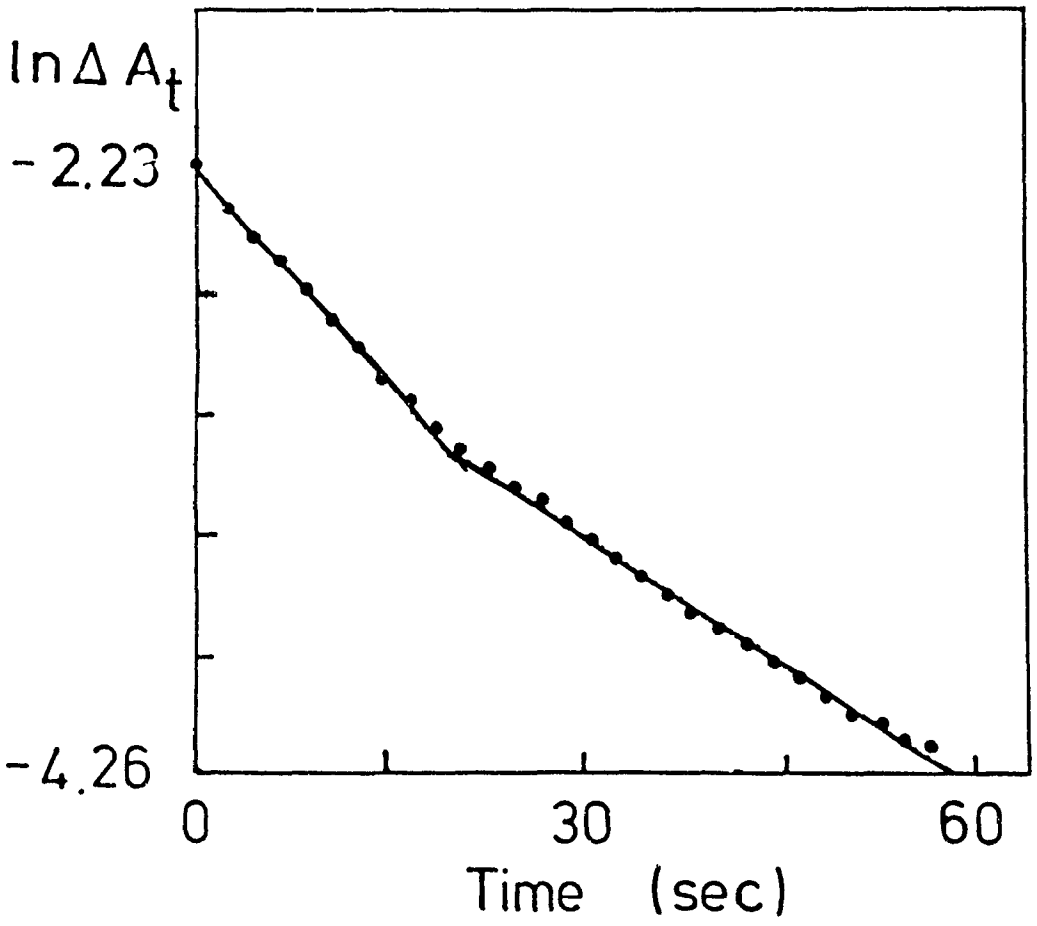

Table 4.3 Kinetic Analysis of the Oxidation of Ferrocytochrome c Peroxidase by Horse Ferricytochrome c vs. Ionic Strength[a,b]

μ (M)[a]	k_f (s^{-1})[b]	k_s (s^{-1})[b]	ß[c]
0.01	0.22 (2)	-	>0.9
0.02	0.23 (2)	0.02 (2)	0.8 (0.5)
0.05	0.20 (3)	0.03 (1)	0.5 (1)
0.1	-	0.02 (0.4)	0.2 (0.5)
0.2	-	0.02 (0.2)	0
0.4	-	0.02 (0.2)	0
1	-	0.02 (0.2)	0

[a]Estimated ionic strength of the phosphate buffers, pH 7.0, 24 °C.

[b]The kinetic traces were analysed as outlined in Section 4.2.4. k_f and k_s are the first-order rate constants for the fast and slow phases, respectively. The numbers in brackets are the errors in the rate constants in units of the last digit.

[c]ß is the fraction of the fast phase (see eq.4.3) at a given μ, and the numbers in brackets are the errors in ß in units of the last digit.

Table 4.4 Kinetic Analysis of the oxidation of Ferrocytochrome c Peroxidase by Yeast[d] Ferricytochrome c vs. Ionic Strength[a]

μ (M)[a]	k_f (s^{-1})[b]	k_s (s^{-1})[b]	ß[c]
0.02	1.6 (5)	0.04 (1)	0.8 (1)
0.05	1.2 (2)	0.04 (1)	0.7 (1)
0.1	0.7 (1)	0.03 (1)	0.7 (1)
0.2	0.6 (1)	0.03 (1)	0.6 (1)
0.4	-	0.03 (0.3)	0
1.0	-	0.02 (0.3)	0

[a] [c]Refer to Table 4.3.

[d]From Saccaromyces cerevisiae.

C reactions, since it only drops from 0.8 to 0.6 between μ = 0.02 and 0.20 M, compared to the drop from 0.9 to 0.5 for horse C between μ = 0.01 and 0.05 M. In Table 4.5, kinetic analyses are given for the reduction of five C's at μ = 0.02 M. The k_f values for yeast (cerevisiae), horse and tuna C's (1.6 ± 0.5, 0.23 ± 0.2 and 0.52 ± 0.08 s^{-1}, respectively) are similar to the electron transfer rates, k_{el}, between CCP(FeII) and C(FeIII) obtained by pulse radiolysis in 1 mM phosphate, pH 7, [k_{el} = 3.4 ± 0.2, 0.3 ± 0.1 and 0.2 ± 0.1 s^{-1} for yeast, horse and tuna C's, respectively (22)]. For the four eukaryotic C's, the ß values are ≥ 0.7; while for C_{551}, ß = 0.4. Another noteworthy feature of the data in Table 4.5 is the small variation (0.02 - 0.04 s^{-1}) in k_s for the slow phase for all five C's; conversely, k_f for the fast phase differs by an order of magnitude on changing from horse C to yeast C.

4.3.5 Temperature dependence of oxidation reaction:

The temperature dependence of the electron transfer rate between horse C and CCP at μ = 0.02 and 0.20 M was examined in phosphate buffer, pH 7.0. These ionic strengths were chosen since the reaction kinetics are predominantly monophasic (Table 4.3) under these conditions. The rates were measured between 0 and 26 °C because at temperatures higher than 30 °C, CCP(FeII) undergoes a heme-linked transition, which gives rise to a species with a Soret maximum at 428 nm. This temperature-induced transition is fully reversible and parallels the acidic-alkaline transition of CCP(FeII) (pK_a = 7.7) reported by Conroy et al. at room temperature (16). At pH 8.0, the alkaline form of CCP(FeII)

Table 4.5 Kinetic Analysis of the Oxidation of Ferrocytochrome c Peroxidase by Ferricytochromes c at 0.02 M Ionic Strength[a]

Cytochrome[d]	k_f (s^{-1})[b]	k_s (s^{-1})[b]	ß[c]
Yeast (S)	1.6 (5)	0.04 (1)	0.8 (1)
Yeast (C)	1.7 (5)	0.04 (2)	0.8 (1)
Horse	0.23 (2)	0.02 (2)	0.8 (0.5)
Tuna	0.52 (8)	0.04 (2)	0.7 (0.5)
C_{551}	0.65 (5)	0.02 (2)	0.4 (0.5)

[a] 'refer to Table 4.3.

[d]Yeast (S) and (C) denote cytochrome c from Saccaromyces cerevisiae and Candida krusei, respectively.

(Soret maximum at 428 nm) can be converted to a species spectrally similar to the acidic form (Soret maximum at 440 nm) by reducing the temperature below 10 °C.

The observed rate constants at μ = 0.02 and 0.2 M are listed in Table 4.6 and Eyring plots are shown in Figure 4.6. At μ = 0.02 M, the rate constant decreases from 0.23 to 0.11 s^{-1} on reducing the temperature from 24 to 0 °C; however, at μ = 0.20 M, the observed rates decrease 10-fold over the same temperature range (Table 4.6).

To determine if the kinetics are dependent on specific ion effects, the temperature dependence of electron transfer was also investigated in 0.01 M phosphate buffer containing 0.10 M KCl, and the results are also included in Table 4.6. The observed rate constants, as well as the temperature dependence are essentially the same in the 0.1 M KCl and 0.1 M phosphate solutions. Therefore, it is unlikely that the unimolecular kinetics at high salt results from phosphate binding to either of the proteins.

The analysis of the temperature dependence of the rates gives similar free energies of activation ($\Delta G^{\#}$) at each ionic strength ($\mu \approx$ 0.02, 0.1 and 0.2 M, $\Delta G^{\#}$ = 18, 20 and 20 kcal mol^{-1} respectively; Table 4.7). However, the entropies ($\Delta S^{\#}$) and enthalpies ($\Delta H^{\#}$) of activation at low and high ionic strength are significantly different (μ = 0.02 and 0.2 M, $\Delta H^{\#}$ = 17 and 4.6 kcal mol^{-1} and $\Delta S^{\#}$ = -7.8 and -46 eu, respectively).

4.4 Discussion:

4.4.1 Oxidation reaction mechanism at low ionic strength:

At μ = 0.02 M, the reaction kinetics of CCP(FeII) with horse C are dominated by the

Table 4.6 Temperature Dependence of the Oxidation of Ferrocytochrome c Peroxidase by Horse Ferricyctochrome c in Phosphate Buffers, pH 7.0[a]

μ ≈ 0.02 M (0.01 M Pi)		μ ≈ 0.2 M (0.1 M Pi)		μ ≈ 0.1 M (0.1 M KCl[b])	
T (°C)	k_{obs} (s^{-1})	T (°C)	k_{obs} (s^{-1})	T (°C)	k_{obs} (s^{-1})
0	0.11	0	0.0015	4	0.0020
5	0.12	8	0.0032	9	0.0041
8	0.15	16	0.0086	13	0.0059
18	0.18	24	0.020	16	0.0090
24	0.23			21	0.015
				26	0.025

[a]The error in the observed rate constants is <10 %.

[b]0.1 M KCl in 0.01 M phosphate buffer, pH 7.0 (see Section 4.3.5).

Figure 4.6

Eyring plots of ln(k/T) vs. 1/T for the oxidation of ferrocyochrome c peroxidase by horse ferricytochrome c in 0.01 M ($\mu \approx 0.02$ M) and 0.1 M ($\mu \approx 0.2$ M) phosphate buffers, pH 7.0. Data from Table 4.6.

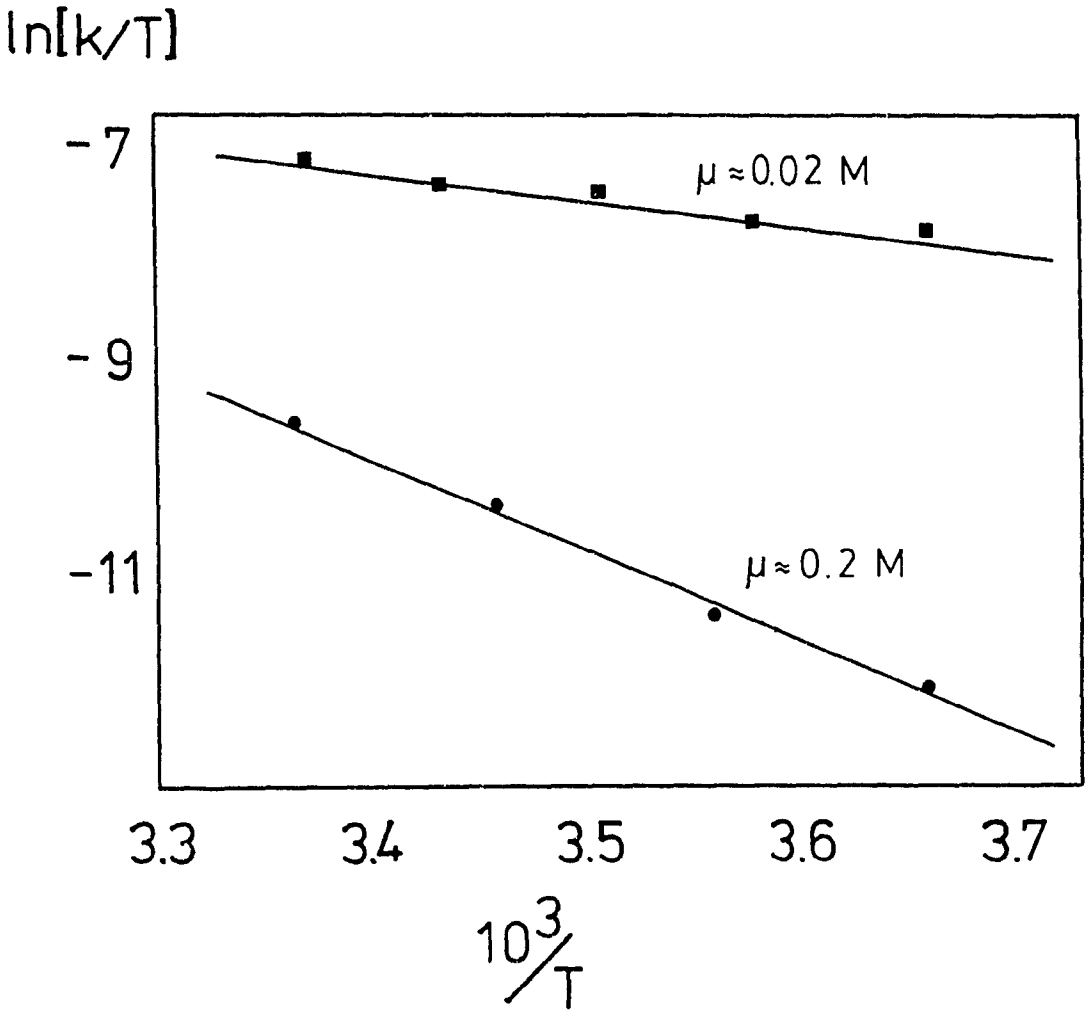

Table 4.7 Activation Parameters in the Oxidation of Ferrocytochrome c Peroxidase by Horse Ferricytochrome c in Phosphate Buffers, pH 7.0[a]

	$\mu \approx 0.02$ M (0.01 M Pi[b])	$\mu \approx 0.2$ M (0.1 M Pi[b])	$\mu \approx 0.1$ M (0.1 M KCl[c])
$\Delta G^{\#}$ (kcal mol^{-1})[d]	18 (11)	20 (0.8)	20 (0.4)
$\Delta H^{\#}$ (kcal mol^{-1})	4.6 (0.5)	17 (0.8)	17 (0.4)
$\Delta S^{\#}$ (eu)	-46 (30)	-7.8 (0.1)	-7.9 (0.1)

[a]The activation parameters were determined from Eyring plots of ln(k/T) vs. 1/T using the data in Table 4.6. Standard errors are listed in brackets. Correlation coefficient = 0.959, 0.996 and 0.997 for the plots using data obtained at $\mu \approx 0.02$, 0.2 and 0.1 M, respectively.

[b,c]Refer to Table 4.6.

[d]Calculated at T = 295 K.

fast phase (ß = 0.8) with k_f = 0.2 s^{-1}. The fluorescence quenching data show that at the same ionic strength, PorC emission is efficiently quenched (I_o/I' = 1.24 at 680 nm; Table 4.1). The quenching at low ionic strength is most probably due to the binding of CCP and PorC since an increase in the polarization (P) of PorC upon the addition of CCP is also observed. Furthermore, the levelling-off of P (Figure 4.3) at [CCP]/[PorC] = 1 indicates the formation of a 1:1 PorC:CCP complex. Thus, the fast phase of the redox reaction most probably arises from electron transfer within the CCP(FeII):C(FeIII) complex. These results support a reaction scheme involving rapid complex formation between the proteins on mixing, followed by slow electron transfer within the complex (Scheme I):

$$\text{C(FeIII)} + \text{CCP(FeII)} \underset{k_2}{\overset{k_1}{\rightleftharpoons}} \text{C(FeIII):CCP(FeII)} \xrightarrow{k_{el}} \text{C(FeII):CCP(FeIII)} \qquad \text{(Scheme I)}$$

where the colon denotes noncovalent complexation and the observed rate constant, k_{obs}, is given by

$$k_{obs} = \frac{k_{el}\,[\text{C(FeIII)}]}{K_d + [\text{C(FeIII)}]} \qquad \text{(eq.4.4)}$$

where $K_d = k_2/k_1$. Using absorbance difference (17) and fluorescence quenching (14)

measurements, K_d's of ≈0.1 μM were reported for the C(FeIII):CCP(FeIII) and PorC:CCP(FeIII) complexes at μ = 0.02 M, pH 6.0. Therefore, it is reasonable to assume that under our experimental conditions the K_d for the C(FeIII):CCP(FeII) complex is also ≈0.1 μM at μ = 0.02 M. Since [C(FeIII)] >> K_d, thus, $k_{obs} = k_{el}$.

4.4.2 Oxidation reaction mechanism at high ionic strength:

At μ = 0.2 M, binding of PorC and CCP is not detected by the methods used in the present study. The K_d estimated by other studies (14, 17) was ≈0.1 mM. Thus, at the protein concentration (≤ 3 μM) used, complexation is not expected. In fact, electron transfer between C and CpdI is clearly second-order at high ionic strength (18), which is further evidence for dissociation of the CCP:C complex at high salt.

Since phosphate is known to bind to C (19) and possibly also to CCP (20), it is necessary to establish that the rate-limiting step in 0.1 M phosphate is not due to phosphate dissociation from the proteins. The kinetics in 0.1 M KCl are identical to those observed in 0.1 M phosphate for oxidation by horse C (Table 4.6); therefore, we conclude that ion-specific binding effects are not involved in the rate-limiting steps.

The occurrence of first-order kinetics at μ = 0.2 M raise the possibility of a more complex reaction mechanism than that given in Scheme I. Since the observed rate constants are independent of protein concentration, an unimolecular rate-limiting step must precede protein association at high ionic strength. A reaction scheme that involves a slow conformational change of CCP(FeII) prior to the electron transfer step is proposed:

$$\text{CCP(FeII)} \underset{k_2}{\overset{k_1}{\rightleftharpoons}} {}^{*}\text{CCP(FeII)} + \text{C(FeIII)}$$

$$k_3 \Big\downarrow \quad \Big\uparrow k_4 \qquad \text{(Scheme II)}$$

$$\text{C(FeIII)}:{}^{*}\text{CCP(FeII)} \xrightarrow{k_{el}} \text{C(FeII)}:\text{CCP(FeIII)}$$

where k_1 is the rate constant for the CCP conformational change which gives *CCP(FeII). k_{obs} for the reduction of C(FeIII) by Scheme II is given by eq.4.5:

$$k_{obs} = \frac{k_1 k_3 k_{el} [\text{C(FeIII)}]}{(k_2 + k_3 [\text{C(FeIII)}])(k_4 + k_{el}) - k_3 k_4 [\text{C(FeIII)}]} \qquad \text{(eq.4.5)}$$

Since the association of C and CCP is diffusion-controlled, we assume that k_3 [C(FeIII)] >> k_2; therefore, $k_{obs} = k_1$.

Evidence for a kinetic barrier due to a protein conformational change prior to electron transfer comes from a comparison of the activation parameters at high and low salt concentrations. At μ = 0.02 M, the reaction is moderately temperature dependent ($\Delta H^{\ddagger}$ = 4.6 kcal mole^{-1}, $\Delta S^{\ddagger}$ = -46 eu), whereas, at μ = 0.2 M the reaction is strongly temperature dependent ($\Delta H^{\ddagger}$ = 17 kcal mole^{-1}, $\Delta S^{\ddagger}$ = -7.8 eu). Such a large variation in the observed activation parameters supports a change in mechanism at high ionic strength. A high

enthalpy is not expected for electron transfer; for example, $\Delta H^{\#}$ measured for intracomplex electron transfer in covalently-linked $Ru(NH_3)_5$-cytochrome c is < 1.5 kcal mol^{-1} (25).

In summary, it is concluded that at low ionic strength, electron transfer between the bound proteins is at least partially rate-limiting. However, rearrangement of the protein interface cannot be eliminated, since the contribution of rearrangement to the overall $\Delta H^{\#}$ at low ionic strength cannot be resolved in the present study. At high ionic strength, the observed first-order kinetics are rationalized by a mechanism that involves a slow conformational change of CCP(FeII) prior to the electron transfer (Scheme II).

4.4.3 Electrostatic effects on the reaction kinetics using different species of C:

The observed first-order rate constants (k_f) as well as the ß values for the fast phase show a significant species-dependency (Table 4.5). At μ = 0.02 M, where ß for both C's are >0.8, the reactivity of yeast C ($k_f = 1.6 \pm 0.5\ s^{-1}$) is about eight times higher than horse C ($k_f = 0.23 \pm 0.02\ s^{-1}$). This is not surprising since yeast C should be the best adapted to yeast CCP. On the other hand, C_{551} is expected to be the poorest partner for CCP due to the large difference in sequence between bacterial and eukaryotic cytochromes (21). However, the relatively large k_f for C_{551} reduction suggests an efficient electron transfer pathway, but the low ß value in Table 4.5 shows that the reactivity edge of C_{551} over the tuna and horse C's is rapidly lost since the reaction favors the slow component (ß = 0.4) even at relatively low ionic strength (μ = 0.02 M). Other measurements of nonphysiological intracomplex electron transfer in the PorC:CCP (22)

and C:ZnCCP complexes, where ZnCCP is the Zn-substituted protein (23), also show species-dependent rates with the yeast C rates ~10 times faster than the horse or tuna rates.

The observed first-order rate constants for the slow phase (k_s) are essentially independent of the sequence of C (Table 4.5). This observation corroborates the high salt mechanism (eq.4.6) proposed above for the reduction of horse C by CCP, where the rate limiting step is assigned to a conformation change of free CCP(FeII) to *CCP(FeII). On the formation of a transient complex, rapid reduction of C(FeIII) by *CCP(FeII) follows the rate-limiting step.

The biphasic kinetics at intermediate ionic strengths are attributed to the existence of low and high salt forms of CCP(FeII). CCP(FeIII) was previously assigned low and high salt forms to explain its biphasic enzyme kinetics (24). The steady-state enzyme kinetics reveal large changes in V_{max}, with little change in K_m, on changing ionic strength, and the oxidation of both horse and yeast C(FeII) by CpdI is biphasic at ionic strengths similar to those where the ß values are ≈0.5 in the present study. Kang et al. (24) proposed the presence of low and high salt forms of CCP(FeIII) to account for this observation and suggested that yeast and horse C stabilize the high and low salt forms, respectively. Since optimal enzyme activity at saturating H_2O_2 requires minimal binding and maximal electron transfer rates between the proteins, these ionic strengths must represent the best compromise values for the binding and redox rates. If high and low salt forms of CCP do exist, then the conformation change, CCP(FeII) ⇌ *CCP(FeII), proposed in Scheme II, must occur in the high salt form. The low salt form of CCP(FeII) may undergo a similar

con.· rmation change, but such a transition would obviously not be rate-limiting in electron transfer to C(FeIII).

The results presented in this study are in contrast to the oxidation of CCP(FeII) by ferricyanide (Chapter 3), where bimolecular kinetics are observed under all experimental conditions, suggesting that the inorganic redox reagent does not discriminate between the two forms of CCP(FeII). A different reaction mechanism is also involved, an observation which is expected for reactions that are not regulated by protein-protein interactions.

4.5 **References**:

1 Poulos, T.L.; and Kraut, J.; J. Biol. Chem. 1980, 255, 8199.

2 Swanson, R., Mandel, N., Mandel, G., Kallai, O.B., Trus, B.L., Dickerson, R.E., J. Biol. Chem. 1977, 252, 759.

3 Poulos, T.L.; and Kraut, J.; J. Biol. Chem. 1980, 255, 10322.

4 Poulos, T.L.; and Finzel, B.C.; Protein Peptide Rev. 1984, 4, 115.

5 Leonard, J.J.; and Yonetani, T.; Biochem. 1974, 13, 1465.

6 Kang, D.S.; and Erman, J.E.; J. Biol. Chem. 1982, 257,12775.

7 Dowe, R.J.; Vitello, L.R.; and Erman, J.E.; Arch. Biochem. Biophys. 1984, 232, 566.

8 Both, L.R.; and Erman, J.E.; Biochim. Biophys. Acta. 1984, 788, 151.

9 Coulson, A.F.W.; Erman, J.E.; and Yonetani, T.; J. Biol. Chem. 1971, 246, 917.

10 Jordi, H.C.; and Erman, J.E.; Biochem. 1974, 13, 3734.

11 Poulos, T.L., et al.; J. Biol. Chem. 1982, 257, 6073.

12 Waldmeyer, B.; and Bosshard, H.R.; J. Biol. Chem. 1985, 260, 5184.

13 Bechtold, R.; and Bosshard, H.R.; J. Biol. Chem. 1985, 260, 5191.

14 Kornblatt, J.A.; and English, A.M.; Eur. J. Biochem. 1986, 155, 505.

15 English, A.M.; and Achkouti, C.M.; Inorg. Chim. Acta. 1986, 123, 41.

16 Conroy, C.W., Tuma, P., Daum, P.H., Erman, J.E., Biochim. Biophys. Acta. 1978, 537, 62.

17 Erman, J.E.; and Vitello, L.B.; J. Biol. Chem. 1980, 255, 6224.

18 Hazzard, J.T.; Poulos, T.L.; and Tollin, G.; Biochem. 1987, 26,2836.

19 Osheroff, N.; Brautigan, D.L.; and Margoliash, E.; Proc. Natl. Acad. Sci. USA 1980, 77, 4439.

20 Smulevich, G., Evangelista-Kirkup, R., English, A.M., Spiro, T.G., Biochem. 1986, 25, 4426.

21 Dickerson, R.E.; Scientific American 1980, 242, 136, and references therein.

22 Cheung, E., Taylor, K., Kornblatt, J.A., English, A.M., McLendon, G., Miller, J.R., Proc. Natl. Acad. Sci. USA. 1986, 83, 1330.

23 Ho, P.S., Sutoris, C., Liang, N., Mangoliash, E., Hoffman, B.M., J. Am. Chem. Soc. 1985, 107, 1070.

24 Kang, C.H.; Ferguson-Miller, S.; and Margoliash, E.; J. Biol. Chem. 1977, 252, 919.

25 Nocera, D.G., Winkler, J.R., Yocum, K.M., Bordignon, E., Gray, H.B., J. Am. Chem. Soc., 1982, 104, 5145.

26 Strottmann, J.M., Stellwagen, A., Bryant, C. and Stellwagen, Eur. J. Biol. Chem. 1984, 259, 6931.

27 Lakowicz, J.R., Maliwal, B.P., Cherek, H. and Balter, A. Biochem. 1983, 22, 1741

28 Dixit, B.P., Waring, A.J., Wells, K.O., Wong, P.S., Woodrow, G.V., Vanderlooi, J.M. Eur. J. Biochem. 1982, 126, 128.

29 Vitello, L.B. and Erman, J.E. Arch. Biochem. Biophys. 1987, 258, 621

Chapter 5

SUMMARIES AND SUGGESTIONS FOR FUTURE STUDIES

5.1 Summaries:

5.1.1 Reactions between proteins and inorganic complexes:

The interactions between cytochrome c (C) and ruthenium polypyridine complexes (Ru^*L_3) can be classified as (i) hydrophobic and (ii) electrostatic. Since no electrostatic effect is observed in the quenching of ruthenium complexes with neutral polypyridine ligands (ie. bpy, phen and DIP), the charge on the ruthenium metal appears to be insulated by these π conducting ligands. The observed static quenching of $Ru^*(DIP)$ suggests binding of the complex tc C(FeIII), probably at a hydrophobic region of the protein surface near the exposed heme edge because of the high quenching efficiency. Electrostatic effects are most significant for the quenching of $Ru^*(DIPS)_3^{4-}$ which has negatively charged sulfonic groups on it surface. Based on the observed saturation kinetics for the quenching of $Ru^*(DIPS)_3^{4-}$ at μ = 0.01 M, it is speculated that an electrostatically stabilized precursor complex between the protein and the $Ru(DIPS)_3^{4-}$ is involved in the reaction mechanism. Also, the ionic strength dependence of the Φ_{max} values for the $Ru^*(DIPS)_3^{4-}$ photosensitized steady-state reduction of C(FeIII) is consistent with strong electrostatic interactions between this complex and C, since Φ_{max} = 0.0039 and 0.158 for $Ru^*(DIPS)_3^{4-}$ at μ = 0.07 and 0.16 M, respectively.

The large K_{sv} ($= k_q\tau_o$) values for $Ru(phen)_3^{2+}$ and $Ru(bpy)_3^{2+}$ obtained from the steady-state experiments are 5- to 26-fold greater than those calculated from the lifetime data. It is possible that the increase is caused by the ion pairing of the anionic EDTA (present in the steady-state experiments) with C and $Ru(phen)_3^{2+}$ or $Ru(bpy)_3^{2+}$. The small (< 1.7-fold) increase in the K_{sv} of $Ru(DIPS)_3^{4-}$ relative to K'_{sv} is expected, since ion pair formation between two negatively-charged species is unlikely.

The oxidation of CCP(FeII) by $Fe(CN)_6^{3-}$ follows bimolecular kinetics and exhibits marked dependence on the ionic strength of the medium at pH 7.0. The results allow an estimate of -9 for the surface charge of CCP(FeII) at pH 7.0. The self-exchange rate constant (k_{11}^{∞}) calculated for the FeIV/III couple is 4 orders of magnitude slower than that of the CCP(FeII/III) couple. The k_{11}^{∞} for the FeII/III couple of CCP is ~5 orders of magnitude slower than k_{11}^{∞} for the FeIII/II couple of myoglobin and ~8-9 orders of magnitude slower than that of the c type cytochromes.

5.1.2 Reaction between C and CCP:

The direct oxidation of CCP(FeII) by C(FeIII) shows biphasic kinetics with fast and slow unimolecular rates dominating at low and high ionic strengths, respectively. The rate constants measured at μ = 0.02 M for yeast (Saccaromyces), horse and tuna C's agree with those obtained by pulse radiolysis in 1 mM phosphate (1). Results from the fluorescence polarization studies show that a 1:1 CCP:C complex is formed at μ = 0.02 M but not at μ = 0.2 M. Thus, the k_f represents the oxidation rate of CCP(FeII) by C(FeIII) within the CCP:C complex. At μ = 0.2 M, the measured rate constants are

independent of the sequence of C. Since the binding between the two proteins is abolished, it is speculated that the measured first-order rate constants represent the conversion of CCP(FeII) to an intermediate *CCP(FeII) prior to the electron transfer. This interpretation is supported by the temperature dependence of the reaction at μ = 0.02 and 0.2 M. The measured activation enthalpies and entropies are 4.6 kcal mol^{-1} and -46 eu at μ = 0.02 M, and 17 kcal mol^{-1} and -7.8 eu at μ = 0.2 M. The high activation enthalpy at μ = 0.2 M supports a reaction mechanism that involves a conformational change of CCP(FeII) as a rate determining step. A likely candidate for such a change is the acidic-alkaline transition of CCP (2,3). At pH 7.0, a temperature-inducible absorption spectral shift at the Soret region at T $\approx$ 30 °C was observed, and this spectral shift is identical to that observed for the acidic-alkaline transition of CCP(FeII) by changing the pH from 7.0 to 8.0.

5.2 **Suggestions For Future Studies**:

1. In order to fully understand the photochemical processes involved in the Ru^*L_3 reactions with C, a few key questions have to be addressed: (i) The rate constant for $Ru^*(bpy)_3^{2+}$ quenching by C(FeIII) is about 4 times higher than the literature value. This discrepancy raises the question of the dependence of k_q on the excitation wavelength. Therefore, the effect of excitation wavelength on the quenching rate constants should be investigated. (ii) Results from the steady-state Ru^*L_3-photosensitized reduction of C(FeIII) indicate that quenching rates may increase in the presence of EDTA; thus, quenching rate constants should be measured in the presence of EDTA. (iii) To date, no direct evidence

has been reported for the reductive quenching of Ru^*L_3 by C(FeII). Recently, hexamethyl-tetraazacyclodecane-Nickel(II) ($Ni^{2+}Me_6ane$) has been employed as scavenger for $Ru(bpy)_3^{1+}$ (4). It may be possible to identify the quenching of Ru^*L_3 by C(FeII) as an electron transfer process.

2. The dependence of the electron transfer rate constant (k_{el}) on the donor-acceptor separation has been analyzed by Marcus and Sutin (5) using the following empirical equation: $k_{el} = A \exp(-\alpha R)$, where A = preexponenial factor, α = electronic coupling factor and R = separation distance. Substituting the values for A (= 10^{13} s^{-1}), α (= 1.2 $Å^{-1}$) and assuming the decay rate constant at saturation (k_{sat} = 3 x 10^6 s^{-1} at μ = 0.01 M) for the quenching of $Ru^*(DIPS)_3^{4-}$ by C(FeIII) equals to k_{el}, a separation distance of 12.5 Å is estimated between the donor and acceptor. In order to establish that $k_{sat} = k_{el}$, the presence of electron transfer products generated by the quenching of $Ru^*(DIPS)_3^{4-}$ by C(FeIII) should be examined by transient absorption measurements. Similar experiments on CCP should also be carried out, and the results obtained could be used to compare differences in the heme accessibility of C and CCP.

3. In the direct oxidation of CCP(FeII) by C(FeIII), an interesting observation is that biphasic kinetics (50 % fast and 50% slow phase) occur at μ = 0.2 M for yeast C and μ = 0.05 M for horse C. These ionic strengths correspond to the conditions that give the highest catalytic rate for the respective C's in the CCP-catalyzed steady-state oxidation of C(FeII). Thus, C and CCP reaction kinetics are highly dependent on the sequence of the C and ionic strength. The effects of protein-protein complex formation on the observed reaction kinetics are further demonstrated by porphyrin cytochrome c (PorC)

fluorescence intensity quenching, and fluorescence polarization titrations in the presence of CCP(FeIII). Since only PorC isolated from horse heart was used here, it would be of interest to repeat the fluorescence intensity quenching and polarization measurements using yeast PorC.

5.3 References:

1 Cheung, E., Taylor, K., Kornblatt, J.A., English, A.M., McLendon, G., Miller, J.R., Proc. Natl. Acad. Sci. USA. 1986, 83, 1330.

2 Yonetani, T., Wilson, D.F., and Seamonds, B., J. Biol. Chem. 1966, 241, 5347.

3 Conroy, C.W., Tyma, P., Daum, P.H. and Erman, J.E., Biochim. Biophys. Acta, 1978, 537, 62.

4 Lieber, C.M., Karas, J.L., and Gray, H., J. Am. Chem. Soc., 1987, 109, 3778.

5 Marcus, R.A., Sutin, N., Biochim. Biophys. Acta, 1985, 811, 265.

Appendix A

Emission Lifetimes of Ruthenium(II)polypyridyl Excited States in the Presence of Cytochrome c

The emission lifetime (τ) at different cytochrome c concentrations [Q] are listed in the following tables. Measurements were carried out using 100 µl of deoxygenated samples containing 20 µM Ruthenium(II) polypyridyl complex with different amount of cytochrome c in phosphate (pH 7.0) or biphthalate (pH 3.0 or 4.0) buffers, at 24 ± 1 °C. Photoexcitation at 337 nm was carried out using a 300-ps pulse from a nitrogen laser, and the emission intensity was monitored at 610 nm. Instrumental set up and experimental procedures are described in Section 2.3.3 and in Figure 2.2.

Table 1 Emission Lifetimes of $Ru(phen)_3^{2+}$ vs. Ferricytochrome c Concentration at pH 7.0

µ = 0.1 M		µ = 0.01 M	
[Q] (mM)	τ (ns)	[Q] (mM)	τ (ns)
0	1027	0	932
0.10	907	0.10	851
0.30	798	0.21	786
0.40	642	0.31	689
0.50	695	0.42	615
0.60	541	0.52	580
0.80	510	0.62	536
1.0	463	0.83	464
1.2	428	1.04	412
1.4	381		
1.6	333		

Table 2 Emission Lifetimes of $Ru(phen)_3^{2+}$ vs. Ferrocytochrome c Concentration at pH 7.0

μ = 0.1 M		μ = 0.01 M	
[Q] (mM)	τ (ns)	[Q] (mM)	τ (ns)
0	1058	0	964
0.09	928	0.10	899
0.18	902	0.22	806
0.27	885	0.33	769
0.30	868	0.44	691
0.40	790	0.55	689
0.44	750	0.66	652
0.50	769	0.77	594
0.70	676	0.88	578
0.79	616	0.99	552
0.88	586		
0.97	586		
1.06	564		

Table 3 Emission Lifetimes of $Ru(phen)_2(CN)_2$ vs. Ferricytochrome c Concentration at pH 7.0

μ = 0.1 M		μ = 0.01 M	
[Q] (mM)	τ (ns)	[Q] (mM)	τ (ns)
0	686	0	636
0.25	533	0.05	629
0.5	469	0.1	589
0.75	417	0.16	564
1.0	395	0.21	548
1.25	314	0.26	533
1.5	284	0.31	515
1.75	273	0.37	493
2.0	239	0.42	484
2.25	231	0.47	454

Table 4 Emission Lifetimes of $Ru(phen)_2(CN)_2$ vs. Ferrocytochrome c Concentration at pH 7.0

μ = 0.1 M		μ = 0.01 M	
[Q] (mM)	τ (ns)	[Q] (mM)	τ (ns)
0	716	0	650
0.14	647	0.10	613
0.28	639	0.20	553
0.42	582	0.30	505
0.56	567	0.40	454
0.83	509	0.50	419
1.11	462	0.60	404
1.39	403	0.70	382
1.94	346	0.80	364
		0.90	342

Table 5 Emission Lifetimes of $Ru(bpy)_3^{2+}$ vs. Ferricytochrome c Concentration at pH 7.0

μ = 0.1 M		μ = 0.01 M	
[Q] (mM)	τ (ns)	[Q] (mM)	τ (ns)
0	618	0	621
0.1	554	0.2	546
0.2	550	0.4	500
0.3	512	0.5	482
0.4	467	0.6	455
0.5	474	0.8	421
0.6	427	0.9	398
0.8	413	1.0	382
0.9	407	1.2	379
1.0	385		
1.2	347		
1.4	350		
1.6	333		
1.8	310		
2.0	295		

Table 6 Emission Lifetimes of $Ru(bpy)_3^{2+}$ vs. Ferrocytochrome c Concentration at pH 7.0

μ = 0.1 M		μ = 0.01 M	
[Q] (mM)	τ (ns)	[Q] (mM)	τ (ns)
0	650	0	608
0.14	629	0.1	588
0.20	610	0.22	553
0.28	581	0.33	526
0.35	579	0.44	508
0.42	575	0.55	490
0.50	552	0.66	476
0.56	533	0.77	465
0.70	524	0.88	436
0.83	492	0.99	424
1.11	467		
1.39	425		
1.94	383		

Table 7 Emission Lifetimes of $Ru(DIPS)_3^{4}$ vs. Ferricytochrome c Concentration at pH 7.0

μ = 0.1 M		μ = 0.01 M	
[Q] (mM)	τ (ns)	[Q] (mM)	τ (ns)
0	3750	0	3730
0.05	2620	0.05	1900
0.10	1960	0.11	910
0.15	1840	0.16	720
0.21	1470	0.19	590
0.26	1290	0.21	495
0.31	1200	0.27	500
0.36	1120	0.32	397
0.41	960	0.42	405
0.46	830	0.53	365
		0.64	375
		0.74	364
		0.86	376
		0.95	365
		1.06	357

Table 8 Emission Lifetimes of $Ru(DIPS)_3^{4-}$ vs. Ferrocytochrome c Concentration at pH 7.0

μ = 0.1 M		μ = 0.01 M	
[Q] (mM)	τ (ns)	[Q] (mM)	τ (ns)
0	3810	0	3835
0.09	2740	0.05	2040
0.19	1940	0.11	1480
0.29	1410	0.16	975
0.39	1320	0.22	787
0.49	1140	0.27	652
0.58	970	0.33	522
0.68	920	0.38	454
0.78	870	0.44	403
0.87	850	0.49	375
0.97	730		

Table 9 Emission Lifetimes of $Ru(bpy)_2(CN)_2$ vs. Ferricytochrome c Concentration at pH 7.0

μ = 0.1 M	
[Q] (mM)	τ (ns)
0	254
0.10	249
0.20	238
0.30	223
0.40	236
0.50	219
0.60	208
0.80	199
1.0	200
1.2	176
1.4	171

Table 10 Emission Lifetimes of $Ru(bpy)_2(CN)_2$ vs. Ferrocytochrome c Concentration at pH 7.0

μ = 0.1 M

[Q] (mM)	τ (ns)
0	272
0.09	258
0.18	247
0.25	235
0.27	247
0.35	234
0.44	234
0.50	224
0.53	220
0.62	203
0.79	213
0.97	184
1.01	190
1.06	183

Table 11 Emission Lifetimes of $Ru(bpy)_3^{2+}$ vs. Ferricytochrome c at μ = 0.1 M, in biphthalate buffer

pH 3.0		pH 4.0	
[Q] (mM)	τ (ns)	[Q] (mM)	τ (ns)
0	621	0	628
0.05	569	0.11	562
0.11	536	0.17	535
0.15	495	0.23	529
0.22	470	0.28	484
0.28	448	0.34	478
0.32	437	0.4	466
0.39	421	0.45	457
0.45	397	0.51	443
0.50	358	0.57	425
0.56	327		

Table 12 Emission Lifetimes of $Ru(bpy)_3^{2+}$ vs. Ferrocytochrome c at μ = 0.1 M, in biphthalate buffer

pH 3.0		pH 4.0	
[Q] (mM)	τ (ns)	[Q] (mM)	τ (ns)
0	630	0	620
0.12	576	0.1	578
0.24	580	0.2	550
0.36	553	0.3	532
0.48	560	0.4	523
0.61	499	0.5	511
0.73	486	0.6	490
		0.7	485
		0.8	480

Appendix B

Stern-Volmer Plots of Emission Lifetime Quenching of Ruthenium Polypyridyl Complexes by Cytochrome c

Plots of the inverse of measured emission lifetime ($1/\tau$) vs. cytochrome c concentration [C] using data listed in Appendix A are given in the following figures. For experimental details see p.117. The bimolecular quenching rate constants obtained from the slopes of the plots are listed in Tables 2.2 and 2.3 in the text.

Figure 1

Quenching of $Ru(DIPS)_3^{4-}$ by C(FeII) at pH 7.0

μ = 0.1 M

$k_q = 11 \times 10^8\ M^{-1}s^{-1}$

corr. coef. = 0.9880

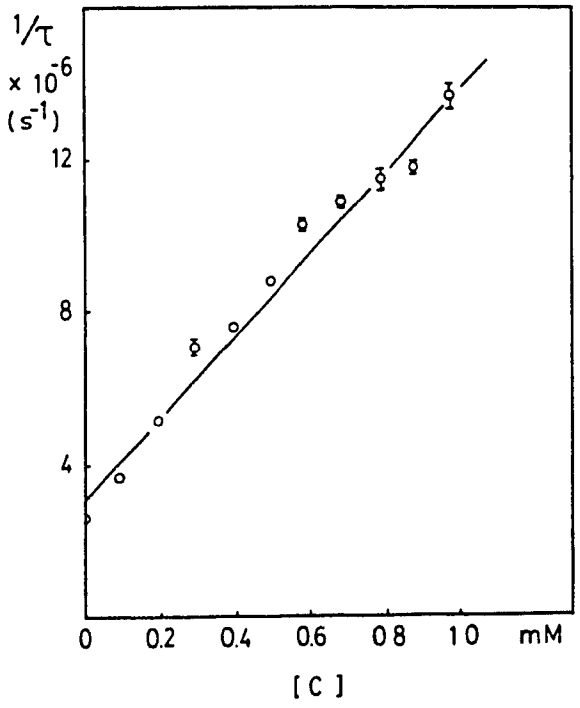

μ = 0.01 M

$k_q = 51 \times 10^8\ M^{-1}s^{-1}$

corr. coef. = 0.9980

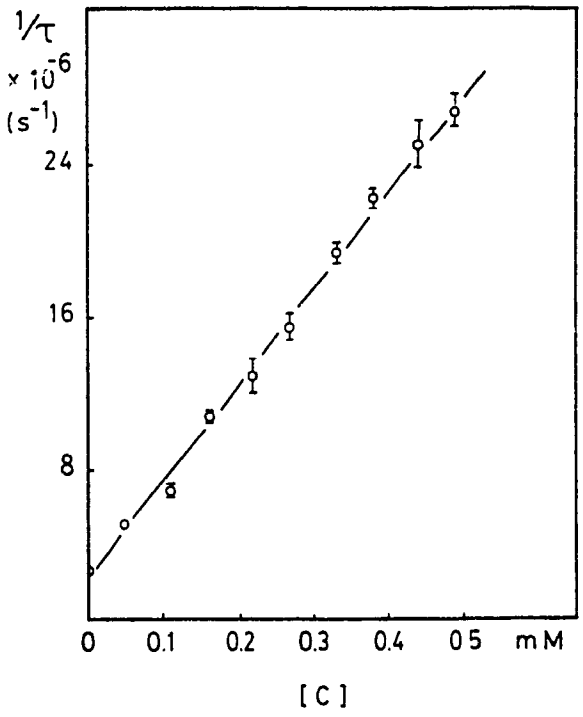

Figure 2

Quenching of $Ru(bpy)_2(CN)_2$ by (A) C(FeIII) and (B) C(FeII) at μ = 0.1 M, pH 7.0

(A) C(FeIII)

$k_q = 14 \times 10^8\ M^{-1}s^{-1}$

corr. coef. = 0.9770

(B) C(FeII)

$k_q = 16 \times 10^8\ M^{-1}s^{-1}$

corr. coef. = 0.9640

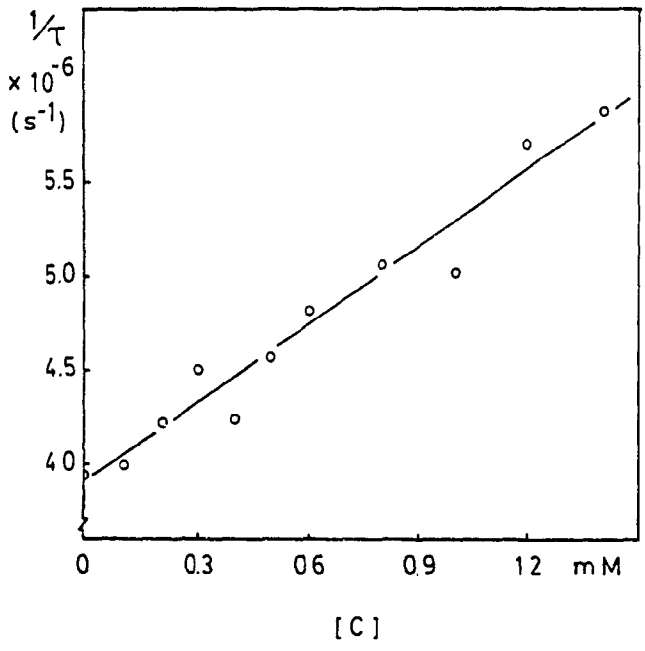

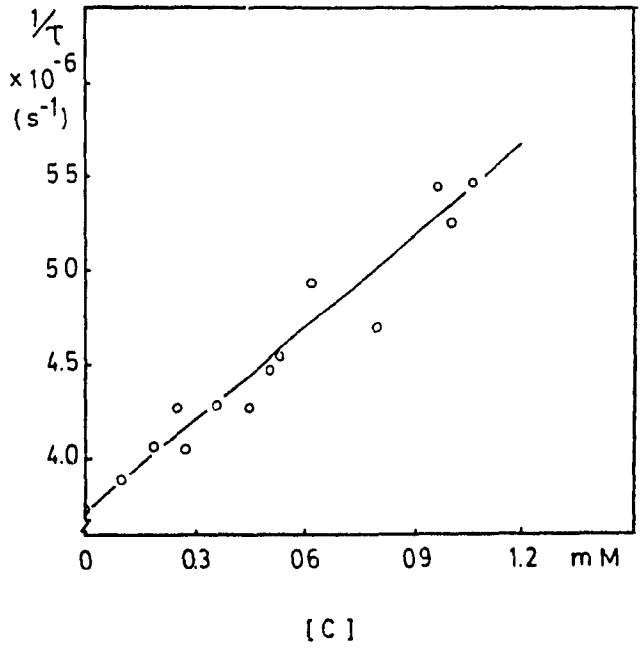

Figure 3

Quenching of $Ru(phen)_2(CN)_2$ by C(FeIII) at pH 7.0

μ = 0.1 M

$k_q = 13x10^8\ M^{-1}s^{-1}$

corr. coef. = 0.9950

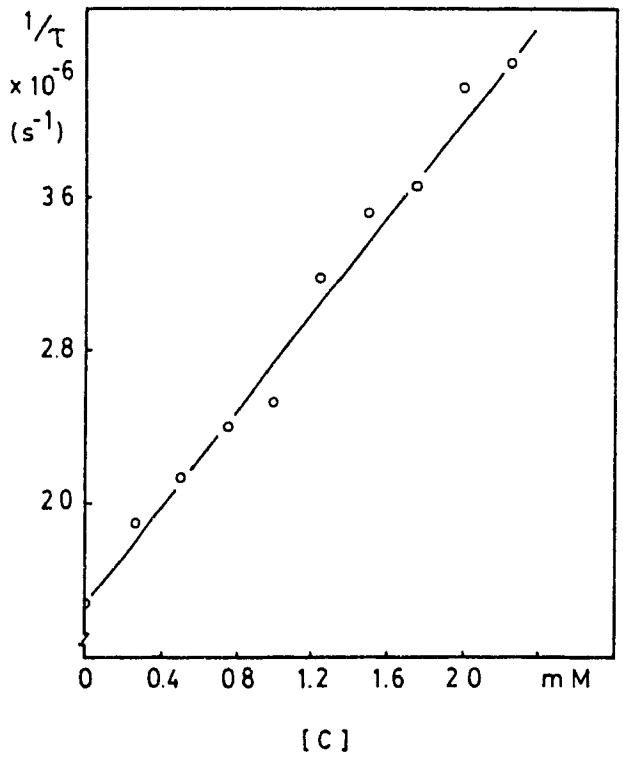

μ = 0.01 M

$k_q = 13x10^8\ M^{-1}s^{-1}$

corr. coef. = 0.9939

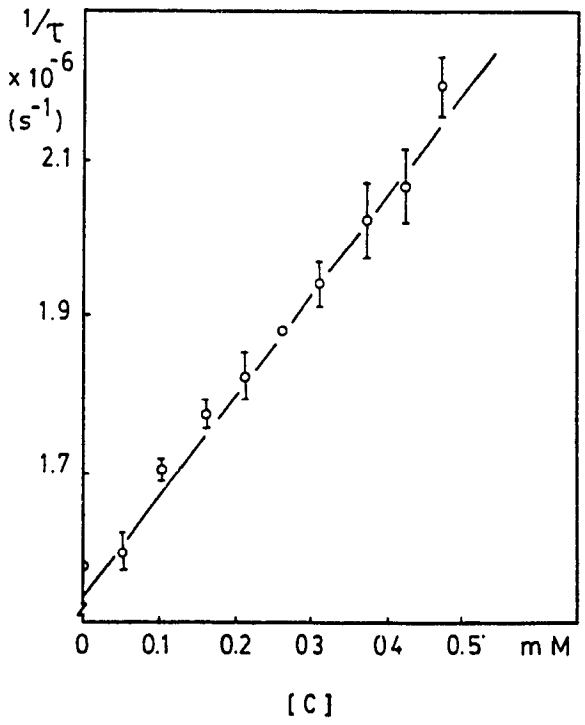

Figure 4

Quenching of $Ru(phen)_2(CN)_2$ by C(FeII) at pH 7.0

μ = 0.1 M

k_q = 7.6×10^8 $M^{-1}s$-1

corr. coef. = 0.9950

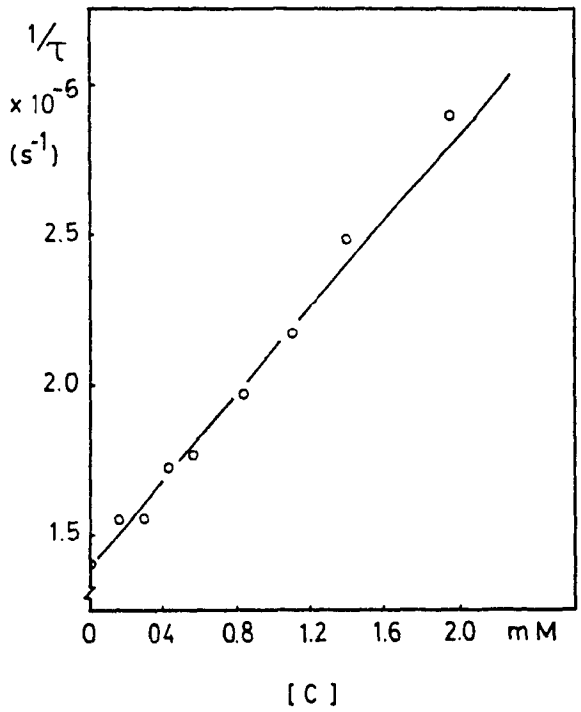

μ = 0.01 M

k_q = 16×10^8 $M^{-1}s^{-1}$

corr. coef. = 0.9950

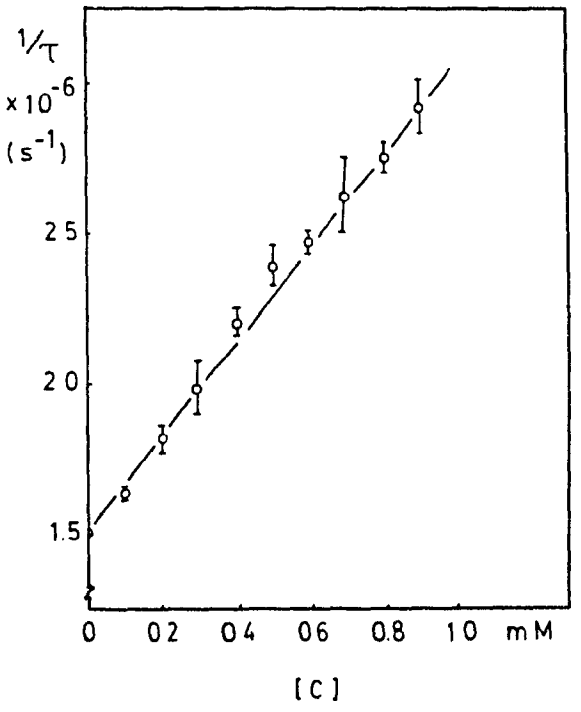

Appendix C

Kinetic Scheme for the Quenching of Ru^*L_3 Involving Precursor Complex Formation

$$RuL_3 \underset{k_o}{\overset{h\nu}{\rightleftharpoons}} Ru^*L_3$$

$$Ru^*L_3 + Q \underset{k_{-1}}{\overset{k_1}{\rightleftharpoons}} Ru^*L_3{:}Q \xrightarrow{k_2} \text{PRODUCTS}$$

$$Ru^*L_3{:}Q \xrightarrow{k_o'} RuL_3 + Q + h\nu$$

Where $k_2 = k_{en} + k_{el}$ and products are $Ru^+L_3{:}Q^-$ for electron transfer (k_{el}) and $RuL_3{:}Q$ for energy transfer (k_{en}).

$$\frac{-d[Ru^*L_3]}{dt} = k_{obs}\,[Ru^*L_3]_{total} \qquad (1)$$

$k_{obs} = 1/\tau$ where τ is the observed lifetime for Ru^*L_3.

Assuming k_o for Ru^*L_3 and k_o' for $Ru^*L_3{:}Q$ are equal:

$$k_{obs}\,[Ru^*L_3]_{total} = k_o\{[Ru^*L_3] + [Ru^*L_3{:}Q]\} + k_2[Ru^*L_3{:}Q] \qquad (2)$$

$$k_{obs} = k_o + k_2 \frac{[Ru^*L_3{:}Q]}{[Ru^*L_3]_{total}} \qquad (3)$$

Since $[Ru^*L_3]_{total} = [Ru^*L_3] + [Ru^*L_3{:}Q]$ (4)

$$\frac{[Ru^*L_3{:}Q]}{[Ru^*L_3]_{total}} = \frac{[Ru^*L_3{:}Q]}{[Ru^*L_3] + [Ru^*L_3{:}Q]} \qquad (5)$$

$$= \frac{\dfrac{k_1\,[Q]}{k_{-1} + k_o + k_2}}{1 + \dfrac{k_1\,[Q]}{k_{-1} + k_o + k_2}} \qquad (6)$$

$$\text{Let } K = \frac{k_1}{k_{-1} + k_o + k_2} \qquad (7)$$

$$\frac{[Ru^*L_3{:}Q]}{[Ru^*L_3]_{total}} = \frac{K\,[Q]}{1 + K\,[Q]} \qquad (8)$$

Substituting (8) into (3) gives;

$$k_{obs} = k_o + \frac{k_2\,K\,[Q]}{1 + K\,[Q]} \qquad (9)$$

Since $k_{obs} = 1/\tau$

$$1/\tau = 1/\tau_o + \frac{k_2 K [Q]}{1 + K [Q]} \qquad (10)$$

$$\tau_o/\tau = 1 + \frac{\tau_o k_2 K [Q]}{1 + K [Q]} \qquad (11)$$

Where Q = concentration of ferricytochrome c

At low [Q]:

$$\tau_o/\tau = 1 + \tau_o k_2 K [Q]$$

Thus the initial slope gives $k_q = k_2 K$

At high [Q]:

$$\frac{1}{\tau_s} - \frac{1}{\tau_o} = k_2 = k_{el} + k_{en}$$

where τ_s is the observed excited state lifetime of Ru^*L_3 at saturation.

Appendix D

Determination of Bimolecular Rate Constants for The Oxidation of CCP(FeII) by $Fe(CN)_6^{-3}$

The oxidation of CCP(FeII) by $Fe(CN)_6^{3+}$ follows the general second order rate law:

$$\text{rate} = k\,[A][B] \qquad (1)$$

where A and B are the two reactants and k is the bimolecular rate constant. At 1:1 stoichiometric amounts of CCP(FeII) and $Fe(CN)_6^{-3}$, the integration of the above expression gives:

$$1/[\text{CCP(FeII)}]_t = 1/[\text{CCP(FeII)}]_0 + kt \qquad (2)$$

where $[\text{CCP(FeII)}]_t$ is the concentration of CCP(FeII) at time t after the reaction was started and $[\text{CCP(FeII)}]_0$ is the initial CCP(FeII) concentration.

Since $[\text{CCP(FeII)}]_0 = (A_0 - A_\infty)/\Delta\varepsilon$ and $[\text{CCP(FeII)}]_t = (A_t - A_\infty)/\Delta\varepsilon$,

where A_0 and A_∞ are the absorbance of CCP(FeII) and CCP(FeIII), respectively, A_t is the absorbance at time t, and $\Delta\varepsilon = \varepsilon_{re} - \varepsilon_{ox}$ is the molar absorbtivity difference for CCP. It is assumed here that the absorbances of $Fe(CN)_6^{3-}$ and $Fe(CN)_6^{4}$ at the monitoring wavelengths are negligible (see Section 3.3) Thus:

$$(A_t - A_\infty)^{-1} = (A_0 - A_\infty)^{-1} + (k/\Delta\varepsilon)t$$

and k is obtained from a plot of $(A_t - A_\infty)^{-1}$ vs. t.

Appendix E

Computer Analysis of Kinetic Data for

The Reduction of C(FeIII)

by CCP(FeII)

The following BASIC program runs on the built-in HP85 microcomputer of the HP8451A spectrophotometer. It automatically extracts the time-dependent absorbance values recorded on the spectrophotometer and analyzes the data by either Guggenheim, Swinbourn or natural Log methods. The corresponding x,y values generated by the algorithm are fitted by a linear least square regression subroutine to determine the curve parameters such as the correlation coefficient, slope and intercept. These parameters are used to determine rate constants of the spectophotometrically monitored reactions.

```
PROGRAM "KINETIC"

 10  DIM X(150),Y(150),V(15)
 20  CLEAR
 30  DISP "INPUT INTERVAL(SEC), BASE LINE"
 40  TIME BASE
 50  INPUT B,C
 60  DISP "INPUT START TIME(SEC), END TIME(SEC)"
 70  INPUT D,E
 80  TIME SCALE D TO E
 90  PLOTTER @ WAIT 2000
100 ALPHA
110 ON KEY# 1,"LN" GOSUB 470
```

```
120 ON KEY# 2,"GU" GOSUB 210
130 ON KEY# 3,"SW" GOSUB 340
140 ON KEY# 8,"END" GOSUB 1040
150 KEY LEBEL
160 GOTO 160

210 REM GUGGENHEIM'S METHOD
220 GOSUB 610
230 FOR I=D TO STEP B
240 Y(I)=LOG(ABS(VALUE(I)-VALUE(I+G)))
250 X(I)=I
260 NEXT I
270 GOSUB 670
280 K=ABS(V(11))
290 L=ABS(V(15))
300 M=VALUE(D)+EXP(V(10))/1-EXP(-(K*G)))
310 N=ABS(EXP(V(14)-EXP(-V(14)))/(1-EXP(K*G)))
320 GOSUB 930
330 RETURN

340 REM SWINBOURNE'S METHOD
350 GOSUB 610
360 FOR I=D TO H STEP B
370 Y(I)=VALUE(I)
380 X(I)=VALUE(I+G)
390 NEXT I
400 GOSUB 670
410 K=LOG(ABS(V(11)))/G
420 L=LOG(ABS(V(11)+V(15))/(V(11)-V(15)))/G
430 M=V(10)/1-EXP(K*G))
440 N=ABS(V(14))/(1-V(11))
450 GOSUB 930
460 RETURN

470 REM NATURAL LOG METHOD
480 H=E
490 J=(E-D)/B+1
500 FOR I=D TO E STEP B
510 Y(I)=LOG (ABS(VALUE(I)-C))
520 X(I)=I
530 NEXT I
540 GOSUB 670
550 K=ABS(V(11))
560 L=ABS(V(15))
```

```
570 M=C
580 N=0
590 GOSUB 930
600 RETURN

610 REM NUMBER OF DATA POINTS
620 F=(E-D)B+1
630 G=INT((F-1)/2)*B
640 H=D+G
650 J=(H-D)/B+1
660 RETURN

670 REM LEAST SQUARE FIT
680 V(1)=0
690 V(2)=0
700 V(3)=0
710 V(4)=0
720 V(5)=0
730 V(6)=0
740 FOR I=D TO H STEP B
750 O=X(I)
760 P=Y(I)
770 V(1)=V(1)+1
780 V(2)=V(2)+O
790 V(3)=V(3)+P
800 V(4)=V(4)+O^2
810 V(5)=V(5)+O*P
820 V(6)=V(6)+P^2
830 NEXT I
840 V(9)=V(1)*V(4)-V(2)^2
850 V(10)=(V(4)*V(3)-V(2)*V(5))/V(9)
860 V(11)=(V(5)*V(1)-V(2)*V(3))/V(9)
870 V(12)=J-2
880 V(13)=(V(6)+V(10)^2*V(1)+V(11)^2*V(4)-2*(V(10)*V(3)+V(11)*V(5)-
          V(10)*V(11)*V(2)))/V(12)
890 V(14)=SQR(V(13)*V(4)/V(9))
900 V(15)=SQR(V(13)*V(1)/V(9))
910 R=(V(1)*V(5)-V(2)*V(3))/SQR(V(9)*(V(1)*V(6)-V(3)^2))
920 RETURN

930 REM OUTPUT
940 CLEAR
950 KEY CLEAR
960 KEY LABEL
```

```
 970 PRINT "# OF POINTS";J
 980 PRINT "K CONSTANT";K
 990 PRINT "STD ERR OF K";L
1000 PRINT "% ERR OF K";L/K*100
1010 PRINT "CORR. COEF.";R
1020 PRINT"BASE LINE";M
1030 PRINT "STD ERR OF BASE";N
1040 RETURN

1050 REM GRAPHIC OUPUT
1060 CLEAR
1070 GCLEAR
1080 SCALE X(D),X(H),Y(D),Y(H)
1090 XAXIS (Y(D)+Y(H))/2,(H-D)/10
1100 YAXIS X(D),(Y(D)-Y(H))/10
1110 FOR I=D TO H STEP B
1120 PLOT X(I),Y(I)
1130 NEXT I
1140 WAIT 2000
1150 ALPHA
1160 RETURN
```